Copyright Warning & Restrictions

The copyright law of the United States (Title 17, United States Code) governs the making of photocopies or other reproductions of copyrighted material.

Under certain conditions specified in the law, libraries and archives are authorized to furnish a photocopy or other reproduction. One of these specified conditions is that the photocopy or reproduction is not to be "used for any purpose other than private study, scholarship, or research." If a, user makes a request for, or later uses, a photocopy or reproduction for purposes in excess of "fair use" that user may be liable for copyright infringement,

This institution reserves the right to refuse to accept a copying order if, in its judgment, fulfillment of the order would involve violation of copyright law.

Please Note: The author retains the copyright while the New Jersey Institute of Technology reserves the right to distribute this thesis or dissertation

Printing note: If you do not wish to print this page, then select "Pages from: first page # to: last page #" on the print dialog screen

ABSTRACT

THREE-DIMENSIONAL STRESS ANALYSIS OF THE FEMUR WITH PROSTHETIC HIP STEM UTILIZING COMPUTED TOMOGRAPHY SCANS OF THE FEMUR FOR GEOMETRY AND MATERIAL PROPERTIES

by
Thomas J. Lavin

Three-dimensional finite element stress analyses of the femur with prosthesis hip stem were performed for two cases, one male and one female, using ideally bonded cemented titanium prostheses. Computed tomography data files were used to derive the three-dimensional femur geometry and material properties for each cortical bone element. The maximum shear stress (4.7 MPa) in the cement was greater then the maximum tensile stress and occurred at the cement-bone interface. The tensile stresses in the cement were less then the fatigue strength of the cement. The stress patterns were quite similar for the two cases.

A data analysis program was developed to processes computed tomography data files of a proximal femur into a finite element model file with prosthesis. The program utilizes Microsoft Excel, it Visual Basic Modules, Math Soft Mathcad, dynamic data exchange, custom menus and user input boxes to make the user interface as efficient as possible.

THREE-DIMENSIONAL STRESS ANALYSIS OF THE FEMUR WITH PROSTHETIC HIP STEM UTILIZING COMPUTED TOMOGRAPHY SCANS OF THE FEMUR FOR GEOMETRY AND MATERIAL PROPERTIES

by
Thomas J. Lavin

A Thesis
Submitted to the Faculty of
New Jersey Institute of Technology
in Partial Fulfillment of the Requirements for the Degree of
Masters of Science in Biomedical Engineering

Biomedical Engineering Committee

January 1997

APPROVAL PAGE

THREE-DIMENSIONAL STRESS ANALYSIS OF THE FEMUR WITH PROSTHETIC HIP STEM UTILIZING COMPUTED TOMOGRAPHY SCANS OF THE FEMUR FOR GEOMETRY AND MATERIAL PROPERTIES

Thomas J. Lavin

Dr. Martin J. Linden, Thesis Advisor — Date
Professor of Mechanical Engineering
of the Department of Mechanical Engineering, NJIT

Dr. Rong - Yaw Chen, Committee Member — Date
Professor of Mechanical Engineering
of the Department of Mechanical Engineering, NJIT

Dr. David Kristol, Committee Member — Date
Professor of Chemistry
of the Department of Chemical Engineering and Chemistry,
and Director of the Biomedical Engineering Program, NJIT

BIOGRAPHICAL SKETCH

Author: Thomas J. Lavin

Degree: Masters of Science in Biomedical Engineering

Date: January, 1997

Undergraduate and Graduate Education:

- Masters of Science in Biomedical Engineering,
  New Jersey Institute of Technology, Newark, NJ, 1997

- Bachelor of Engineering in Mechanical Engineering,
  The City College of the City University of New York, New York, 1983

Major: Biomedical Engineering

This thesis is dedicated to my beloved wife Marie Lavin

ACKNOWLEDGMENT

I wish to express my sincere gratitude to my thesis advisor, Dr. Martin J. Linden, for his guidance, patience and encouragement throughout this research. I would like to thank Wei - Chun Chang, whom I have never met, but this work is based on his previous efforts. I would also like to thank Steven Robbins M. D. at Saint Barnabas Medical Center for his continued interest in this project and Chin -Yang Huang for his help in transferring data files and his review of this work.

Additionally, sincere thanks to Dr. Rong-Yaw Chen and Dr. David Kristol for serving as members of the committee.

I especially thank my wife for her love and support.

TABLE OF CONTENTS

TABLE OF CONTENTS
(continued)

TABLE OF CONTENTS
(continued)

LIST OF TABLES

LIST OF FIGURES

LIST OF SYMBOLS

Symbol	Meaning
1/sec	One divide by seconds
2-D	Two dimensional
3-D	Three dimensional
&	And
ρ	Density or apparent density
μm	One million of a meter
σ	Normal Stress
τ	Shear stress
#	Number
%	Percent
+	Plus

LIST OF ABBREVIATIONS

A	Anterior Also used as a constant in the linear equation relating density to computed tomography number
ABG	Anatomique Benoist Giraud (hip prosthesis)
Al	Aluminum
AML	Anatomic Medullary Locking
ANSYS	Is the name of a Finite Element Software Package (Swanson Analysis Systems Inc.)
ASCII	Plain-text file format
b	Constant in linear equation relating bone mineral density to stress
B	Used as a constant in the linear equation relating density to computed tomography number
BW	Body weight
CB	Cortical bone
cm	One hundredth of a meter
CoCrMb	Cobalt-chrome molybdenum
CT	Computed tomography
CT#	Computed tomography number
DXA	Bone mineral density

LIST OF ABBREVIATIONS
(continued)

E	Young's modulus (elastic modulus) Also used as change of the strain in bone remodeling equation
FEA	Finite element analysis
g/cm^2	Grams per centimeter squared
g/cm^3	Grams per centimeter cubed
GPa	One billion Pascal
Hz	Hertz
kg/m^3	One thousand grams per meter cubed
km/hr	One thousand meters per hour
I	Inferior
L	Lateral
m	Constant in linear equation relating bone mineral density to stress
M	Median
MACTAR	The McMaster Toronto Arthritis Patient Preference Disability Questionnaire

LIST OF ABBREVIATIONS
(continued)

MHz	One thousand Hertz
mm	One thousandth of a meter
MPa	One thousand Pascal (1 MPa = 145 psi)
N	Newton
NJ	New Jersey
NJIT	New Jersey Institute of Technology
Nm	Newton meter
P	Posterior
Pa	Pascal
PMMA	Polymethylmethacrylate
psi	Pounds per square inch
QCT	Quantitative computed tomography
r	Correlation coefficient used in regression analysis
S	Superior

LIST OF ABBREVIATIONS
(continued)

THA	Total hip arthroplasty
THR	Total hip replacement
Ti	Titanium
TiAlV	Titanium aluminum vanadium
V	Vanadium
vs.	versus
WOMAC	The Western Ontario and McMaster Universities Osteoarthritis Index

LIST OF COMPUTER DATA FILES AND PROGRAMS

COMPUTER DATA FILES

File Name	Description
CASE1.DAT	5,523,328 byte ASCII text data file containing the CT data for case 1.
CASE2.DAT	4,883,840 byte ASCII text data file containing the CT data for case 1.
CT2BNUM.DAT.Z	Compressed data file containing the CT data for case 1.
CT5NUM.DAT.Z	Compressed data file containing the CT data for case 2.

EXCEL PROGRAMS

Program Name	Description
CTCASE1F.XLS	A Microsoft Excel program containing a Visual Basic module that separates the CASE1.DAT data file into seventeen different data files (one for each cross-section).
CTCASE2F.XLS	A Microsoft Excel program containing a Visual Basic module that separates the CASE2.DAT data file into seventeen different data files (one for each cross-section).
CTPROG.XLS	The main Microsoft Excel program containing all of the Visual Basic modules required to process the CT data into a "3-D" finite element input file. Referred to as the Excel program.
CREATERI.XLS	A Microsoft Excel program containing a Visual Basic module that creates a right hip set of data files from the Case 2 (left hip) set of data files.
FEADATA.XLS	A Microsoft Excel program containing the raw and processed Finite Element Analysis Stress solution for Case 1 and Case 2.

LIST OF COMPUTER DATA FILES AND PROGRAMS
(continued)

MATHCAD PROGRAMS

Program Name	Description
CBLDATA.MCD	Plots the inner and outer cortical bone boundaries versus different CT numbers for a left hip.
CBLEFT.MCD	Plot a color image of the CT data as well as a black and white inner and outer boundary plot for a left hip.
CBRDATA.MCD	Plots the inner and outer cortical bone boundaries versus different CT numbers for a right hip.
CBRIGHT.MCD	Plot a color image of the CT data as well as a black and white inner and outer boundary plot for a right hip.
CB3DPLOT.MCD	Plots the 3-D cortical bone outer boundaries including the rotated layers.
NODEPLOT.MCD	Plots the 2-D nodal boundaries for each cross-section.
STRESSRT.MCD	Computes the von Mises and maximum shear stress from the components of stress obtained from the ANSYS runs. Associated with FEADATA.XLS.
3DCBPLOT.MCD	Plot the 3-D cortical bone inner and outer boundaries.
3DPPLOT.MCD	Plot the 3-D prosthesis outer boundaries.

CHAPTER 1

INTRODUCTION

1. 1 Hip Prosthesis Design Factors

The following factors need to be considered in the design and analysis of a prosthetic hip stem. The existing shape and condition of the femur bone. The prosthesis material and geometry. The method of attachment of the prosthesis to the bone. The loads that the prosthetic and bone will experience. The rate at which these loads will be applied. The fatigue life of the prosthesis. The stress levels that the bone and prosthesis will experience. The changes in the femur stress levels induced by the present of the prosthesis. The most likely mode of failure of the prosthesis and the method of analysis.

Osteoarthritis of the hip, characterized by the chronic degeneration of the cartilage of the hip joint, is the primary diagnoses requiring total hip arthroplasty. Osteoarthritis causes severe pain and severely affects the individual's physical activity, social interactions, as well as overall health. Total hip arthroplasty results in a rapid and complete improvement in the health-related quality of life of the patient, and affects all aspect of the patients overall well-being (Rorabeck 1994).

A total hip arthroplasty involves the replacement of the hip ball and socket joint. The typical hip prosthesis includes a hip stem, a femoral ball, and an acetabular component. Some hip stem prostheses include a collar portion, designed to contact the calcar. This research deals with the hip stem portion of the joint replacement.

A Computed Tomography Data Analysis Program has been developed that uses Computed Tomography data files and ANSYS Finite Element Analysis Software to allow

an engineer to analyze various prosthetic designs for a given femur bone geometry. The following sections elaborate on the various factors that influence the design and finite element modeling of a hip prosthesis.

1.2 Finite Element Method

Given that the femur with prosthesis is a geometrically complex structure composed of materials with different properties, the finite element method of analysis is an ideal way to model this complex structure and has been used in this research. The finite element method is an effective computational method to analyze the displacements and stresses that will occur in a structure under a defined set of loads and boundary conditions. The finite element method allows the modeling of structures with complex geometries containing multiple materials with different properties. It also allows a structure to be analyzed under various load conditions and boundary constraints.

The general procedure involved in the finite element analysis of a structure are as follows: (1) Discretization of the structure into a collection of finite elements of geometrically simple shapes; (2) Formulation of element equations for all typical elements in the model; (3) Assembly of the element equations to obtain the equations of the whole structure; (4) Imposition of the boundary conditions of the problem; (5) Solution of the assembled equations; and (6) Postprocessing of the results (Reddy, 1984).

1.2.1 Discretization of the Structure

The number, type (i.e., linear, quadratic), and shape (i.e., tetrahedral, brick) of elements used to model a structure depends on the accuracy of the results desired. All interfaces where there is an abrupt change in geometry or material properties need to be modeled. The geometrical shape of an element is defined by coordinate points, called nodes.

The solution convergence characteristics of the finite-element approximation should be investigated by refining the mesh (i.e., increasing the number of elements in the model).

1.2.2 Formulation of Element Equations

The variational formulation of the governing differential equation over the typical element is constructed to obtain an element equation in the form

$$[K^{(e)}]\{u^{(e)}\} = \{F^{(e)}\}$$

where K = element stiffness; u = displacement and F = force.

All forces associated with an element are assumed to be concentrated at the nodal points. The above equation called the element stiffness matrix relates the nodal point forces to the nodal points displacements.

1.2.3 Assembly of the Element Equations

The correspondence between the local nodes and the global nodes is expressed in the form of an array, called the Boolean connectivity matrix. The element equations are

expressed in terms of global nodal values and indicate the contribution of each element to the overall problem. Superimposing is used to obtain the global system equation

$$[K^{(G)}]\{u^{(G)}\} = \{F^{(G)}\}$$

The numbering of the nodes directly affects the bandwidth of the global system equation, and therefore the storage requirements and computational cost of running the analysis. To reduce the bandwidth of the global system equation the elements must be ordered for the solution phase so that the element for which each node is mentioned first is as close in sequence to the element for which it is mentioned last. All elements, including those of different types, should be included in this node numbering sequence.

1.2.4 Imposition of the Boundary Conditions

The imposed nodal constrains (i.e. selected nodes fixed in x, y, and z) and loads associated with the problem are incorporated into the global system equation. At this point the finite element input file would contain a nodal point coordinate file containing each node number and its associated coordinates, an element (node-connectivity) file, a material properties file for all of the elements in the model and the locations and magnitudes of all of the applied forces and constraints.

1.2.5 Solution of the Assembled Equations

The global system equation is partitioned into the following form

$$\begin{vmatrix} [K^{11}] & [K^{12}] \\ [K^{21}] & [K^{22}] \end{vmatrix} \begin{vmatrix} \{\Delta^1\} \\ \{\Delta^2\} \end{vmatrix} = \begin{vmatrix} \{F^1\} \\ \{F^2\} \end{vmatrix}$$

where $\{\Delta^1\}$ is the column of known displacements, $\{\Delta^2\}$ is the column of unknown displacements, $\{F^1\}$ is the column of the unknown forces, and $\{F^2\}$ is the column of the known forces (Reddy, 1984).

The above equation can be written as two matrix equations to obtain

$$[K^{11}]\{\Delta^1\} + [K^{12}]\{\Delta^2\} = \{F^1\}$$

$$[K^{21}]\{\Delta^1\} + [K^{22}]\{\Delta^2\} = \{F^2\}$$

The unknown displacements $\{\Delta^2\}$ are determined by solving the second matrix equation, rearranged as shown below

$$\{\Delta^2\} = [K^{22}]^{-1}(\{F^2\} - [K^{21}]\{\Delta^1\})$$

Once the unknown displacements $\{\Delta^2\}$ are determined the unknown forces $\{F^1\}$ can be computed from the first matrix equation.

1.2.6 Postprocessing of the Results

The solution of the global system equation gives the nodal values of the primary unknowns (e.g., displacement). Postprocessing of the results includes the calculation of the strains from the strain-displacement relations and then calculation of the stresses from the stress-strain relations. The results are then represented in tabular and/or graphic form.

The use of the finite element method combined with computer tomography, which provides the 3-dimensional bone geometry and properties, and a pre-processing method to determine the prosthesis geometry is an efficient way to determine the stresses in the femur with prosthesis.

1.3 Bone Properties

In order to develop a finite element input file of the femur with prosthesis the material properties of all of the materials in the model need to be known. The following is a summary of the bone properties reported in the recent literature. Cowin (1995) showed mathematically, using the minimization and maximization of the strain energy density, that the midshaft of a long bone, such as the femur, has the greatest stiffness in the direction of its long axis and its greatest impact loading resistance in the transverse direction. Table 1.1 list the Young's Modulus of Trabecular and cortical bone measured ultrasonically and mechanically, by Rho et al., (1993).

Table 1.1 Young's Modulus of Trabecular and Cortical Bone

	Ultrasonic (2.25 MHz)		Mechanical (Tensile)	
	Young's Modulus	1 Sigma	Young's Modulus	1 Sigma
Material	(GPa)	(GPa)	(GPa)	(GPa)
Trabecular Bone	14.8	1.4	10.4	3.5
Cortical Bone	20.7	1.9	18.6	3.5

Rho et al., (1993) shown that the Young's modulus of cortical bone cannot be extrapolated from the Young's modulus vs. density relationship for cancellous bone, yet the Young's modulus of trabeculate can be predicted by extrapolation from the relationship between Young's modulus vs. density of the cancellous bone. This implies that mechanically cortical and trabecular bone are not the same material. Trabecular bone being the bone tissue within cancellous bone.

The two most frequently used methods to determine the Young's modulus of bone is ultrasonic and microtensile or microcompression testing. In Ultrasonic testing, ultrasonic waves propagated through the bone specimen at a given frequency (i.e. 2.25 MHz). The Young's modulus in a specific direction is equal to the bone density multiplied by the through the thickness propagation velocity squared (Kohles et al., 1994). The bone specimens are saturated with physiological saline during the tests (Rho et al., 1993). In microtensile tests the bone specimen are often glued to an attachment using a cyanoacrylate glue (Rho et al., 1993).

Rho et al., (1993) states that the actual Young's modulus of trabecular bone material probably falls nearer to the upper end of values obtained by bending test (3.2 - 7.8 GPa) and towards the lower end of the range found using microtensile and other tests (8.7 - 12.7 GPa). There is not a single value for Young's modulus of trabeculae, as the properties may vary depending upon the location, age, density, species, and state of health. Since the trabecular bone undergoes a considerably higher rate of turnover than cortical bone, there is a great deal of variation in its properties. Rho et al., (1993) found that Ultrasonic testing gave higher values for Young's modulus for both microspecimens of cortical bone and individual trabeculae then microtensile testing. They state that it is possible that this discrepancy is due to the dependence of Young's modulus in bone upon strain rate, and may indicate that the very slow strain rate used in the microtensile tests (5.5×10^{-6}/sec) was not equivalent to the strain associated with the elastic wave propagation used in Ultrasonic testing. For the bone specimens measured by Rho et al.,

(1993) the following equation, which is valid for both cancellous bone cubes and trabecular bone material, was derived:

$$E = -0.29 + 0.0042\ \rho + 1.8 \times 10\text{-}6\ \rho^2, \quad (r^2 = 0.97)$$

where E is in GPa and ρ is in kg/m^3.

As stated previous Rho et al., (1993) found that the Young's modulus of cortical bone could not be extrapolated from cancellous bone data.

Van Rietbergen et al., (1995) developed a realistic three dimensional model of trabecular bone, representing a 5.15 by 3.64 by 5.12 mm cube, consisting of 296,679 elements. The geometry for the model was obtained by using micro-CT-scanning to digitize a 7 by 7 by 7 mm trabecular bone cube. There was a total of 176 slices each with a resolution of 176 by 248 pixels. The model represented the center section of the cube. All elements were assigned isotropic material properties. A Young's modulus of 1000 MPa was used so that the results could be scaled (analysis was linear elastic) to any isotropic Young's modulus with a Poisson's ratio of 0.3 (as used in their model). Based on experimental data (88 to 400 MPa) they estimated the tissue Young's modulus for trabecular bone to be between 2.23 GPa and 10.1 GPa.

Keaveny et al., (1993) points out, that because the ends of any bone specimen is machined there is a damage artifact which results in a lower experimentally measured Young's modulus. There may also be frictional artifacts which depend on the specimen-platen interface conditions. The frictional artifacts increase the experimentally measured Young's modulus. The experimentally measured artifacts are sensitivity to the specimen size, aspect ratio and the Poisson's ratio of the bone being tested. Based on a series of

finite element models used to represent different specimen sizes and frictional effects Keaveny et al., (1993) discovered that the error in the Young's modulus measurement can be substantial for certain specimen geometries. They also reported that the platens Young's modulus may vary from less than 30 % to over 175 % of the Young's modulus of the bone specimen. They concluded that one needs to question the accuracy of the Young's modulus data so far obtained with the conventional compression test, and that any inter-study comparisons, where the aspect ratio, Poisson's ratio, frictional characteristics, and specimen size differ, are invalid.

They also discovered that when strain is measured by an extensometer, there is no initial, nonlinear "toe" in the stress-strain curve. Thus, the trabecular bone specimen behaves in a linear fashion up to yielding. Therefore, the initial nonlinearity seen during testing of trabecular bone may also be an experimental artifact due to specimen-platen damage. Keaveny et al., (1993) recommended the use of ultrasound or direct attachment of extensometers to material away from the platens to overcome problems with accuracy.

In this research the Young's modulus of cortical bone was assumed to following the Carter and Hayes (1977) equation listed below

$$E = 3790(\text{strain rate})^{0.06}(\text{Density})^{3} \quad \text{(MPa)};$$

where strain rate is in units of (1/sec) and density is in g/cm^3

and the Young's modulus of cancellous bone was assumed to be a constant and equal to 1000 MPa, as used by Chang (1994).

1.4 Computed Tomography Number vs. Density

Computed Tomography (CT) scans of the femur are used in this research to determine the 3-dimensional geometry of the femur and the material properties of the cortical bone to be used in the finite element model. This research is a continuation of the procedure used by Marom and Linden (1985) and further developed by Chang (1994) to created a 3-D finite element model from Computer Tomography (CT) data. In computed tomography two dimensional cross-sectional views of a object are obtained. These two dimensional cross-sectional views can be combined to form a three-dimensional image. The three-dimensional image gives a much more accurate geometrical representation of the bone structure then can be obtained from the review of anteroposterior and lateral x-rays. This three-dimensional image can be used as the basis for designing a custom prosthesis.

A CT number is associated with every pixel location in the cross-section. There is a relationship between the pixel CT number and the density of the object at that location. In this research the relationship between cortical bone density and CT number is assumed to be linear. The equation used to relate CT number to cortical bone density is of the following form:

$$\text{Density} = (A)(CT\#) + B \quad (g/cm^3)$$

The Computed Tomography Data Analysis Program allows the user to vary the values of A and B so that this CT data analysis program can be used with any CT scanner that gives a CT number that is linearly related to the cortical bone density. Studies have show that there is a relationship between the density of cortical bone and its Young's

modulus. Therefore, not only does a CT scan give an accurate geometrical representation of the bone structure it also allows one to determine the Young's modulus of the bone. The following rate dependent equation has been used to relate the density of the cortical bone to its Young's modulus (E):

$$E = 3790(\text{strain rate})^{0.06}(\text{Density})^3 \quad \text{(MPa)}; \quad \text{Carter and Hayes (1977)}$$

where strain rate is in units of (1/sec) and density is in g/cm^3

The program allows the user to input various strain rates. The Young's modulus of cancellous bone was assumed to be a constant in this research and not a function of the density (CT number) of the cancellous bone.

1.5 Prosthesis Material/Geometry

In order to develop a finite element input file of the femur with prosthesis the material properties and geometry of all of the materials in the model need to be known. This section discusses the prosthesis materials and geometries reported in the recent literature. The goal of a hip prosthesis is to restore the natural kinematic motion of the joint. This must be accomplished in such a way that the prosthesis does not cause pain. Ideally the life of the prosthesis should exceed the life expectancy of the patient. In reality the prosthesis sometimes fails and revision surgery is required. The typical prosthesis materials are titanium aluminum vanadium (TiAlV) and cobalt-chrome molybdenum alloy (CoCrMb). Stem length as well as stem cross-section plays a major role in the stability of

the prosthesis. The use of a calcar support (collar) on a hip prosthesis has received both support and disapproval.

Head et al., (1995) suggests that titanium alloy is the material of choice for cementless femoral components even though they state that the most widely used cementless femoral component in the United States is the Anatomic Medullary Locking (AML; DePuy, Warsaw, IN) which is made of CoCrMb alloy. Their reasoning was that TiAlV has a much lower Young's modulus then CoCrMb and therefore a lower bending stiffness which results in less stress shielding (less bone reabsorption), especially for stem with diameters larger than 13.5 mm. Since the bending stiffness is proportion to the Young's modulus times the radius raised to the fourth power. Lower incidence of thigh pain is also associated with the decreased rigidity of TiAlV. Superior biocompatibility of TiAlV was also pointed out. However, advantages with respect to implant fixation has not been confirmed. TiAlV was not recommended to be used as a bearing surface because of its poor wear resistance. CoCrMb stems were preferred for cemented femoral stems because FEA shown that titanium alloy stems placed greater stress on the cement.

Sotereanos et al., (1995) on the other hand, stated that chrome-cobalt femoral prostheses have the following three advantages over titanium stems. Cobalt-chrome implants have been used successfully for a longer period than titanium ones. Secondly, the porous coating can be applied to the entire surface of the prosthesis stem with a low incidence of fatigue failure. This ability to apply a porous surface to an entire implant has distinct advantages in revision surgery. Applying a similar coating to a titanium stem increases the risk of stem fracture. The third advantage of cobalt-chrome implants over a

titanium alloy implant, being the greater surface hardness of cobalt-chrome, which results in less abrasive wear in the uncoated distal portions.

Callaghan (1993) also states the advantages of cobalt-chromium as being its material hardness which should result in less wear debris, and it's ability to more readily maintain strength, through the sintering process of applying porous beads, since it has less notch sensitivity. Titanium however is believed to have the potential of obtaining greater bone ingrowth since pure titanium can bond chemically to bone. Titanium also has decreased material stiffness, therefore less stress shielding will occur in the bone and there are less biocompatibility concerns associated with its use. As seen from the above there is not universal agreement of the choice of stem material.

Typically, stems are either straight or curved. The advantage of a straight stem is that it is more versatile for use in patients who have an abnormal femoral anatomy. However, a curved stem allows for better initial torsional stability in patients with normal femoral anatomy. Modular stem designs also exist. They allow for a more custom fit but fretting at the modular tapers which results in the production of wear debris is a concern. Some hip prosthetic stems contain a collar to allow for proximal medial stress transfer and increased initial stability of the implant. However, initial collar contact is not always obtained and when it is obtained initially it is not maintained in a relatively large percentage of patients due to bone remodeling. Another concern with the use of a collared stem is that by the collar making contact it may inhibit adequate seating of the prosthesis, and prevent the desired press fit of the prosthesis from being obtained.

Munting and Verhelpen (1995) performed a pre-clinical biomechanical evaluated of a femoral implant that has no intramedullary stem. It fits into an angular resection of the femoral neck. The stemless prosthesis was made of titanium alloy (Ti, 6% Al, 4% V) and had a hydroxyapatite coating. An 8 mm diameter trans-trochanteric screw is used to provide immediate strong fixation. There is an ongoing clinical trial with consenting patients under the age of 50.

The Computed Tomography Data Analysis Program developed in this research allows the user to vary the prosthesis material and geometry.

1.6 Prosthesis/Bone Interface

One of the areas of greatest concerns in the hip stem joint is the interface between the femur bone and prosthesis. This interface plays a major role in the transfer of loads (stress) from the prosthesis to the bone. The important of stress transfer is discussed in Section 1.9. This section discusses the present methods used to attach the prosthesis to the bone.

The three most popular means of attaching the prosthesis to bone are bone cement, porous surfaces and bone compatible coatings. The most common bone cement is Polymethylmethacrylate (PMMA) pioneered by Charnley in 1970. Simplex P bone cement (Howmedica, Rutherford, NJ) is also commonly used. To reduce the chance of an inflection an antibiotic, such as cephalosporin, is often added to the bone cement. The techniques employed in the use of bone cement has evolved. The original method consisted of finger packing the cement into the femur without a medullary plug ("first-

generation cementing techniques"). Around 1976, the use of a medullary plug and cement gun for cement delivery was incorporated. In 1978, some surgeons began using a Water Pik (Daval, Cranston, Rhode Island) to clean the bone interstices of blood and marrow. Cement pressurization through the use of a cement compactor was incorporated later that year. Newer cementing techniques now, also use cement porosity reduction techniques, e.g., vacuum mixing or centrifugation and a layer of methylmethacrylate precoated on the metal (Estok and Harris 1994).

The goal of proximally porous-coated femoral prosthesis is to provide a lifelong biologic fixation between the implant and bone without severe femoral stress shielding. Coating materials include porous layers (beads or mesh), plasma-sprayed metals, hydroxyapatite, and tricalcium-phosphate (approximately fifty micrometers thick, used to enhance bone ingrowth). This alternative method of fixation is being pursued because the cement joint is believed to be the weak link in the bone/prosthesis interface. The ideal of a biological bond to the bone in theory can extend the life of the prosthesis which is required for younger more active patients. The bond between hydroxyapatite and the prosthesis may turn out to be the weak link, rather than the bond between hydroxyapatite and bone. The strength requirements of a prosthesis prohibits the use of a fully porous implant, so a porous coating is placed on a solid substrate. Sintering, diffusion-bonding, and plasma-spraying are the commonly used methods to create porous surfaces.

Sintering is a high-temperature process that fuses spherical beads (cobalt-chrome or titanium), differing only in bead size, to the substrate and to each other at the contact points. The sintering technique works for either a cobalt-chrome or titanium substrate.

The spherical beads are initial held in place on the substrate with a jelly-like binder which dissipates during the heating process. Sintering reduces the fatigue strength of the implant material. The process of sintering redistributes carbide phases in the case of chromium alloys and creates notches at the sites of attachment in the case of titanium alloys. There is also a reduction in strength in the area without the porous coating due to phase transformation that occurs during sintering. This would include the smaller-diameter neck (Callaghan 1993, Bourne et al., 1994).

Diffusion-bonding is a process which uses heat and pressure (less heat than sintering) to attach titanium fiber metal porous pads to a titanium alloy substrate. The fatigue strength of the titanium alloy components reduces from 78,000 to 30,000 psi as a result of diffusion bonding or sintering, largely because of notch sensitivity (Callaghan 1993, Bourne et al., 1994).

The optimum pore size for bone ingrowth is believed to be in the range of 100 to 400 micrometers. Since the porous coating does not result in an immediate bond, the initial strength of fixation that is achieved is less than that achieved with the cured bone cement, however, within two weeks the interfacial strengths are equivalent to those obtained in cancellous bone (1.4 to 2.6 MPa) (Callaghan 1993).

Metal ion contamination is a potential concern with porous-coated implant because of the large surface area exposed to bone. Wear, electrochemical corrosion, and fretting corrosion all result in the release of metallic ions.

Plasma-spraying involves the partial melting of metal powders in a hot plasma flame within the spray nozzle (only the coating material is heated) and the delivery of this

product (i.e. titanium coating powder) to the substrate through a carrier pressurized gas mixture, under an applied electrical field. A textured surface results. The plasma spray process reduces the fatigue strength of a titanium alloy implant from 78,000 to 70,000 psi due to the notch-sensitivity (Callaghan 1993, Bourne et al., 1994).

The major concerns with these coating processes are the fact that they reduce the bulk mechanical strength of the implant, have the potential for debonding between the porous surface and substrate and cause an accelerated rate of corrosion (due to the large surface area).

The relative motion between the prosthesis and the adjacent bone effects the type of tissue that grows within the porous surfaces. There appears to be a relative motion threshold. If the relative motion exceeds the threshold, bone ingrowth will not occur, instead a fibrous tissue layer will result. The threshold has been estimated to be as low as 40 μm and as high as 150 μm. If stability is achieved and maintained, the following three phases of primary fracture-healing occur at the porous interface: first, there is an initial inflammatory phase; then, there is reparative woven bone which occurs at one to two weeks; and finally there is the remodeling lamellar-bone phase which occurs at four weeks (Gilbert et al., 1992, Callaghan 1993).

Using rigid-body motion mechanics Gilbert et al., (1992) developed a method to measure the three-dimensional motion of a femoral prosthesis with respect to the femur containing it. They obtained the following relative motions. "For an uncemented prosthesis the total migration was 193 μm in magnitude (with 12 μm in the anterior direction, 150 μm in the medial direction, and 122 μm distally) and the micromotion at

the end of the test was 52 μm in magnitude (with 21 μm anterior, 44 μm medial, and 17 μm axial micromotion)". The difference in magnitudes observed by Gilbert et al., (1992) between the relative motion at the peak loads and the prosthesis migration are at or exceed the relative motion threshold believed to result in the development of a fibrous tissue layer. The exact prosthesis used by Gilbert et al., (1992) was not specified.

The most important factor for the maximization of bone ingrowth into porous surfaces is the achievement of stability between the implant and bone. The percentage of available porous surface in which bone ingrowth actual occurs is believed to be somewhere between 0 to 65 per cent (Callaghan 1993). There is greater proximal cortical bone loss with the use of more extensively coated stems and of stems that have a diameter of more than 13.5 millimeters due to proximal stress shielding. However, many investigators prefer extensively coated stems because they question the durability of the fixation attained with proximally coated stems, especially in view of the potential destruction of bone that has recently been realized to occur due to the biological response to particulate debris. There is also a lower incidence of thigh pain associated with the use of extensively coated stems.

A greater rate of intraoperative fractures occur with procedures performed without cement, due to the fact that cementless prosthesis tend to be thicker and require a press fit for initial stabilization.

The development of connective soft tissues at the interface between implants and bone can endanger the stability of the implant fixation. This is a biological reabsorption process of the bone facing the implant, which sometimes occurs after many years of

successful functioning. The interface bone is replaced by a soft tissue layer which can easily deform under compression and is not capable of transmitting shear and tensile stresses. The soft tissue formation between implant and bone results in a clinically loose implant (Weinans et al., 1993).

Huiskes and Reitbergen (1995), point out that the long-term survivorship of noncemented hip stems in total hip arthroplasty is subject to incompatible design goals. Stated slightly differently we have, the goals of minimal bone loss and maximal interface security are incompatible. To reduce bone absorption, bones should be stressed to their normal physiologic levels and loads should be transferred proximally. This is achieved by using short, flexible, proximally bonded stems. Conversely to maximized bone ingrowth and minimize micromotions stems ought to be long, rigid and bond over their entire length.

Rorabeck (1994) conducted a double-blind study of 250 cases comparing the cemented Mallory Head Implant (Biomet, Inc. Warsaw, Indiana) to the cementless version. They found no difference in impact on patients health-related quality of life between cemented and cementless total hip arthroplasty at two years. They compared Harris Hip score, D'Aubine Score, WOMAC Osteoarthritis Index, MACTAR index, Sickness Impact Profile, Time Trade-Off (how many of their current years of life are patients willing to give up to achieve full health), Six-Minute Walk, and Economic factors. Rorabeck et al., (1994) plan to follow this group of patients for ten years to determine the relative revision rates of the cemented and cementless implants.

The Computed Tomography Data Analysis Program developed in this research allows the user to vary the interface properties used in the 3-dimensional finite element model of the femur with prosthesis. For the two cases analyzed in this study, a titanium prosthesis with an ideally bonded cemented interface was modeled. Section 1.11 discusses methods that can be used to model other interface conditions.

1.7 Hip Forces

The boundary conditions used in the finite element models created in this study consisted of assigning zero displacement constraints to the distal most portion of the femur (e.g. the distal most set of nodes were fixed in X, Y, and Z). In addition a joint load was applied to the top of the prosthesis neck and a muscle reaction force was assigned to femur nodes associated with the greater trochanter muscle attachment site. This section discusses the hip joint and muscle reaction forces found in the literature.

Telemetering total hip implants (Bergmann et al., 1993) allow one to measure the magnitudes, directions and moments of force in real time. Instrumented prostheses were implanted in the left and right hips of an 82 year old male patient (650 N body weight (BW)) with severe arthritis (first patient). This patient is a healthy active individual being able to run at 8 km/hr 30 months after implantation. In the frontal plane the left prosthesis restored the femur preoperative location relative to the femur to within 3 mm. The right prosthesis caused the femur to be 1.3 cm more lateral and 1 cm more distal after the implantation.

The second patient a 69 year old female (470 N BW) has a unilateral idiopathic femoral head necrosis and received a right hip prosthesis. This patient also suffered from a neurologic disorder which caused an abnormal gait pattern. The median peak forces of this patient were about 20-30 % larger than those of the first patient at the same speed. The second patient was unable to run.

Bergmann et al., (1993) reported median peak forces of about 550 % of BW for jogging and very fast walking in the first patient using telemetering total hip prostheses. In the second, less active, patient a median peak force of 410 % of BW for 3 km/hr walking was reported. In instances of stumbling a force of 720 % and 870 % of BW was reported for patient one and two respectively. Tests with the first patient showed that he was unable to willingly create forces of this magnitude with any kind of exercise. Torsional moments around the stem of the implant were 40.3 Nm and 24 Nm for patient one and two respectively. Torsional moments can lead to high bone stresses and large motion between implant and bone. The data obtained indicate that an increase of the torsional moments with a smaller anteversion angle is probable. Therefore, implant anteversion must be carefully considered by the surgeon.

Since the peak forces and moments were much larger when the patients stumbled then measured with walking or running, Bergmann et al., (1993) points out that the role "accidental" forces play in the initiation of prosthetic loosening must, therefore, be considered.

Bergmann et al., (1995) investigated the loads and moments produced by staircase walking. Staircase walking has been thought as one activity that places the highest loads

and moments on the hip joint. Bergmann et al., (1995) reported that although the joint force and bending moments are greater for going up or down stairs then for level walking, walking at 5 km/hr causes forces and moments of similar magnitudes. The torsional moments observed in vivo (Bergmann et al., 1995), greater than 5% of body weight, are probably close to the torsional strength limits of implant fixations. Therefore high torque around the stem axis may contribute to implant loosening.

Delp and Maloney (1993) developed a three-dimensional biomechanical model of the human lower extremity to determine how a 2 cm displacement of the hip center affects the moment-generating capacity of four muscle groups: the hip abductors, adductors, flexors, and extensors. Their results show that the functional result of an otherwise satisfactory hip reconstruction may be compromised, if the capacity of the muscles to generate moments is greatly reduced, due to post surgical displacement of the hip center. For example, if the hip center is displaced superiority the hip abductors may be unable to develop the moments needed to counteract the moment from body weight during single-leg stance, and a limp is likely to result. Posterior hip center displacement may reduced the hip extensors moment generating capability sufficiently that climbing stairs, or rising from a chair may be impossible.

Surgical changes that alter the hip center may reduce the force-generating capacity of a muscle group, by altering the length-tension relationships of the muscles in the group, and change their moment arms about the joint, by altering the distances between the muscles and the hip center.

The Computed Tomography Data Analysis Program developed in this research allows the user to vary the magnitude and direction of the joint force and greater trochanter muscle force to be applied to the 3-dimensional finite element model. The joint and greater trochanter muscle force used for the two cases analyzed in this study are listed in Table 3.5.

1.8 Stress Analysis

The goal of the finite element analysis of the femur with prosthesis is to estimated the resulting stress levels. If the stress levels are to great, failure of the hip joint may occur and if the stress levels in the femur are to low, bone reabsorption (stress shielding) may occur which eventually leads to failure of the joint. Modes of failure are discussed in Section 1.10 and stress shielding is discussed in Section 1.9. This section discusses the maximum shearing stress and maximum distortion energy theories of failure.

The complete description of stress at a point requires the specification of the stress on all planes passing through the point. A total of nine scalar stress components define the state of stress at a point. The Stress Tensor shown below indicate the nine stress components.

$$\tau ij = \begin{vmatrix} \tau xx & \tau xy & \tau xz \\ \tau yx & \tau yy & \tau yz \\ \tau zx & \tau zy & \tau zz \end{vmatrix} = \begin{vmatrix} \sigma x & \tau xy & \tau xz \\ \tau xy & \sigma y & \tau yz \\ \tau xz & \tau yz & \sigma z \end{vmatrix}$$

where: τij = shear stresses; i = x, y, or z; j = x, y, or z

σn = normal stresses; n = x, y, or z

The components of stress generally vary from point to point in a stressed body. The variation of stress with position may be expressed by the following differential equations of equilibrium

$$\frac{\partial \sigma x}{\partial x} + \frac{\partial \tau xy}{\partial y} + \frac{\partial \tau xz}{\partial z} + Fx = 0$$

$$\frac{\partial \tau xy}{\partial x} + \frac{\partial \sigma y}{\partial y} + \frac{\partial \tau yz}{\partial z} + Fy = 0$$

$$\frac{\partial \tau xz}{\partial x} + \frac{\partial \tau yz}{\partial y} + \frac{\partial \sigma z}{\partial z} + Fz = 0$$

Three principal planes of zero shear stress exist that are mutually perpendicular with normal stresses that have maximum or minimum values. These normal stress are referred to as principal stresses (σ_1, σ_2, and σ_3). The algebraically largest stress is represented by σ_1, and the smallest by σ_3. The principal stresses can be determine by solving the following determinant for the three roots of σ_p (σ_1, σ_2, and σ_3).

$$\begin{vmatrix} \sigma x - \sigma p & \tau xy & \tau xz \\ \tau xy & \sigma y - \sigma p & \tau yz \\ \tau xz & \tau yz & \sigma z - \sigma p \end{vmatrix} = 0$$

The values of the principal stresses are used to predict the likelihood of failure. Two theories of failure are discussed below. The maximum shear stress theory and the maximum distortion energy theory. The maximum shear stress theory predicts that yielding will start when the maximum shear stress in the material equals the maximum shear stress at yielding in a simple tension test. The maximum shear stress at the yield point (τyp) in a tension test equals the maximum principal stress (σyp) at the yield point divide by two. Therefore we have in a simple tension test

$$\tau yp = \sigma yp/2$$

The value of the maximum shearing stress is given by the following equation:

$$\tau max = (1/2)(\sigma_1 - \sigma_3)$$

At the yield point we have

$$(1/2)(\sigma_1 - \sigma_3) = \tau yp = \sigma yp/2$$

or

$$\sigma yp = (\sigma_1 - \sigma_3).$$

In the maximum distortion energy theory failure by yielding occurs when, at any point in the body, the distortion energy per unit volume in a state of combined stress become equal to that associated with yielding in a simple tension test. Mathematically this is written as

$$\sigma yp = \{(1/2)[(\sigma_1 - \sigma_2)^2 + (\sigma_2 - \sigma_3)^2 + (\sigma_3 - \sigma_1)^2]\}^{(1/2)}$$

This stress is known as the von Mises yield stress.

The stresses obtained from postprocessing of the finite element model displacement solution are used to predict whether the prosthesis will fail. ANSYS the finite element package used in this research allows the user to obtain the stress levels in various formats (e.g., nodal stresses, principal stresses, von Mises stresses).

1.9 Bone Adaptation/Stress Shielding

Although a bone remodeling routine was not part of this research, the maximum principal stress and maximum shear stress calculated in the femur with prosthesis, at the time of implantation can be used to accurately predicts the bone density remodeling caused by the prosthesis (Skinner et al., 1994). The following is a brief review of bone adaptation and how it relates to hip prostheses.

Wolff's law states that there is a natural bone remodeling processes that adjust the structure and the microstructure of bone to support the loads borne by the skeleton with a minimal amount of material. It has been shown that there is a direct connection between the bone remodeling process as a point-by-point reaction to mechanical strain energy density and bone remodeling as a process which produces a structure which satisfies an overall structural goal (Harrigan & Hamilton 1994). It is generally accepted that bone adapts to mechanical loading. A decrease in mechanical load causes reabsorption of bone (atrophy), whereas an increase in mechanical load leads to bone formation (hypertrophy) (Mullender et al., 1994). The degree of bone stress shielding that occurs around a femoral stem is affected, first of all by the bonding conditions of the implant/bone interface and secondly by the stem stiffness (i.e., stem thickness and Young's modulus)

(Weinans et al., 1994). A common, though not universal, biologic reaction for partially porous coated cementless hip prostheses observed clinically is bone hypertrophy (increased bone density or perhaps new endosteal bone formation) at the junction of the porous coated and smooth surface of the stem. As stated previously there is a trade-off between stress shielding and relative motion for cementless hip implants (Keaveny and Bartel 1994).

When too much bone is lost, the fixation strength of the implant is jeopardized and the prospects for a successful revision operation are diminished (Weinans et al., 1994). If excessive stress shielding (proximal bone loss) or excessive degenerative arthritis occurs the proximal femur may need to be replaced. Chandler (1994) reported on a technique of reconstruction using proximal femoral allograft-prosthetic composites. In this technique a modular long-stemmed prosthesis was cemented to an allograft proximal femur and press-fitted into the host bone. This procedure involves the adding of bone stock to the deficient femur while loading the remaining host bone in a physiologic manner.

Sadegh et al., (1993), employed surface bone remodeling theory (shape evolution of bone due to a change in the bone's strain distribution) and the boundary element method (only the boundary and not the whole domain needs to be discretized) to investigate the microstructural remodeling of bone at the bone-implant interface. They determine that in order to achieve a successful mechanical interlocking between implant and bone, one needs to ensure the existence of a normal compressive strain in the bone tissue in the region close to the implant and in the direction perpendicular to the direction

of ingrowth. Their models show that not only does the depth of ingrowth increase with increasing applied stress but the rate of ingrowth increase at higher applied stresses.

Harrigan & Hamilton (1994), have shown that a remodeling rate equation, that uses density taken to a power as a state variable, can be part of a process that optimizes a weighted sum of the strain energy in the structure and the total mass of the structure. Specialized cells, the osteoclasts and osteoblasts are responsible for bone reabsorption and bone formation. It has been suggested that bone contains mechanoreceptors which regulate bone at a local level. Mullender et al., (1994) developed a bone adaptation simulation model in which osteocytes act as sensors by appraising a mechanical signal. Each sensor then produces a stimulus for bone mass regulation which diminishes exponentially with distance from the sensor's location. Unlike the previous models, in which each element is assumed to have one sensor cell which regulates bone mass in that element (uniform density in an element), which has produced discontinuous structures (alternating checkerboard pattern) and were mesh dependent (Weinans et al., 1992), this model which separates the sensor density and range of action from the element mesh, produces results that are more physiologically and mechanically consistent with the continuum assumption. The predicted trabecular morphology in this model is dependent on the actual relationship between local load, sensor density and range of influence.

Fyhrie and Schaffler (1995), developed a bone remodeling theory that assumes for a given constant strain E there will exist a steady-state or homeostatic relationship between density and the mechanical variable as given below:

$$\rho_a = M(E)$$

where the exact form of M is to be determine.

The remodeling equation based on the 'error' term ρ_a - M(E) is

$$(\partial\rho_a/\partial t) = - B\{\rho_a - M(E)\} \text{ or } (\partial\rho_a/\partial t) + B\rho_a = BM(E)$$

where B is an unknown constant.

They further stated that:

$$\rho_a(t) = Ce^{-Bt} + Be^{-Bt}\int e^{Bt}M(E)dt$$

where, C is an unknown constant of integration.

This remodeling equation differs from the others in the fact that there is no constant goal state. Due to the fact that the time scales for the rates of change of the strain E and of the change in apparent density ρ_a are completely different the function M must include some type of time averaging of the strain. M(E) is defined as the homeostatic (or steady-state) value of apparent density that the bone would attain under a constant strain. This remodeling equation has been shown to be stable for the cases which are known to be spatially unstable for other formulations. The fundamental character of this remodeling equation is also exponential which is consistent with the experimental observations of bone density changes that occur during disuse, after hip replacement surgery, during growth and during aging.

Pritchett (1995) reported on the use of dual energy xray absorptionmetry scans to determine the relative bone loss in the proximal femur for 50 stems of 5 different types. The bone mineral density in the neck medial of the hip receiving the prosthesis was compared to the hip without the prosthesis. A data summary is presented in Table 1.2.

Table 1.2 Bone Loss After Hip Replacement

Number of Patients	Prosthesis	Collar Remarks	Interface	Measure Loss of Bone Density Compared With Opposite Side (%)	Standard Deviation
15	Physiological Stress Loading	Large horizontal collar	Proximal porous coating	8	14
13	Conical Collar (C-2)	Large collar perpendicular to the resultant forces	Cementless	14	19
6	Anatomic Medullary Locking	Collarless	Cementless	34	15
6	Harris Precoat	Collarless	Cemented	43	13
10	Mueller	Collarless	Cemented	57	13

As seen from the above table, the percent of loss of bone density associated with total hip arthroplasty can be quite significant (> then 50%) and plays a major role in the likelihood of long term survival of the prosthesis joint.

The patients with the Physiologic Stress Loading stem had the smallest average bone loss, 8%. Five of the 15 patients with the Physiologic Stress Loading stem had a gain of 5 to 20 %. Eighth of the 15 have a loss of 5 to 20%. The collar of the stem in the remaining two was not in contact with the medial femoral neck. These two patients had a loss of 30%.

The patients with the Mueller straight stem prosthesis shown the greatest average bone loss, 57%. All 10 patients with a Mueller straight stem prosthesis showed a loss of bone mineral density (range, 42% - 85%).

Rubin and Mc Leod's (1994) experiments on the turkey ulna showed that brief exposure to extremely low-amplitude mechanical strains can enhance the biologic fixation of cementless implants. The degree of ingrowth is dependent on the frequency of the

applied strain. These low-magnitude (< 500 με), frequency-specific (15 - 30 Hz) strains are potentially osteogenic and since they are far below those strain levels that jeopardize the structural attributes of bone, these mechanical signals are an attractive alternative for the promotion of bone ingrowth into non cemented prostheses. This method allows one to harness bone tissue's capacity to adapt to biophysical stimuli which reduces the burden of inducing bone ingrowth solely through the design attributes of the component or the bioreactivity of its surface.

The resulting stress levels that occur with the implantation of a prosthesis into a femur and the resulting bone adaptation that occurs plays a significant role in the survival of the prosthesis joint. The finite element method of analysis combined with the Computed Tomography Data Analysis Program developed in this study allows one to obtain an estimate of the resulting stress levels in the actual femur in which the prosthesis will be implanted.

1.10 Modes of Failure

As stated previously, the goal of the finite element analysis of the femur with prosthesis is to estimated the resulting stress levels to predict the likelihood of failure. In order to be able to predict failure of the structure one must first understand the modes of failure that can occur. This section discusses the common modes of failure for prosthesis hips.

A hip prosthesis needs to be resistance to processes such as fatigue, corrosion-fatigue, stress-corrosion, wear, cracking, etc. The following are the most common causes of femoral prosthesis revision: loosening of component (due to bone reabsorption,

micromotions at the interfaces and/or interface debonding), pain, fracture of femur, inflections, component fracture, and excessive wear. Femoral component loosening is the most common mode of failure in total hip arthroplasty (Havelin et al., 1993). Patients who have a porous-coated implant have a greater potential to be exposed to metal ions because of the large surface area exposed to bone. Wear, electrochemical corrosion, and fretting corrosion are mechanisms for the release of metallic ions.

Initial loss of fixation for a cemented prosthesis occurs primarily by debonding at the prosthesis-cement interface or crack initiation in the cement itself associated with voids and pores (Harrigan & Harris 1991).

The reabsorption of interface bone and the subsequent generation of fibrous tissue that is associated with aseptic loosening may be caused by one or more of the following factors; a bone-implant gap left when inserting the implant, by foreign body reactions against wear particles i.e. debris of polyethylene, polymethyl-metacrylate, or metal, by physiological bone remodeling resulting from stress shielding or local overloading. For cemented implants, it is also likely that the heat generation in acrylic cement during polymerization plays a role (Weinans et al., 1993, Munting and Verhelpen 1995).

As stated above, connective soft tissues at the interface between implant and bone can endanger the fixation of the implant. Weinans et al., (1993) described the problem as a biological reabsorption process of the bone adjacent to the implant. This reabsorption process can occur after many years of successful functioning. The interface bone is replaced by a soft tissue layer which can easily deform under compression and is not capable of transmitting shear and tensile stresses. Interface bone reabsorption and the

formation of a soft tissue layer depends on several factors including the relative motion between the bone and implant at the interface and the deformation of the interfacial material. At any location that the implant is not mechanically bonded to the surrounding bone it can move with respect to the bone (micromotion). The body reacting to this repetitive micromotion can form a soft tissue layer between the implant and bone, which can finally result in a clinically loose implant. Weinans et al., (1993) hypothesized that interface debonding is dependent on the interface stress and soft tissue interface interposition is dependent on relative interface motions. Interface disruption and fibrous tissue interposition are interrelated and can possibly enhance each other leading to a progressive debonding. Local debonding occurs when the interface stresses exceed the strength of the bond. At these locations relative motion can occur. It is believed that if these relative motions exceed a certain threshold level, bone will be absorbed and replaced by a soft fibrous tissue.

Mathematically, interface failure will occur if

$$[(\sigma - \sigma_a)/\sigma_o]^2 + (\tau/\tau_o)^2 > 1$$

where σ and τ are the actual normal and shear stresses

and σ_o, σ_a, and τ_o are constants (Weinans et al., 1993).

The finite element method allows one to investigate the mechanical modes of failure (e.g., stress shielding, fatigue stress cracking, excessive relative motions). Section 1.11 discusses finite element modeling methods reported in the literature and Section 1.13 summaries the Clinical results actually obtained.

1.11 Finite Element Analysis

A review of the hip stem prosthesis finite element models in the literature was performed. Table 1.3 list the interface modeling parameters, material properties, loads applied, model size, etc., for five of the models reviewed. The newer models have used CT data to obtain bone geometry and bone material properties. In all of the models reviewed the same relationship between density and Young's modulus was used for both cortical and cancellous bone. The following is a highlight of some of the modeling techniques used and the results reported.

Harrigan & Harris (1991) investigated the effect of partial cement-metal debonding. They reported that the cement interface around a partially debonded implant is at a substantial risk for developing radial cracks due to elevated hoop stresses. This also sharply increases the risk of pore-based crack initiation.

Keaveny & Bartel (1993a and b), described the effect of porous coating and collar support on early load transfer and relative motion for a cementless hip arthroplasty in the early post operative situation. They used thin (0.2 mm thick), nonlinear no-tension interface elements over the entire bone-prosthesis interface, with an upper bound on the coefficent of friction (Coulomb-friction) of 1.73 over coated surfaces, and zero friction over smooth surfaces. This was done to accentuate the frictional effects of the coating. The Coulomb-friction interface condition was also employed at the calcar-collar interface to model ideal initial calcar-collar contact. This allowed separation at this interface upon loading. It was noted that the use of an infinite friction interface results in a high shear stress with low normal compressive stress.

Table 1.3 Finite Element Hip Stem Prosthesis Models

	Harrigan & Harris	Keaveny & Bartel	Skinner et al.,	Huiskes & Van Rietbergen	Mann et al.,
	(1991)	(1993 a & b)	(1994)	(1995)	(1995)
Model Type	3-D	3-D	3-D	3-D	3-D
Nodes per Element	8 - node			8 - node	15/20 - node
Element Type	linear brick	solid quadratic isoparametric	linear isoparametric	isoparametric brick	linear, elastic quardric
No. of elements	7,019	1,424	12,971	2,106	1,128
Femur	Right	Left	Right	Right	Left
Prosthesis	HD-2 total hip prosthesis with collar	AML with & without collar	AML straight stem	Omniflex Number 9 implant	4 different stem configurations
Interface	Cement	Porous coating; full, 2/3 & none	Porous coating; 5/8 & 1/3	Porous coating, full proximal, stripes & none	Cement

Table 1.3 Finite Element Hip Stem Prosthesis Models
(continued)

Interface modeling parameters	Three cases of partial cement-metal debonding, using contact elements with a zero coefficient of friction to model a slipping cement-metal interface.	Calcar - collar support with ideal initial contact with separation allowed upon loading. No-tension interfaces over the entire bone-prosthesis interface. 1.73 coulomb friction over coated surfaces and zero friction over smooth surfaces.	100% porous coating fixation. 100% calcar-collar contact. Non-linear gap elements used in non porous coated areas.	Full bonding between bone and implant at the coated areas. Uncoated areas no bonding and no friction. Nonlinear interface elements used that allowed local slip and tensile separation to occur.	Coulomb friction interface with normal and shear-strain models used.
Material Properties					
Prosthesis E	200 GPa	200 GPa	220 GPa	110/210 GPa	110/210 GPa
Cortical Bone E	26 GPa	Based on QCT data	Based on CT data	Based on CT data	Based on CT data
Cancellous Bone E	1 GPa	Based on QCT data	Based on CT data	Based on CT data	Based on CT data
Cement	2.8 GPa				2.2 GPa
Poisson ratio	0.3	0.3	.342 for stem & .4 for bone	n/a	0.3
Maximum Load Case	Stair Climbing	Gait	3 x BW	Walking	Gait
Joint Load	1652 N	3409 N	3200 N	2132 N	3409 N
	461 N (L)	1492 N (L)	930 N (L)	n/a	1492 N (L)
	745 N (P)	915 N (P)	880 N (P)	n/a	915 N (P)
	1401 N (S)	2925 N (I)	2930 N (I)	n/a	2925 N (I)
Greater Trochanter	608 N	2592 N	2150 N	n/a	2592 N
	304 N (L)	1342 N (M)	790 N (M)	n/a	1342 N (M)
	306 N (A)	832 N (A)	770 N (A)	n/a	832 N (A)
	431 N (S)	2055 N (S)	1840 N (S)	n/a	2055 N (S)

Each bone element in Keaveny & Bartel's (1993a and b), model was assigned an unique Young's modulus based on the mean value of the Quantitative Computed Tomography (QCT) data sampled at 27 points within each element. This resulted in a bone moduli ranged of 0.1 MPa, used to represent a gap, to 20 GPa with an average Young's modulus of 17.1 GPa in the mid diaphysis and 332 MPa in the center of the femoral head. The model assumed the reamed shape of the bone was exactly the same as the shape of the prosthesis (thus, interference stresses were not modeled). Thin (in the radial direction) elements were used adjacent to the prosthesis to accurately describe the Young's modulus distribution of the material (either bone or a gap) immediately adjacent to the prosthesis.

This modeling assumption assumes that the prosthesis is well fitted in the bone so that the relative displacements do not fully close the "gaps" upon loading. The load is transferred from the prosthesis to the bone primarily through the bone, and that only negligible loads are transferred through the very low Young's modulus material which represents a gap. This method of using a very low Young's modulus material to represent a gap eliminated the need to model gaps explicitly with geometrically non linear contact elements.

The finite element mesh was chosen based on convergence studies of ideally bonded interfaces. To minimize the errors associated with the model assumptions used and the mesh selected they compared all results for the bone-prosthesis analyses to a corresponding analysis of the bone without the prosthesis.

Keaveny & Bartel (1993a), reported for the early postoperative situation (no bone-ingrowth or fibrous tissue) minimal load transfer of the mediolateral, anteroposterior, and axial forces over the proximal 30 mm of the fully coated prosthesis with collar support with gradual load transfer all along the remainder of the prosthesis. The maximum load transfer occurred at the stem tip.

They found that the use of a full porous coating reduces the torsional and axial loads acting on the distal bone, and that load transfer through the collar substantially improves axial and torsional loading of the proximal bone. Collar support and porous coating can only be used to control the transfer of bending loads to the proximal bone, and even here the effect is marginal. These design variables did affect the manner by which the axial force and torsional moment were transferred to the bone more distally for the early postoperative situation. The amount of stress shield would change substantially if the stem size and the Young's modulus (stiffness) of the prosthesis was revised. The flexural stiffness of the implant should be used to control transfer of the bending moments, and the proximal geometry (a collar or strong tapers) and surface treatment should be used to control the transfer of the axial and torsional loads.

It was also noted that the load transfer patterns for this model would change substantially if a combination of sparse bone ingrowth and fibrous tissue formation was modeled.

Since there is substantial proximal remodeling with fully coated devices the potential advantage in improving immediate fixation and long-term fixation may well be offset by the consequences of distal bone ingrowth. The bone hypertrophy which occurs

at the stem tip is related to the large magnitude of the laterally directed force predicted at this site. Compressed stresses of up to 100 MPa were observed in this region.

Keaveny and Bartel (1993b) showed that a porous coating could be used to reduce early relative motion. Relative motion is usually highest at the stem tip. This relative motion at the lateral stem tip could lead to abrasion of the endosteal bone, which could lead to thigh pain or metal ion release. The use of a collar or porous coating did affect the lateral contact forces at the stem tip. It is possible that thigh pain can be reduced by reducing the contact stress at the stem tip. The reduction of the stem flexural stiffness or the use of a shorter stem or the formation of a fibrous tissue layer should accomplish this.

Even if initial collar support contact is obtained it may be lost in vivo if there is bone death at the resected surface due to interruption of the blood supply or if proximal stress shielding occurs. Keaveny and Bartel (1993b) reported that for the fully coated device with ideal initial collar contact, early relative motion was dominated by twisting due to the resultant torque about the hip joint. Subsidence increases substantially for the case without a collar. Distal twist was found to increase as the length of the uncoated portion of the stem increases.

In a concentric cylinder finite element model of a cementless hip stem, Keaveny and Bartel (1994), used a nonlinear interface element. A no-tension interface was modeled allowing debonding to occur if the normal strains were positive. Shear failure could occur in the model if the product of the shear strain and the shear modulus exceeded the shear strength as specified by Coulomb friction. They reported that

regardless of the precise initial fit, the stiffness of the stem, or the type or extent of surface treatment, the distal transfer of the bending load occurs only over a small portion of the bone-prosthesis interface. It was found to be concentrated within approximately one stem diameter of the lateral stem tip.

Skinner et al., (1994) using a 3-D finite element model demonstrated that the maximum principal stress and maximum shear stress calculated in the femur with prosthesis, at the time of implantation accurately predicts the bone density remodeling caused by the prosthesis. Skinner et al., (1994) used computed tomography scans, (thickness of 3.0 mm, pixel size 1.06 mm, 320 by 320 matrix) of a specific cadaveric femur (53 year old male) to generate the 3-D finite element model. The chromium alloy AML straight stem, porous coated type prosthesis (Depuy, Warsaw, IN) was modeled. Dual energy xray absorptiometry (a noninvasive method of bone mineral density measurement) scans were obtained in the anteroposterior plane on the operated proximal femoral region of the six male patients that had undergone total hip arthroplasty for osteoarthritis. The relationship of bone mineral density (DXA; g/cm^2) to stress (σ; Pa) at the time of implantation is given by the following linear equation

$$DXA = m\sigma + b$$

However, the terms of the equation (m, b) varied from patient to patient and also varied for the case with and without a prosthesis. The difference noted by Skinner et al., (1994) may result from differences in age, activity levels, genetic variation, preoperative bone density and placement of the prosthesis.

Mann et al., (1995) investigated four stem cross-sectional geometries, two stem Young's moduli and two loading conditions in a cemented prosthesis finite element model. All of which had only limited effects on the stress distributions in the cement. A single element thick (0.05 mm) stem-cement interface layer was incorporated into the model around the stem. An 3.0 mm constant-thickness cement interface was used. Cement elements extended distal to the stem tip in all models. CT scan data of a normal proximal left femur was used to obtain the outer geometry of the bone. A grayscale density-Young's modulus relationship was used to determine the Young's moduli for each bone element.

In the Coulomb friction interface model normal and shear-strain models were employed. In the normal direction a Young's modulus of 2,200 MPa in compression and zero in tension was used. In shear, a Coulomb friction model with a shear modulus of 1,100 MPa before interface slip was used. After the friction limit was reached, the model set the shear stress across the interface to the product of the coefficient of friction (0.3) and the normal compressive stress across the interface.

Three regions of high stress were evident in the proximal cement interface for the model with the frictional interface. There were two large region of debonding on the anterior and posterior surfaces of the stem, for that model. A region of debonding was evident on the anterior surface of the stem from the stem collar to the tip of the stem. On the posterior surface of the stem, a region of debonding also existed. It extended from the collar to within two stem diameters of the tip of the stem.

The use of a realistic Coulomb friction stem-cement interface resulted in the largest tensile stresses in the proximal cement interface increasing by 95% over the ideally bonded interface model. For the strenuous load case the cement stresses in the proximal femur (10.8 MPa) exceed the fatigue strength (8-10 MPa) of PMMA cement. Therefore, fatigue failure of the cement in the proximal third of the cement interface is a possibility under strenuous cyclic loads. Failure due to fatigue for less active patients would not be anticipated. They hypothesize that loosening of the cemented femoral stem could be initiated by failure of the cement interface in the proximal femur due to radially directed cracks in the cement interface. This in turn would result in a less constrained cemented femoral component allowing increased relative motion between the stem and cement, which would cause a redistribution of load transfer in the cemented hip system. Subsidence of the stem in the cement interface could then occur resulting in a loose prosthesis having a stem-cement gap in the lateral region of the proximal stem.

Weinans et al., (1994) used a 2-D finite element model with a side plate to determine cortical bone loss versus prosthesis fit and coating area. A non-site specific adaptive bone remodeling feedback loop based on strain energy per unit of bone mass, averaged over a particular loading history, was applied to the model. A titanium (Young's modulus 110 GPa) stem was used in all of the models. At the noncoated areas of the bone-prosthesis interface smooth contact was assumed without any friction, hence at these locations only compressive stresses can be transferred. This model predicted 54 percent and 38 percent bone loss in the proximal femur for the medial and lateral side, respectively, for the completely coated (titanium) implant. For a partial coated stem (1/3)

the model predicted 50 percent and 22 percent bone loss in the proximal femur for the medial and lateral side. A model with a proximal press fit and a overreamed distal end produced the least proximal bone loss, 18 percent and 13 percent for the medial and lateral side. Whereas, a distally press fit model with the proximal portion overreamed produced a 91 percent bone loss proximal/medially and a 48 percent bone loss proximal/laterally.

Huiskes and Van Rietbergen (1995), used a 3-dimensional finite element model of a proximal right femur containing 2106, 8-node isoparametric brick elements based on computed tomographic data (27, 4 mm slices). A simplify finite element model of an Osteonics Omniflex Number 9 implant with a 16 mm diameter distal dip was fitted in the femoral model. The maximal CT density value was set equal to an apparent density value of $\rho = 1.9$ g/cm^3. Linear interpolation was used to transform the CT numbers to apparent densities. The maximal density in an element in the model was normalized at 1.73 g/cm^3. The Carter and Hayes equation (1977) was used to convert from ρ to Young's Modulus. A value of 110 GPa was used for the Young's modulus of the titanium stem and 210 GPa was used for the cobalt chrome alloyed distal tip.

To represent the reamed medullary canal, the elements at the lateral proximal side of the stem and around its distal part were given a low apparent density of 0.01 g/cm^3. Full bonding between bone and implant was assumed at the coated regions. No bonding and no friction were assumed at the uncoated areas, including the distal tip. A 10-μm gap was interpositioned in these areas to represent a thin fibrous interface. Special nonlinear interface elements were used to allow local slipping and tensile separation to occur. The

fully coated model showed 47.5% to 59.3% bone loss in the proximal medial region. The proximal coated model showed 47.3% to 60.2% bone loss in this region.

Hollister et al. (1993), pointed out that the cellular processes controlling bone ingrowth are significantly influenced by the mechanical environment that exist at the bone-implant interface. As a result of surgery a fracture healing response occurs at the implant interface. Hollister et al. (1993), used a plane stress two-dimensional finite element model combining 14,698 four-node linear quadrilateral elements, to model an implant-bone porous coating interface, and compared their results to animal retrieval studies.

Hollister et al. (1993), reported that the amount of bone ingrowth may be related to the stiffness of the porous coating. It is believed that bone ingrowth and apposition occur in areas where it is best suited to support the implant under load. However, unlike cortical bone, trabeculae bone rarely contain haversian systems and the osteocytes within trabeculae must receive nutrition by diffusion. Hollister et al., (1993) concluded that (1) bone adaptation is not solely a global optimization process, both mechanical and nutritional demands are reflected in the final bone structure; (2) the porous coating stiffness itself may stress-shield initially ingrown tissue, and (3) implant shape significantly affects the bone adaptation process.

The two finite element models created in this study using the Computed Tomography Data Analysis Program used CT data files to obtain the femur 3-dimensional geometry and material properties. A titanium prosthesis with an ideally bonded cement joint was fitted into the femur based on the femur size and shape. Linearly elastic,

ANSYS element type 45 (3-dimensional, 8 node, homogeneous and isotropic, 3 degree of freedom elements allowing only translation about the X, Y and Z axis), were used for all of the elements in the model. There were 2,544 elements and 2,691 nodes in each model. The prosthesis was modeled using two elements in the radial direction per cross-section. The interface, cancellous bone and cortical bone were modeled with one element in the radial direction per cross-section.

The material properties used in the finite element models are listed in Table 3.4. The Young's modulus of the cortical bone elements varied as a function of density. The maximum cortical bone Young's modulus was 24,724 MPa and 27,194 MPa for Case 1 and Case 2, respectively. The minimum cortical bone Young's modulus was 3,556 MPa and 2,927 MPa for Case 1 and Case 2, respectively.

As stated above, the interface was modeled as an ideally bonded cement joint using linearly elastic elements to minimize the run time and to allow a direct comparison with the results of Chang 1994 for the same CT data files.

1.12 Norway National Resister for Total Hip Replacement

Havelin et al., (1993) reported on 17,444 total hip replacements. This was the largest single source of hip replacement data I found in the literature and it proved to be a valuable source of general information on total hip replacements and is summaries below.

A national register for total hip replacements was established in Norway on September 15, 1987. Havelin et al., (1993) reported on the first 17,444 total hip replacements recorded (September 1987 through December 1990); 2,350 of these were

revisions (13.5 percent). Sixty nine percent of the patients were women. Table 1.4 list the age of the total hip replacement patients. The median age was 70 (12-97) years for primary operations and 71 (18-93) years for revisions. The revision rate for men was 17.4 percent (801/4607) and 14.8 percent (1549/10487) for women. Table 1.5 list the reasons for the primary operations. Primary arthritis was the diagnosis in 68 percent of the primary operations. Ninety percent of the revised prostheses had been operated into the patients before the period of registration. Table 1.6 list the reasons that the revision operations were required. The Christiansen prosthesis was the most common of the revised prostheses. It accounted for twenty three percent of the revisions. The total number of Christiansen prosthesis implanted was not available so the actual revision rate of this prosthesis was not reported. Loosening of the acetabular component was the reason for revision in 56 percent of the revisions. Loosening of the femoral component was the reason for revision in 64 percent of the revisions. The percentage for loosening of one or both components was 87 percent. Pain was listed as the indication for revisions in 11 percent, deep infection in 4 percent, dislocation in 4 percent, and fracture of femur in 4 percent, also. Multiple causes are possible for each revision. The frequency of femoral fractures increased to two percent for the revisions operations from 0.2 percent for primary operations. A fissure in proximal femur or fracture of the major trochanter occurred in 3 percent of the operations when an uncemented femoral prosthesis was used in the primary operations, and 0.7 percent when cemented femoral components were used. These complications occurred in 3 percent of the revision operations regardless of use or non-use of a cemented prosthesis.

The use of antibiotic prophylaxis increased from 84 percent in 1987 to 95 percent in 1990. It was used in 90 percent of the primary operations, and in 95 percent of revisions. The median operative time increased from 95 (30 - 430) minutes for primary operations to 135 (25 - 390) minutes for revisions. Operations using cemented prostheses and operations with trochanteric osteotomy required some 10 - 20 minutes more than those without cement or osteotomy. A lateral surgical approach was used in 61 percent, and a posterolateral approach was used in the remaining 29 percent. A trochanteric osteotomy was required in 24 percent of the operations. In 53 percent of the primary and 84 percent of revision cases using uncemented prostheses, some kind of bone transplant (not specified) occurred. A bone transport occurred in only 7 percent of the patients receiving a cemented prosthesis.

In Norway during this time, 12 different types of cements were applied. In 45 percent of the primary operations with a cemented prostheses a cement with antibiotics was used. The use of cement with antibiotics was 96 percent for revision operations with cemented prosthesis.

A very large number of different components and sizes were used, in fact, there was a total of 422 different designs and sizes of acetabular implants, and 398 different femoral implants used. Some surgeons used prosthesis designed for uncemented use, with cement. Uncemented acetabular implants were used in 17 percent of the primary operations. Uncemented femoral implants were used in 12 percent of the primary operations. In revision operations an of uncemented acetabular implants used was 21 percent of the time, and an uncemented femoral implants was used 17 percent of the time.

Table 1.4 Age of Total Hip Replacement Patients vs Number of Operations (Norwegian Arthroplasty Register 9/87 - 12/90)

Age	Revisions	Primary
<20	2	15
20-29	13	62
30-39	40	191
40-49	101	541
50-59	184	1543
60-69	675	4866
70-79	1012	6500
>80	322	1374
Total	2349	15092

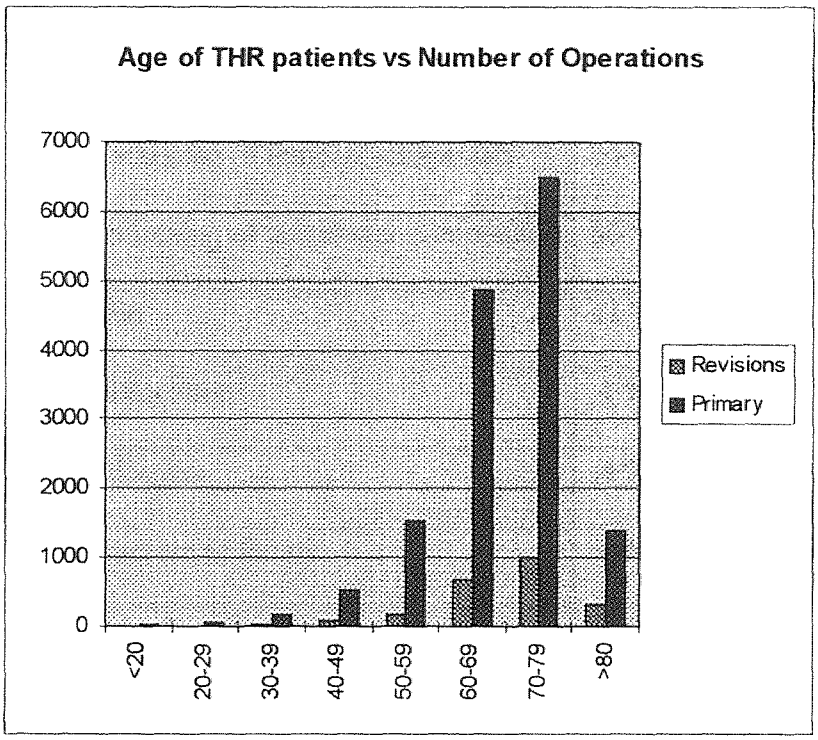

Figure 1.1: Age of Total Hip Replacement Patients vs Number of Operations (Norwegian Arthroplasty Register 9/87 - 12/90)

Table 1.5 Diagnoses at primary operations
(Norwegian Arthroplasty Register 9/87 - 12/90)

Primary arthritis	68 %
Rheumatoid arthritis	4 %
Sequelae after hip fracture	13 %
Sequelae after dysplasia	8 %
Dysplasia with dislocation	2 %
Other pediatric hip disease	1 %
Ankylosing spondylitis	0.4 %
Other	2 %

Table 1.6 Diagnoses at revision operations
(Norwegian Arthroplasty Register 9/87 - 12/90)

Loosening of femoral component	64 %
Loosening of acetabular component	56 %
Pain	11 %
Dislocation	4 %
Infection	4 %
Fracture of femur	4 %
Other	5 %

The Charnley cemented acetabular was used in 59 percent of the operations and the Charnley cemented femoral prostheses was used in 57 percent of the operatives. The use of a combination of a cemented and an uncemented component in the same hip was

rather common. Twenty-five percent of the uncemented acetabular prostheses were used with a cemented femoral prosthesis.

Because of the fact that loosening of the femoral component was the reason for revision in 64 percent of the revisions and so many different femoral implants (398) were used it appears that a better method is required to design and analysis hip prostheses. The use of the Computed Tomography Data Analysis Program combined with a finite element analysis program can be used to estimate the stress patterns induced in the actual femur in which the implant is to be install and an alternate implant can be chosen and analyzed if required prior to surgery. This tool also allows for the investigation of new prosthesis shapes and materials to be evaluated pre-clinically.

1.13 Clinical Results

One of the fundamental goals of a finite element model is to represent the real world. Therefore one must study the clinical results of total hip arthroplasty to determine if there is a correlation between the failure mode (or lack thereof) predicted by the finite element model and the actual results obtained.

To better understand the long term outcome of total hip arthroplasties a review of the hip stem prosthesis clinical results reported recently in the literature was performed. Table 1.7 list the type of prosthesis used, the prosthesis bone interface, the years during which the surgeries were performed, the number of prosthesis in the study, the male/female ratio, the mean age of the patient at time of surgery, the principal diagnosis,

Table 1.7 Clinical Results

	Dall et al., (1993)	Raut et al., (1995)	Berry et al., (1995)	Estok & Harris (1994)	Katz et al., (1995)	Engh et. al., (1994)
Hip Prosthesis	Charnley low-friction arthroplasties	Charnley low-friction arthroplasties (DePuy)	Six porous coated femoral designs	HD-2 & calcar replacement implant (Howmedica)	Iowa (Zimmer); Charnley (Zimmer); and Richards	Anatomic Medullary Locking (Depuy)
Interface	Cement	Cement	Porous coating	Cement	Cement	Porous coating
Operating Years	1970-1985	1974-1990	1985-1989	1976-1980	1977-1983	1977-1981
Number of prosthesis	811	125	375	38	79	166
Male/Female ratio	2/3	72.8%	59.7%	61.1%	46.6%	n/a
Mean Age	60	67	60	53	64	n/a
Principal Diagnosis	Arthrosis	Fractured Stem	Aseptic loosening	Aseptic loosening	Aseptic loosening	Osteoarthritis
Percentage	72	100	80	100	68	n/a
% of primary procedures	93	0	0	0	0	100
% of revision procedures	0	100	100	100	100	0
Survivorship analysis	87% @ 10 - 12 years	86% @ 8 years	58% @ 8 years	79% @ 11.7 years	74% @ 10 years	89% @ 8.8 years
Stem Revision Percentage	7%	10%	17%	11%	10%	3%
No pain	n/a	67.2%	n/a	58%	45%	n/a
Mid pain	n/a	22.4%	n/a	26%	25%	n/a
Significant discomfort	n/a	10.4%	23%	16%	30%	n/a

Table 1.7 Clinical Results
(continued)

Engh et. al., (1994)	Xenos et. al., (1995)	Tonino et. al., (1995)	Rossi et. al., (1995)	McPherson et. al., (1995)	McPherson et. al., (1995)
Anatomic Medullary Locking (Depuy)	Porous Coated Anatomic (Howmedica)	ABG (Howmedica)	ABG (Howmedica)	Anatomic Porous Replacement-I (Intermedics)	Anatomic Porous Replacement-I (Intermedics)
Porous coating	Porous coating	Hydroxyapatite	Hydroxyapatite	Porous coating	Hydroxyapatite on porous coating
1982-1984	1983-1986	1990-1991	1989-1991	n/a	n/a
227	100	222	100	42	42
n/a	68.1%	57.4%	34.0%	57.1%	57.1%
n/a	58	63	63	56.5	55
Osteoarthritis	Osteoarthritis	Osteoarthritis	Osteoarthritis	n/a	n/a
n/a	62	75	64	n/a	n/a
100	100	100	100	100	100
0	0	0	0	0	0
98% @ 8.4 years	87% @ 7 years	100% @ 2 years	100% @ 2 years	95% @ 3 years	95% @ 3 years
0.4%	2%	0%	0%	0%	2%
n/a	n/a	87.2%	96%	91%	85%
n/a	n/a	12.3%	4%	7%	10%
n/a	n/a	0.5%	0%	2%	5%

percentage of patients having that diagnosis, percentage of primary operations in the study, percentage of revision operations in the study, survivorship estimates, actual stem revision percentage and relative levels of post operative pain for the studies reviewed. The following is a highlight of studies reviewed.

Dall et al., (1993) reported on the survivorship of 811 cemented Charnley low-friction arthroplasties performed between 1970 and 1985. The principal diagnosis was arthritis. Ninety-three percent of the operations were primary procedures, the other seven percent were conversions for failed previous surgery other than total hip replacements. A trochanteric osteotomy was required in the majority of cases. There was an 87 percent probability of survival (Kaplan-Meier survivorship analysis) at 10-12 years for the total hip arthroplasty. Revision of 1 or both components was required in 68 of 811 hips (8 percent), all but 2 within 10 years, see Table 1.8. The authors had a minimum 3-year follow-up on 630 of the remaining 743 unrevised hips. There was evident of radiographic loosening, in 38 of the 630 hips, which is an indicator of impending failure. Twenty-two of the 38 hips with radiographic loosening had good/excellent clinical results, and the other 16 had fair/poor clinical results. Dall et al., (1993) found that certain parameters gave a higher incidence of cases requiring revision surgery, notably male, protrusio, osteonecrosis, medial cup position, and valgus stem position.

It was noted that fewer of the cemented sockets required revisions than the cemented stems and that this is at variance with current perceptions of using a cementless socket and cemented stem.

Table 1.8 Charnley Hip Failures

Cause of Failures	
Sepsis	12
Recurrent Dislocation	3
Loose Sockets	6
Loose Stems	20
Both Components Loose	12
Stem Fracture	15
Total	68

Raut et al., (1995) reported on the use of cemented Charnley revision arthroplasty for fractured stem in 125 patients between January 1974 and December 1990, each patient only having one hip operated on. The fractured stems were made of annealed stainless steel and the proximal fragment of the stem was always loose. None of these authors experienced a fractured stem which the newer design of Charnley prostheses introduced in the mid-1980s. Newer cement mixing techniques such as centrifugation or vacuum mixing of the cement were not performed at the time of these revision arthroplasty. Eighteen hip stems (14.4%) showed radiographic stem loosening. Thirteen hips (10.4%) required further re-revision; seven (5.6%) of these were due to aseptic stem loosening. There were five (4%) additional stem fractures. These stems were also annealed stainless steel stems. The thirteenth one (0.8%) needed a revision because of a loose socket which caused recurrent dislocation. The stem on this hip was well fixed. The authors noted that the "incidence of failure was significantly increased by preoperative endosteal bone loss; need for lateral cortical window for extraction of distal

fragment of the fractured stem; not placing the stem in neutral; and unsophisticated surgical technique, i.e., not using intramedullary femoral cement block and not excavating the lesser trochanter resulting in poor quality femoral cementing".

Berry et al., (1995) reported on the results of proximally porous-coated femoral components used in three hundred seventy-five revision total hip arthroplasty in 356 patients, performed between 1985 to 1989, using six prosthesis designs. More severe preoperative bone loss correlated with poorer survivorship, free of aseptic loosening of the prosthetic and subsidence of ≥ 5 mm. Intraoperative proximal femoral fractures were common (26%). The survivorship free of revision for aseptic failure was 58% at 8 years. The authors caution that the damaged, weaken bone that is often present in the proximal femur, does not provide the required proximal bone environment, for prosthesis that rely on the proximal femoral bone for fixation.

Estok and Harris (1994) reported on the results of cemented femoral revision surgery using second-generation techniques. This includes the use of a medullary plug and cement gun for cement delivery which was incorporated approximately in 1976. Since January, 1978 the cementing technique also employed a Water Pik (Daval, Cranston, Rhode Island) to clean the bone interstices of blood and marrow. Cement pressurization through the use of a cement compactor was incorporated November, 1978. From a group of 38 hips in 36 patients receiving a cemented femoral component during revision surgery, cemented using the above techniques, a survivorship of 90% and a 79% incidence of well-fixed femoral components was observed at an average 11.7 years follow-up. Newer cementing techniques now, also use cement porosity reduction

techniques, e.g., vacuum mixing or centrifugation and a layer of methylmethacrylate precoated on the metal. These revision results compare favorably with the results previously obtained for primary cemented prosthesis.

Katz et al., (1995) reported on 42 revision total hip arthroplasties performed from 1977 to 1983, using improved cementing techniques (distal intramedullary cement plug, cement gun delivery system and pressurized) that had a minimum of 10 year follow-up radiographs. Simplex P cement (Howmedica, Rutherford, NJ) with two grams of a cephalosporin antibiotic was used. The incidence of femoral re-revision for aseptic loosening for the study was 9.5% (4/42). The incidence of radiographic femoral failure which was defined as a revision or definite or probable loosening was 26.1% (11/42). These results were reported as being an improvement compared to the failure rates with the older cementing techniques. The author recommended the incorporation of impaction bone grafting, antibiotics in the cement as well as the new cementing techniques.

Engh et al., (1994) reported on the clinical results obtained using the AML hip prosthesis. There was a 10.8% (18 0f 166) failure rate (5 revisions and 13 stems having radiographic evidence of instability) at a radiographic follow-up period of 106 months, for a single size fully porous coated AML prosthesis implanted prior to 1982. For the variable size AML stems used between 1982 and 1984, with a mean radiographic follow-up period of 101 months there was a 1.8% (4 of 227) failure rate (1 revision and 3 radiographicly graded unstable). Engh et al., (1994) uses the proximal loss of periprosthetic bone loss density (5% - 52%) caused by the stress-shielding characteristic of this prosthesis as a sign that the femoral prosthesis was fixed by bone ingrowth. Bone

ingrowth was observed on 57% of the porous-surface area of the femoral components. The authors commented that the extent of bone reabsorption which occurs is related more to the preoperative condition of the femur bone than to the in vivo duration. They also felt that the articulating surfaces were the weak link in the design rather the porous coated implant.

Periprosthetic bone loss (osteolysis), along the femoral components, was observed by Xenos et al., (1995) in 13 of 100 uncemented total hip arthroplastices performed using a Porous Coated Anatomic (Howmedica, Rutherford, NJ) cobalt-chrome hip prostheses. This femoral prosthesis is porous coated in the proximal third. The 100 hips had a 7 year minimum follow-up. It was noted that the average age at surgery was 10 years younger for the bone loss group than for the non-bone loss group. Osteolysis was defined as any local area of endosteal bone loss >5 mm that appeared adjacent to the femoral component. Eighteen hips showed scalloping of >5 mm in the proximal medial femur (calcar area) due to the stress shielding effects of the prosthesis. Two revisions of the femoral components were done in this series.

Tonino et al., (1995) reported on the results of 222 patients (hips) that received a titanium alloy hip prosthesis, the ABG total hip arthroplasty (Anatomique Benoist Giraud, Howmedica International, Staines, England), with a 60 micron hydroxyapatite coating on the proximal third, from January, 1990 to April, 1991. The stem had a macro relief scaled surface which was designed to transform shear forces on the anterior, posterior, and medial surfaces into compression forces. The proximal portion of the stem was pressed fitted and the distal femoral was over-reamed to promote proximal femoral

stress transfer. The average follow-up was two years. Five trochanteric fractures occurred during hip surgery, and one subtrochanteric fracture occurred on mobilization. None of the fractures required revision. All six fractures headed with bed rest. Minor distal stem migration (<5 mm) was observed in 6 patients. Cortical bone hypertrophy in the transition zone of coated to uncoated was observed in 4 to 6% of the patients (bone densification were observed in 54%). Slight bone reabsorption of the calcar was observed in 21.8%. In 3.6% of the patients there was some form of thigh pain after 2 years. There were no cases of loosening or suspected radiographic loosening. Distal over-reaming was noted as being of paramount importance to shift the load transfer proximally.

Roosi et al., (1995) reported on 100 consecutive patients who received the ABG total hip arthroplasty (Anatomique Benoist Giraud, Howmedica International, Staines, England), during September, 1989 to January, 1991. The titanium femoral stem of this implant is hydroxyapatite coated on the metaphyseal portion. Rossi et al., (1995) points out that immediate stability is essential to achieve long-term biologic integration. Increased cortical bone density and thickness at the junction between the proximal coated portion and the rest of the stem was noted on 20 patients and cancellous bone thickening was evident in another 10. Thigh pain was not reported, even for the 25 patients that had radiolucent lines present (indicative of micromotion) around the distal portions of the stem.

McPherson et al., (1995) reported the results of a matched pair study of 2 groups of uncemented total hip replacements. A titanium alloy Anatomic Porous Replacement-I

primary hip (Intermedics Orthopaedics, Austin, TX) was the prosthesis used in all patients. One group received stems with hydroxyapatite on the proximal femoral patched porous surfaces. The other group received stems without hydroxyapatite on their proximal femoral patched porous surfaces. The proximally patched porous coating was on the anterior, posterior, and medial surfaces. The stem had a porous-coated collar and an anatomic posterior bow. The patients were matched one to one in terms of gender, age (within 5 years), weight (within 25 pounds), bone type, activity level and diagnosis. At a 3-year follow-up the mechanical failure rate was only %5 in each group. However, the incidence of osteolysis, 17% (7 stems in each group) was 10 times higher than in a circumferentially coated Anatomic Porous Replacement-I stem. Patients with hydroxyapatite-coated femoral stems exhibited proximal cancellous hypertrophy at a quicker rate than those without the hydroxyapatite-coating. The authors felt that there was no clinical advantage to the use of hydroxyapatite over the porous coatings. Because of the high incidence of osteolysis, the use of a patched porous coating with or without hydroxyapatite was discouraged. The femoral head in the study was made of titanium alloy. Since titanium alloy burnishes and abrades easily, it should not be used as an articulating surface. It was felt that the used of a titanium alloy femoral head was a contributing factor in the high rate of osteolysis observed.

Kohles et al., (1994) performed unilateral total hip arthroplasty in 15 adult mixed-breed dogs. A collared femoral prosthesis was implanted into nine of the 15. The other six received a collarless femoral prosthesis. A titanium alloy implant (Techmedica Inc., Camarillo, CA) with recessed titanium mesh inserts on the proximal portion of the stem

(cranial and caudal faces) was used. Postoperatively, the 15 dogs were allowed free weight bearing and exercise. The dogs were euthanized four months after the total hip arthroplasty, and transverse sections at the midstem and 1 cm distal to stem locations were obtained. Ultrasonic and densitometric measurements were performed at eight locations circumferentially on each section. The section of bone directly under the collar was not tested and therefore, any changes that may have occurred in this region was not reported. The results obtained showed no difference in 4 month postoperative bone elasticity or bone density between collared and collarless designs. However, there was decreased values in bone mineral densities and Young's modulus when compared to the control values. The degradations were noted to be generally consistent around the perimeter for both the proximal and distal cross-section. Since the distal portion should not be stressed shielded it is believed that reduced limb loading occurred.

As stated previously , one must study the clinical results of total hip arthroplasty to determine if there is a correlation between the failure mode (or lack thereof) predicted by the finite element model and the actual results obtained. A lack of correlation would indicate invalid modeling assumptions or that another phenomena plays the major role and that a different type of analysis and/or correction action may be required (e.g., if infection due to non-biocompatibility of the interface material was the major cause of revision operations, the stress pattern in the femur/prosthesis would not be of paramount importance). However, since the clinical results show that femoral component loosening is the major cause of hip stem revisions a detail finite element analysis should provide useful information as to cause and can be used to develop correction actions (e.g. new prosthesis designs).

CHAPTER 2

OBJECTIVES

There were two objectives in this study. The first objective was to develop a Computed Tomography Data Analysis Program which takes CT data of a proximal femur as an input, and outputs a "3-D" finite element model with prosthesis. The main advantage of this tool is that an estimate of the stress pattern induced in the actual femur in which the implant is to be installed can be assessed prior to surgery, and an alternate implant can be chosen and analyzed if required. The second objective was to run the resulting finite element models for two cases and to compare the results, to the results obtained from the previous modeling process (Chang 1994). The differences between the two modeling processes are discussed in Chapter 3 and Chapter 4. The CT data is used to determine the geometry, density and Young's modulus of the cortical bone section of the finite element model. The CT data analysis program created utilizes two commonly used Windows software packages, Microsoft Excel and Math Soft Mathcad. The program performs the following tasks: (a) determines the area of interest in the CT data files for each cross-section; (b) plots the inner and outer cortical bone boundaries versus a range of CT numbers; (c) creates color plots of area of interest and black and white boundary plots for CT densities chosen by the user for each cross-section; (d) determines the center of each cross-section; (e) plots a 3-D image of the inner and outer cortical bone boundary for each cross-section (as scanned); (f) screens the model created for warped elements and adjust the cortical bone outer boundaries; (g) displays unadjusted and adjusted cortical bone boundaries; (h) determines the node locations for all elements in the finite

element model; (i) plots 2-D nodal boundaries for each cross-section; (j) plots 3-D cortical bone outer boundary, with tilt of bone axis to CT scanner axis removed; (k) determines the average CT number and density for each cortical bone element; and (l) creates a "3-D" finite element model file.

The CT data analysis program allows the user to vary the following parameters: (a) the CT number to be used for the cortical bone inner boundary for each cross-section; (b) the CT number to be used for the cortical bone outer boundary for each cross-section; (c) the angular spacing between elements in the finite element model; (d) the prosthesis size relative to the size of the femur receiving the prosthesis in the medial-lateral and anterior-posterior planes at three locations; (e) the number of prosthesis, interface, cancellous and cortical bone elements in the model; (f) interface thickness; (g) minimum cancellous bone thickness; (h) minimum cortical bone thickness; (i) constants of the linear equation that relate CT number to density; (j) prosthesis material and properties; (k) interface material and properties; (l) cancellous bone properties (note the cortical bone Young's modulus is determined based on the CT number); and (m) joint force and trochanter muscle force to apply.

The data obtained from solving the finite element model can be used to determine what prosthesis changes need to be incorporated to alter the stress pattern (i.e. to prevent proximal stress-shielding, to reduce the stress level in the bone cement, etc.) in the femur to decrease the likelihood of mechanical failure of the prosthesis. As stated previously, the main advantage of this tool is that an estimate of the stress pattern induced in the actual femur in which the implant is to be installed can be assessed prior to surgery, and an alternate implant can be chosen and analyzed if required.

CHAPTER 3

MATERIALS AND METHODS

3.1 Computed Tomography Data Analysis Program

A Computed Tomography Data Analysis Program to process computed tomography data files of a proximal femur into a three-dimensional finite element model file with prosthesis was developed. The computed tomography data analysis program created utilizes two commonly used Windows software packages, Microsoft Excel, it Visual Basic Modules, and Math Soft Mathcad. The material properties of the femur, density and Young's modulus, are determined from the computed tomography data. The program performs the following tasks; displays the CT images, determines the inner and outer cortical bone boundaries, creates the prosthesis, display 3-D images of the prosthesis and bone, corrects warped elements, generates nodes, generates elements, determines material properties, applies boundary conditions and creates a finite element input file for ANSYS (Swanson Analysis Systems Inc.). The program utilizes dynamic data exchange, custom menus and user input boxes to make the user interface as efficient as possible.

This method is useful in determining the resulting stress pattern that would be induced by a particular prosthesis, allowing one to optimize the prosthesis selection for a particular femur geometry and bone state of health. This method also allows the investigation of new prosthesis shapes and materials to be evaluated pre-clinically. One can also used this method to predict the expected failure mode and location, of a particular prosthesis.

The main advantage of this tool is that an estimate of the stress pattern induced in the actual femur in which the implant is to be installed, can be assessed prior to surgery and an alternate implant can be chosen and analyzed if required.

3.2 Scanned Femoral Bone Data

Computed tomography data was obtained for two patients scanned pre-operatively at the Radiology Department of Saint Barnabas Medical Center in Livingston, New Jersey. Case 1; An active, 30-year-old male patient had suffered osteoarthritis in the left femur and was treated by left total hip arthroplasty. The left femur was scanned from 20 mm below the femoral head to the knee. Case 2; An active, 36-year-old female patient had suffered osteoarthritis in the left femur and was treated by left total hip arthroplasty. The left femur was scanned from 10 mm below the femoral head to the mid shaft. Both femora were scanned by Siemens Scatter, Somatom DR. The above patient data was obtained from Chang (1994), page 61.

The pixel data (CT numbers) obtained from the scans represent pixel radiographic densities. The CT numbers are stored in binary CT data files as integers in the range of 0 to 4095, each integer requiring two bytes, each byte consists of 8 bits. The matrix size for each cross-sectional scan was 512 x 512 pixels. The spacing between pixels were 0.257x0.257 millimeters. The spacing between slices was 10 mm. Only the most proximal, seventeen slices (170 mm) for each case was used in this research.

The CT data files scanned at St. Barnabas Medical Center was stored on a 12 inch optical disc. This data was transferred to cassette by Siemens Company in Iselin, New Jersey. The data was then copied to the NJIT computer system. Chang (1994) developed a C language program that separates the CT data from the file header and a FORTRAN program combines with the NJIT HOOPS package to display color images. The user defines the area of interest in the CT image being displayed by entering the coordinate of the starting point (the upper left corner point of the area of interest), as well as, the width and length of the image to be stored. This method significantly reduces the size of the matrix which needs to be stored and processed. For Case 1, the matrix was reduced from 512x512 to 285x225 (24.5%) and to 270x210 (21.6%) for Case 2. This data was stored in ASCII text format (1 character per byte). The ASCII text data for the areas of interest in the seventeen slices of Case 1 and Case 2 occupied 5,523,328 bytes and 4,883,840 bytes, respectively.

3.3 Transfer of Computed Tomography Data

The ASCII text data files for Case 1 (**CT2BNUM.DAT.Z**) and Case 2 (**CT5NUM.DAT.Z**) stored in Dr. Linden's NJIT computer account were copied to the NJIT tmp directory and uncompressed. The uncompressed data files were copied onto a personal computer using binary Kermit modem transfer. Chin - Yang Huang a NJIT doctoral student supplied to me the names of the data files and the instructions for modem transferring of data. The uncompressed copies of the data files in the NJIT tmp

directory were deleted as is customary. On the personal computer the data files were copied to a different directory and renamed **CASE1.DAT** and **CASE2.DAT**.

3.4 Data Conversion back to Binary

A Visual Basic module (**CTCASE1F.XLS**) was created using Microsoft Excel 5.0a to separate the **CASE1.DAT** data file into seventeen different data files (one for each cross-section). The newly created files were created as binary random access files. A similar Visual Basic module (**CTCASE2F.XLS**) was written for the **CASE2.DAT** data file. Each of the Case 1 cross-sectional data files occupied 128,250 (285x225x2) bytes. Each of the Case 2 cross-sectional data files occupied 113,400 (270x210x2) bytes. The total required storage for Case 1 reduced from 5,523,328 to 2,180,250 bytes and for Case 2 from 4,883,840 to 1,927,800 bytes. This reconversion to binary format served three purposes; (1) it reduced the memory storage requirements, (2) by separating the files into cross-sectional files it allows complete files to be copied to floppy disks and (3) the program that was written to create the finite element input file was written to be able to work with the 512x512 CT cross-sectional binary data files with the header removed.

3.5 The Auto-Open Module

A module which runs automatically, when the computed tomography data analysis program (**CTPROG.XLS**) is opened, was created. This modules caused the following message to be displayed on the computer screen.

Computed Tomography Data Analysis Program

This program was created by Thomas Lavin as part of a NJIT Master's Thesis; Dec 95-April 96. The program reads in Femur CT data files and outputs an ANSYS (FEA) input File with prosthesis.

The program utilizes
Microsoft Excel 5.0a (and its Visual Basic Modules)
and MathSoft Mathcad 5.0.

Please open Mathcad 5.0 prior to running this program.

Please select the menu items contained in the above CT_Data menu, in sequential order to run this program.

This message informs the user that they must open Mathcad 5.0 prior to running the modules in this program. Several of the Excel modules access Mathcad programs using dynamic data exchange. In order for the Excel modules to be able to pass the data to the Mathcad programs, Mathcad must be open. The dynamic data exchange commands will then automatically open the required Mathcad program for that procedure.

In order to make the program easy to use a menu item called **CT_Data** was created and appears in the main menu bar of all the Excel sheets in this program. The sub-menus of the CT_Data menu access the nine modules created to process the raw CT data into an ANSYS Finite Element Input File. The program was design so that the user sequentially selects the nine sub-menu items. The names of the nine sub-menu items are as follows: (1) Create CB ASCII Files; (2) Boundaries vs. CT Number; (3) Minimum CB Density; (4) CB Color Plots; (5) Boundaries; (6) Prosthesis Size; (7) Nodes; (8) Average CT Number; and (9) FEA Input File where CB stands for cortical bone.

3.6 Create Cortical Bone ASCII Files

This module determines the area of interest in the CT data file and creates ASCII text files that can be read by Mathcad. All data exchanged between the user and program is handled using Excel Visual Basic Input Boxes. The user is requested to enter the following data file information: (a) the maximum data matrix row number; (b) the maximum data matrix column number; (c) the spacing between pixels rows; (d) the spacing between pixels columns; (e) the height spacing between cross-sections; (f) the total number of cross-sections; (g) the name of the Mathcad directory; (h) the minimum outer cortical bone CT number; and (I) the names of the CT cross-sectional data files.

Based on the matrix size the program determines a column and row pixel spacing to use to quickly scan the data file of each cross-section to determine the area of interest. This method differs from that method used by Chang (1994). Chang (1994) required the user to display the cross-section and then manually pick a coordinate on the screen using the mouse. The user would have to record the x and y coordinate value displayed and then select the opposite corner point. The user was then required to input the values of the coordinates for the first corner point, as well as, the different in length and width between the two corner points. This revised program determines the area of interest using the user supplied minimum cortical bone CT number without requiring the images to be displayed or further user input. Since every pixels value is not compared to the minimum cortical bone density the boundary determined is enlarged slightly to insure that it encompasses all pixels of interest. In order to allow relative size comparison and

geometrically orientation comparisons between the displays of the various cross-sections, a single boundary is determined which is used for all the cross-sections.

Once the boundary to use is determined, ASCII text files of the data contained in the area of interest of each cross-section are created. The Mathcad programs cannot read binary random access data files so ASCII text files are required.

Although the data files processed in this work were already significantly reduced from their original 512x512 matrix size, the program was written to handle any size binary data matrix with the header file already removed.

3.7 Boundaries vs. Computed Tomography Number

The next module in the sequence uses the ASCII text files of the area of interest created in the previous module, and a Mathcad program to plot the inner and outer cortical bone boundaries versus CT numbers ranging from 1200 to 1400 in steps of 40. The user is requested through an input box to enter whether the hip side receiving the prosthesis is the right or left hip. The Mathcad plots display M, P, L, and A for the median, posterior, lateral and anterior side, respectively. Since the medial and lateral call outs are reversed for a left and right hip the Excel program needs to know which Mathcad program (display format) to access. **CBRDATA.MCD** is accessed if the data files are for a right hip and **CBLDATA.MCD** is accessed for a left hip.

The program was designed to automatically plot out the cortical bone inner and outer boundaries versus CT numbers for all of the cross-sections, without requiring user input to issue print commands or next cross-section commands. However, on a personal

computer having only 8 M of RAM, "not enough memory" errors were encountered which resulted in some blank displays. This memory limitation forced the user to manually run one cross-section at a time using only the Mathcad program instead of being able to have this process fully automated through the dynamic data exchange commands of the visual basic module as intended. With the memory on the computer increased from 8 M of RAM to 40 M the program plotted out the displays automatically as intended. The minimum required amount of RAM required to accomplish this was not determined. The cortical bone boundaries versus CT number for cross-section 1 (most proximal cross-section) and cross-section 17 (most distal cross-section), of Case 1 are displayed in Figure 3.1 and Figure 3.2, respectively.

As seen from Figures 3.1 and 3.2 the boundaries of the proximal cross-sections are much more sensitivity to the choice of CT number that the distal cross-sections.

3.8 Minimum Cortical Bone Density

Using the plots obtained from the previous module the user is requested to enter the minimum inner and outer cortical bone CT numbers for each cross-section. The numbers entered are stored in Excel cells that are accessed by other modules in the program.

CT Number ≥ 1200

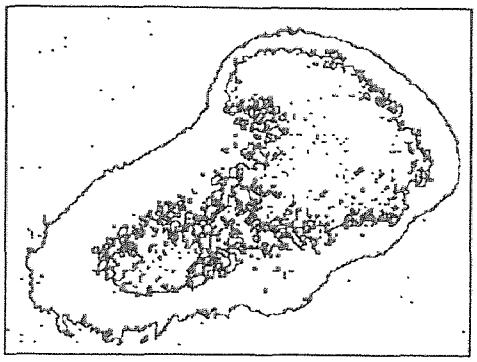

CTa

CT Number ≥ 1240

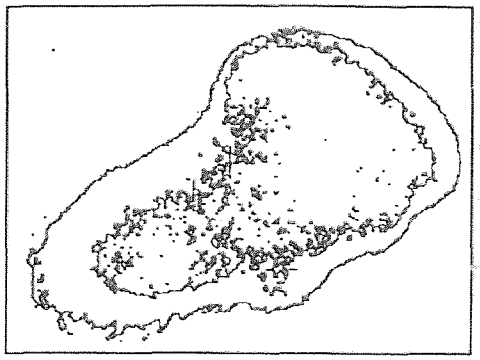

CTa

CT Number ≥ 1280

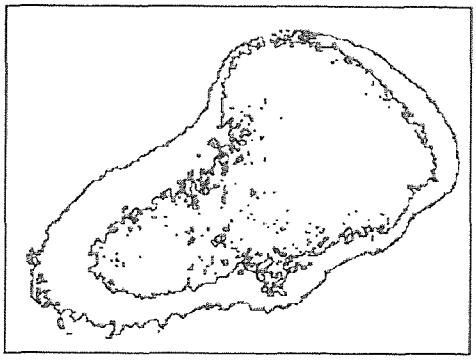

CTa

CT Number ≥ 1320

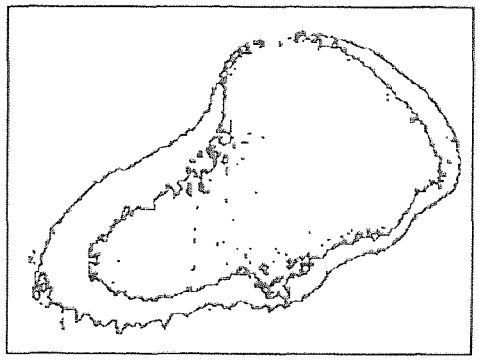

CTa

CT Number ≥ 1360

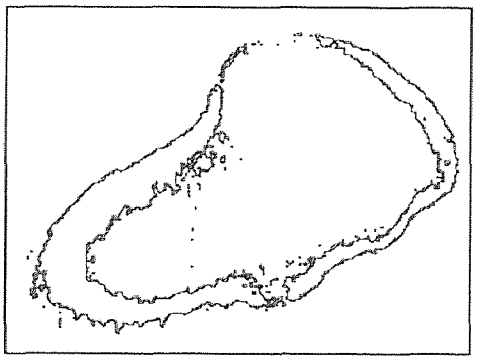

CTa

CT Number ≥ 1400

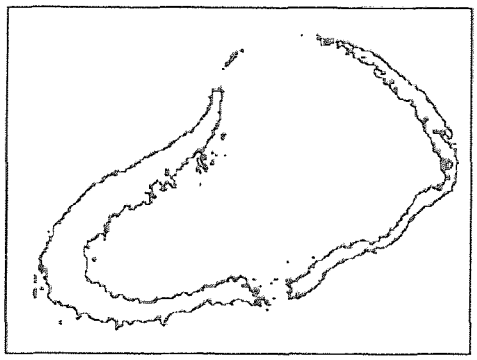

CTa

Figure 3.1 Case 1; Cross-section 1; Cortical Bone Inner and Outer Boundaries vs. CT Number

CT Number ≥ 1200

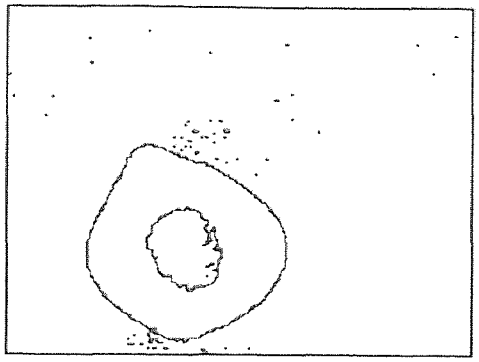

CTa

CT Number ≥ 1240

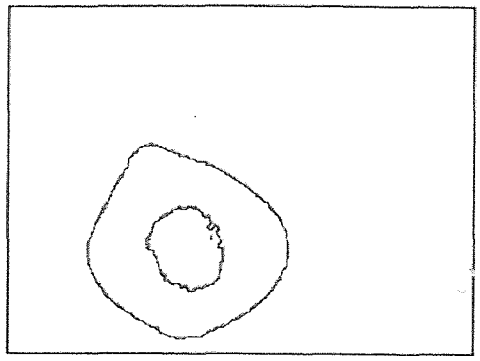

CTa

CT Number ≥ 1280

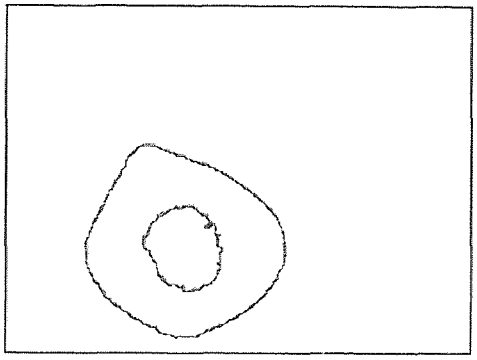

CTa

CT Number ≥ 1320

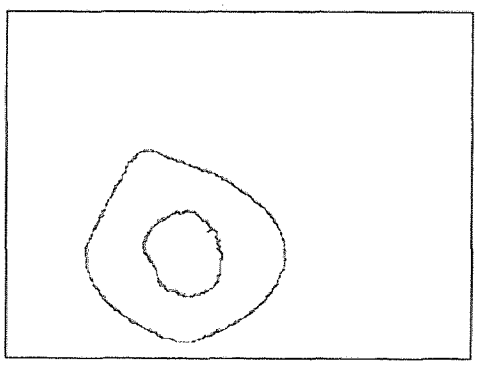

CTa

CT Number ≥ 1360

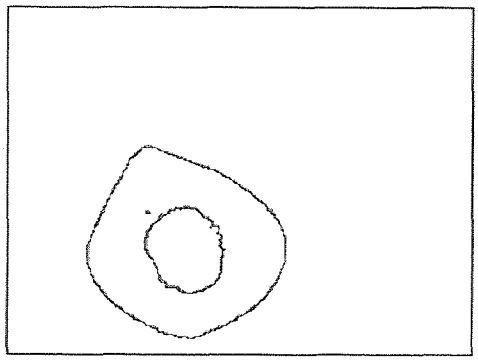

CTa

CT Number ≥ 1400

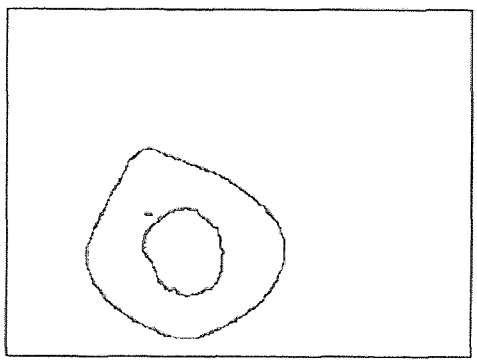

CTa

Figure 3.2 Case 1; Cross-section 17; Cortical Bone Inner and Outer Boundaries vs. CT Number

3.9 Cortical Bone Color Plots

This module creates color plots of the CT data using Mathcad, as well as, a black and white inner and outer boundary plot. The CT number entered in the previous module is used to determine what number to use for the boundary plot. If the prosthesis is for a right hip Mathcad program **CBRIGHT.MCD** will be executed. For a left hip **CBLEFT.MCD** will be executed. A legend displaying color vs. CT number is created for each cross-section. This program was also designed to automatically print out all of the plots for each cross-section without requiring additional user inputs. Due to memory limitations the user may need to run one cross-section at a time directly in the Mathcad program. Once again with the computer memory increased these plots also ran automatically as intended. Figure 3.3 and Figure 3.4 contains the black and white versions of the color plots for cross-section 1 and cross-section 17, of Case 1, respectively.

3.10 Boundaries

This module determines the x, y and z values of the inner and outer cortical boundaries. The user is required to enter the angular spacing angle desired between elements. Ninety divided by the angular spacing angle must be an integer to insure that nodes lie along the medial-lateral and anterior-posterior planes. If the user enters an angular spacing angle that results in ninety divided by that angle, not being an integer i.e. 20 degrees, the program revises the angular spacing angle so that the result will be an integer i.e. the 20 degree value would be revised to 18 degrees, and similarly if 24 degrees was entered it will be revised to 22.5 degrees.

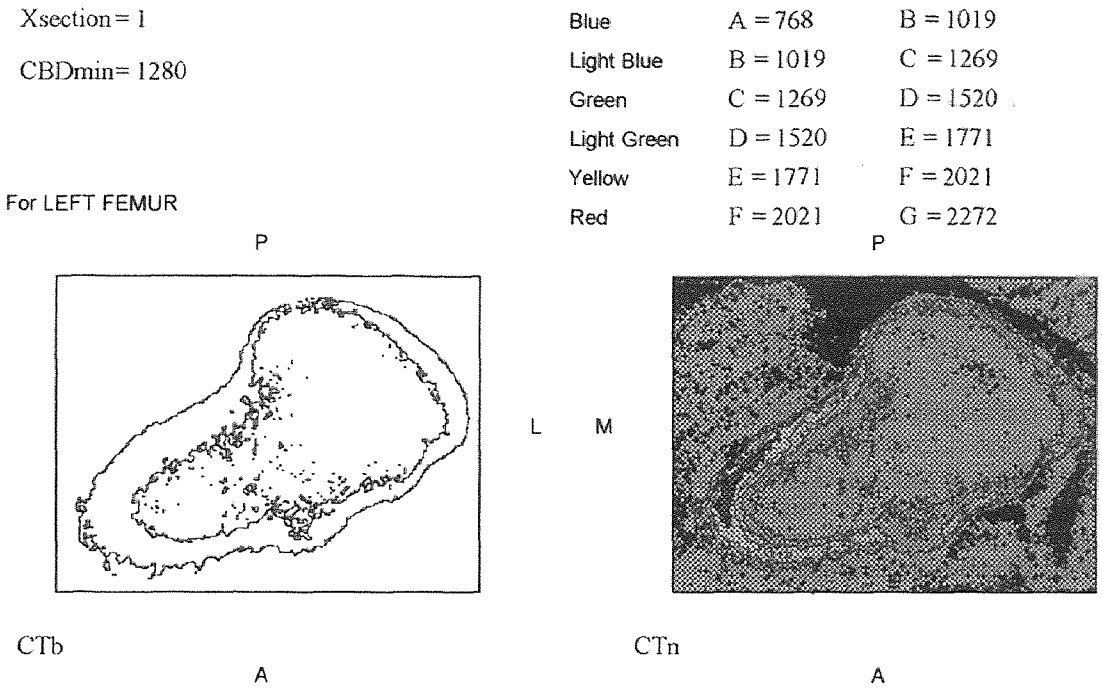

Figure 3.3 Case 1; Cross-section 1; Black and White versions of the Color Plots

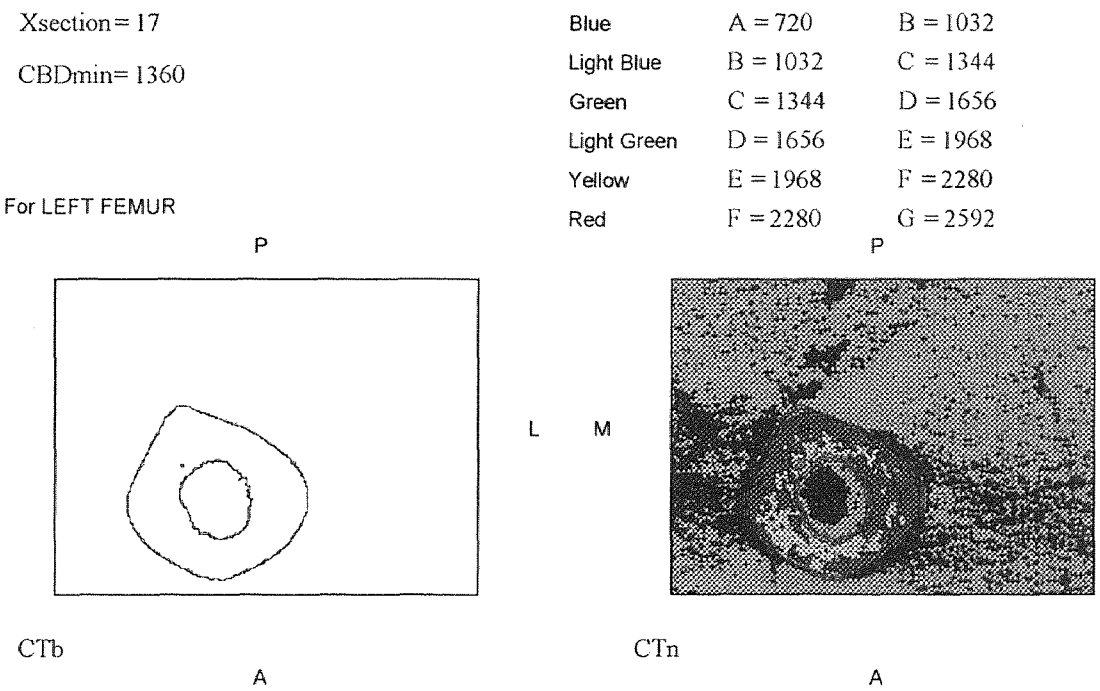

Figure 3.4 Case 1; Cross-section 17; Black and White versions of the Color Plots

Since the CT numbers that are used to determine the cortical bone boundaries may have been revised in a previous module, this modules re-determines the area of interest using the updated CT numbers.

An estimate of the center of the cortical bone is determined for each cross-section in the following manner, using the boundary determined for each individual cross-section a x and y starting point is determined which is at the center of the boundary for that particular cross-section. Since the proximal portion of the femur bone is not circular this point is only used as the starting point. From this point every pixel along a south-east line and along a north-west line is compared to the minimum cortical bone CT number for that cross-section, and the coordinates of the last pixel having a CT number less then the minimum CT number is recorded. The center of the two points, one found during the south-east search and the other found during the north-west search, is used as a starting point for a north-east and a south-west line on which every pixel is compared to the minimum cortical bone CT number for that cross-section. The center of the two points, one found during the north-east search and the other found during the south-west search is taken as the center of that cross-section.

However, since we wish to fit a prosthesis into the bone we need to revise the centers to be along a straight line from distal stem to mid stem, and then along a tapered line from mid stem to proximal stem. This is accomplished by performing two linear regression analysis. The first one uses the centers of the sixth through the seventeenth cross-section, with the seventeenth cross-section being the most distal cross-section. The second linear regression analysis uses the centers of the first, second, fifth and sixth cross-

section. Due to the irregular shape of the third and fourth cross-section their centers were not used in the linear regression analysis. The values from the first linear regression analysis are used to determine the center of the sixth through the seventeenth cross-section. The centers of the five most proximal cross-sections are determined using the values from the second linear regression analysis. The difference between the center determined by the first and second linear regression analysis is determined for the five most proximal cross-sections. These values are used to correctly position these cross-sections in three dimension space relative to one another. All node location calculations are performed from the center of each cross-section.

The node locations for the inner and outer boundaries of the cortical bone are found by performing a x and y sort, and then determining the one which results in a smaller radial length for the inner boundary and the one which results in a larger radial length for the outer boundary. Note that the smallest x and y values of the boundary are location in the upper left corner (see Figure 3.5). Similarly, the largest x and y values are located in the lower right corner i.e. in a 512x512 matrix, pixel 1,1 would corresponds to the upper left corner and pixel 512,512 would corresponds to the lower right corner. Also note, that all angles are given from the center of the inner cortical bone boundary.

At the cardinal headings, angle = 0 and angle = 180 degrees, only a x sort is required. Similarly at cardinal headings, angle = 90 and angle = 270 degrees, only a y sort is required. The x sort is performs as follows, for each angular spacing angle in a quadrant, x is varied from the x center point to either the highest x boundary (for quadrants I and IV) or the lowest x boundary (for quadrants II and III). Where quadrant

I is 0 to 90 degrees; quadrant II is 90 to 180 degrees, quadrant III is 180 to 270 degrees and quadrant IV is 270 to 360 degrees.

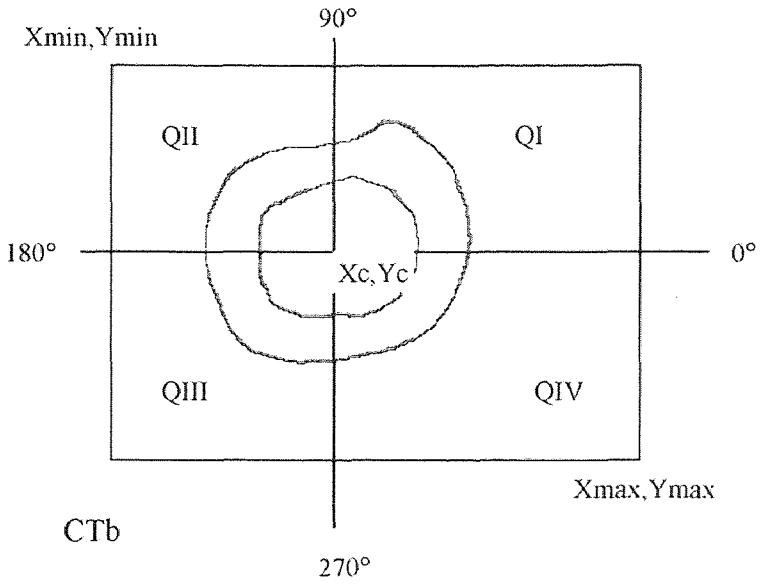

Figure 3.5 Cortical Bone Boundary Display

The y value for a x sort is equal to the x value minus the x center value, times the tangent of the angle for which the boundaries are being determine. The CT number for the corresponding x and y point is compared to the minimum CT number for that cross-section. The smallest and largest radial lengths that have CT numbers greater than or equal to the minimum CT number for that cross-section, are recorded corresponding to the x sort, inner and outer cortical bone boundary for that angle. Since not every pixel is being checked using this method an y sort is performed, for each quadrant y is varied from the y center point to either the lowest y boundary (for quadrants I and II) or the highest y

boundary (for quadrants III and IV). The lowest y value occurs in quadrant I or II and the highest y value occurs in quadrant III or IV. The x value for an y sort is equal to the y center value, minus the y value, divided by the tangent of the angle for which the boundaries are being determine. The CT number for the corresponding x and y point is compared to the minimum CT number for that cross-section. The smallest and largest radial lengths that have CT numbers greater than or equal to the minimum CT number for that cross-section, are recorded corresponding to the y sort, inner and outer cortical bone boundary for that angle. As previously mentioned, the node locations for the inner and outer boundaries of the cortical bone are found by determining if the values for the x or y sort results in a smaller radial length for the inner boundary or a larger radial length for the outer boundary.

Note that by performing the linear regression analysis, the centers of each cross-section (except the most proximal five) are placed at $x = 0$ and $y = 0$ so any angular tilt that may have existed due to the orientation of the patient's leg in the CT scanner has been removed. The calculated boundaries with the tilt removed are listed on sheet 2 of the Excel workbook for all angular spacing angles and all cross-sections. After the calculations to determine the cortical bone boundaries are completed, the user is given the option to plot the bone boundaries. These plots represent the actual bone orientation in the CT scanner, so the above mention tilt has not been removed. Figure 3.6 and Figure 3.7 are the 3-D Mathcad plots of the inner and outer cortical bone boundaries for Case 1 and Case 2, respectively.

For Case 1, a minimum CT number of 1280 was used for cross-sections 1 through 7 and a minimum CT number of 1360 was used for cross-sections 8 through 17.

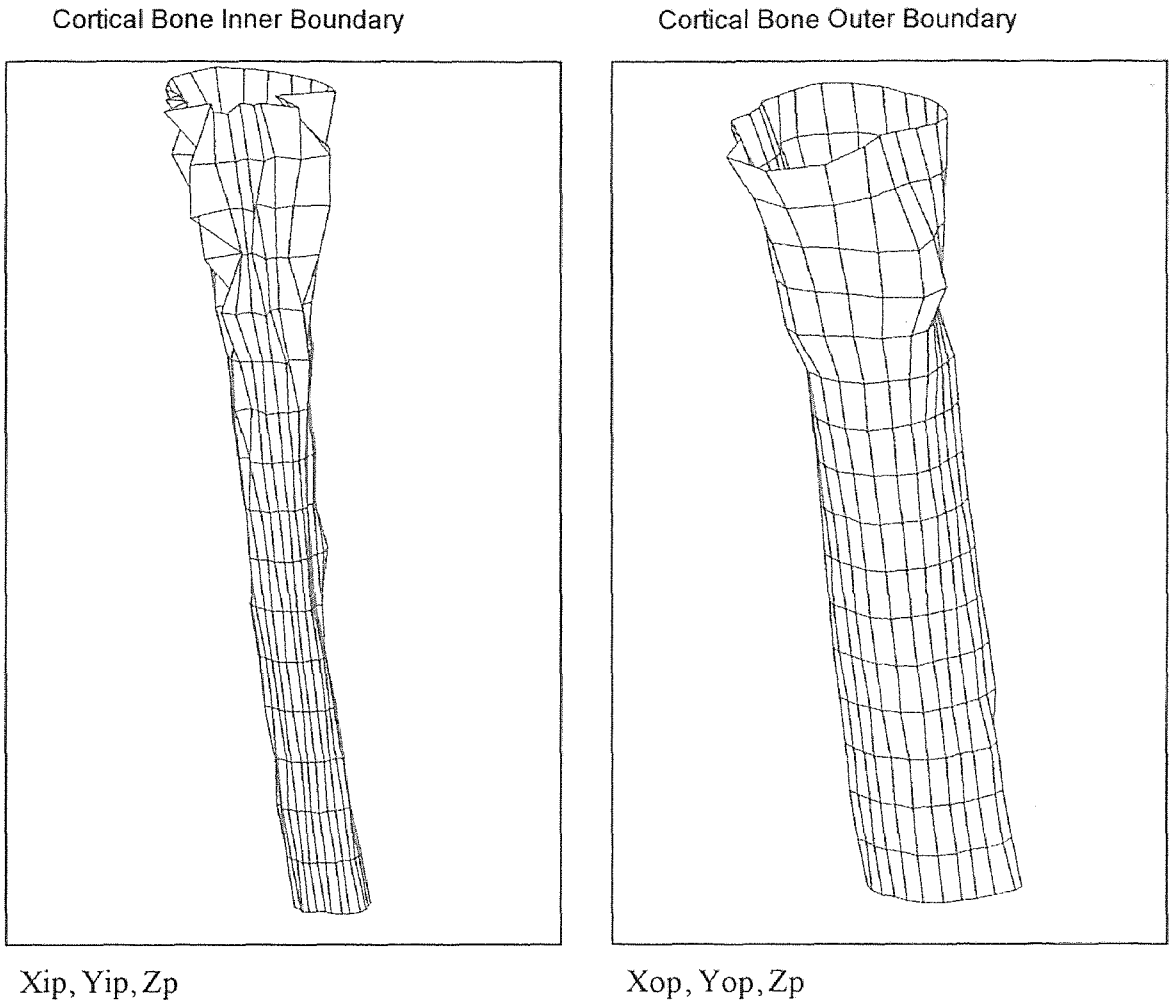

Figure 3.6 Case 1: 3-D Cortical Bone Inner and Outer Boundary Plot

For Case 2, a minimum CT number of 1280 was used for cross-sections 1 through 6 and a minimum CT number of 1360 was used for cross-sections 7 through 17. The Mathcad program (**3DCBPLOT.MCD**) used to create the plots is access using dynamic data exchange through the Excel program.

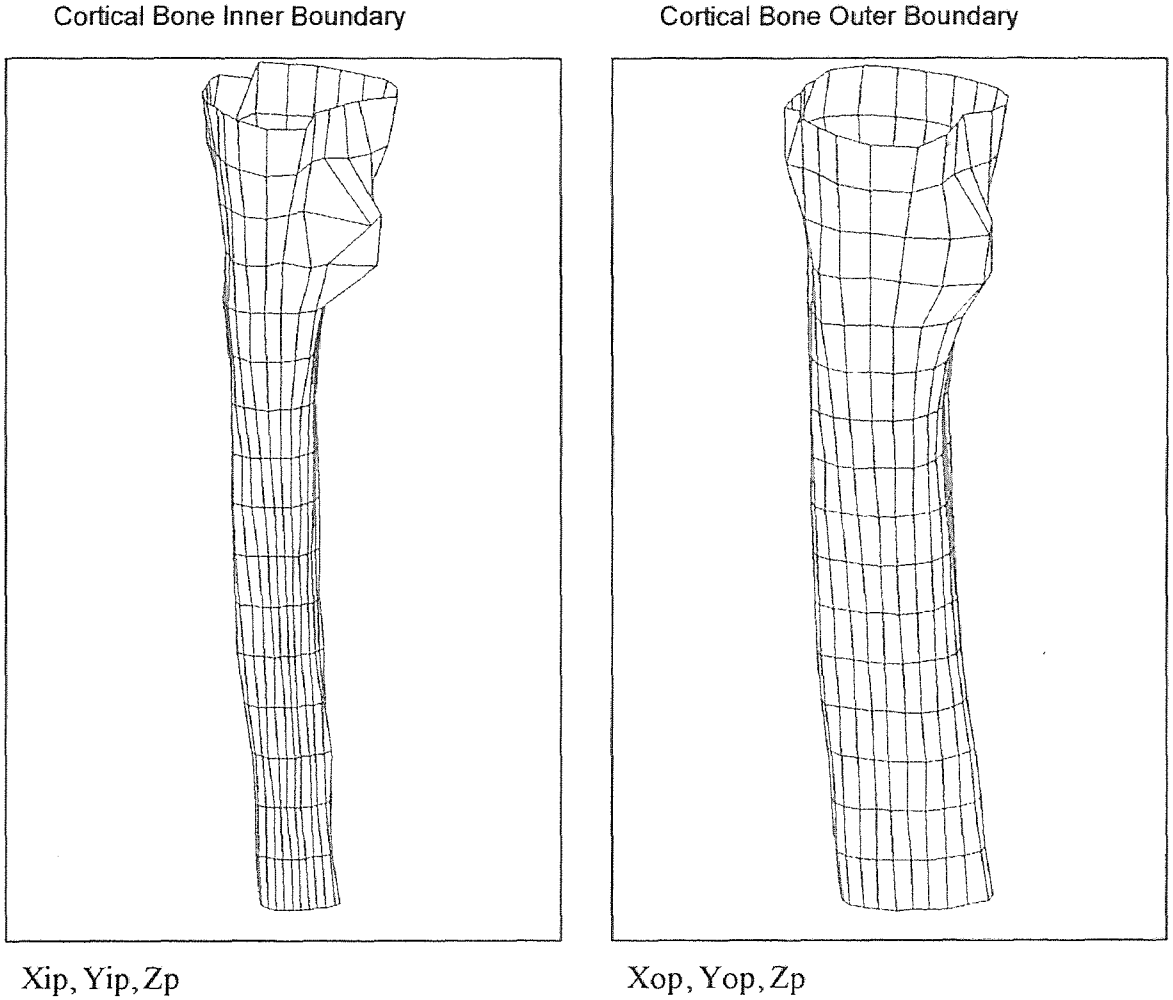

Figure 3.7 Case 2: 3-D Cortical Bone Inner and Outer Boundary Plot

3.11 Prosthesis Size

The next module in the sequence determines the size of the prosthesis using the cortical bone boundaries and user inputs. The user is requested to enter the following prosthesis information: (a) the medial - lateral ratio of prosthesis to cortical bone at the distal stem; (b) the medial - lateral ratio of prosthesis to cortical bone at the mid stem; (c) the medial - lateral ratio of prosthesis to cortical bone at the bone cut surface; (d) the anterior - posterior ratio of prosthesis to cortical bone at the distal stem; (e) the anterior - posterior ratio of prosthesis to cortical bone at the mid stem; (f) the anterior - posterior ratio of prosthesis to cortical bone at the bone cut surface, (all of the above ratios must be within .25 and .75); (g) the bone cut angle; (h) the neck to shaft angle; (i) the width from distal stem center to the center of the neck post in the medial - lateral plane (W1); (j) the prosthesis height from the medial prosthesis bone cut surface to the center of the neck post (H3); (k) the medial - lateral neck post diameter; (l) the anterior - posterior neck post diameter; and (m) the neck post angle. Figure 3.8 contains medial - lateral and anterior - posterior plots of a prosthesis showing the locations of some of the items listed above.

The elements created in the finite element models, in this research are 8 node brick elements. The ideally shaped 8 node brick element would be a cube. A cube has six equal side, each in a flat plane and all corner angles are 90 degrees. As the shape of the finite element deviates from the ideal shape (a cube) one or more sides are no-longer contain with-in a flat plane and the element is distorted. The ANSYS finite element program converts the matrices and load vectors of the element from the points on the flat

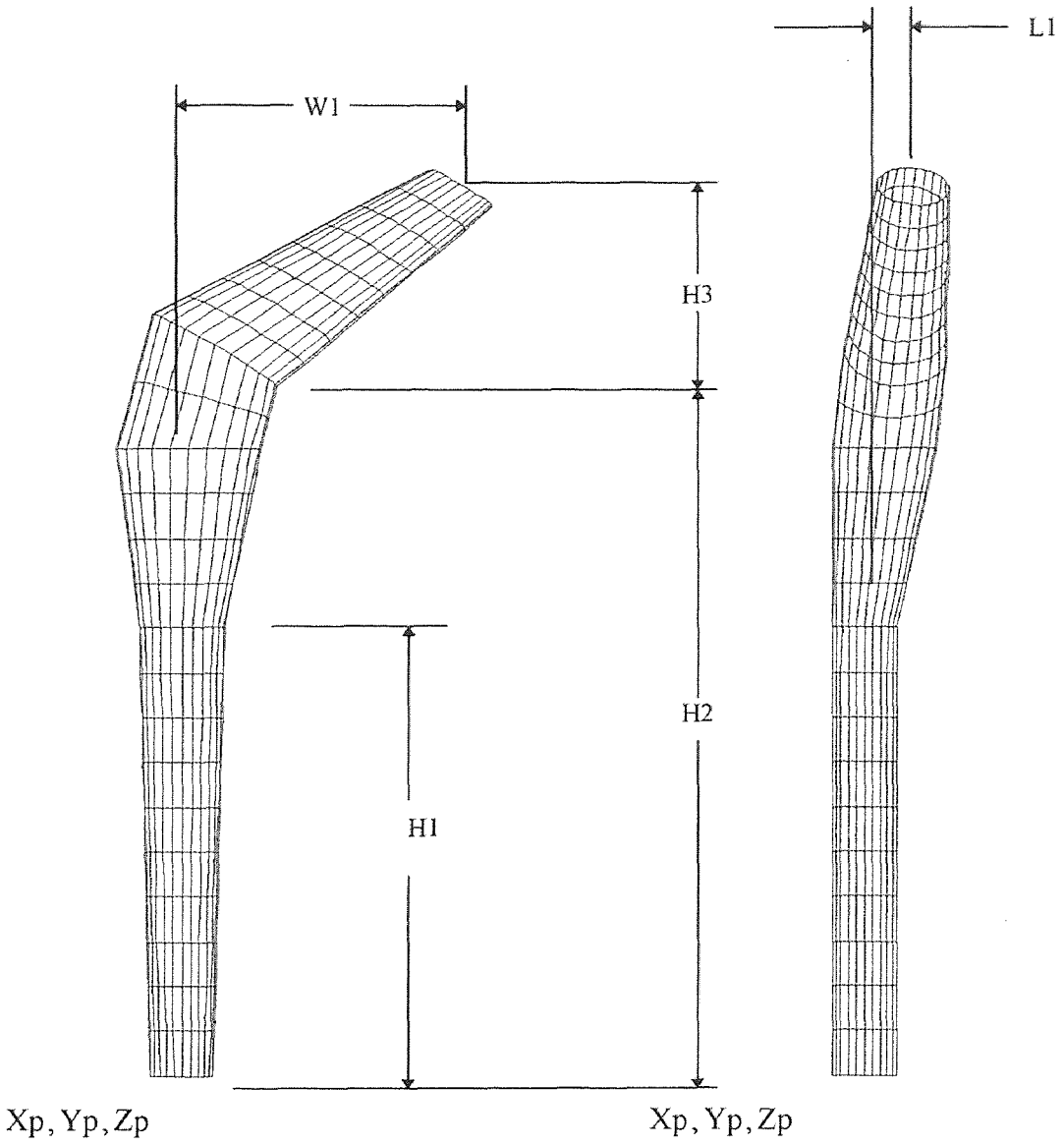

Figure 3.8 Medial - Lateral and Anterior - Posterior Prosthesis Parameters

plane in which the element is derived to the actual nodes. However, if the distortion is excessive the element is consisted warped and the ANSYS finite element analysis program will terminate. Figure 3.9 shows the shape of an ideal and distorted finite element.

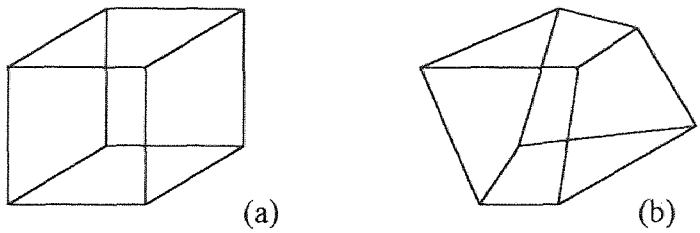

Figure 3.9 Ideal (a) and Distorted (b) Finite Element

In an attempt to reduce the number of warped finite elements created, the outer boundaries of the cortical bone are modified according to the following:

1) If the radius at any angle for any cross-section (i.e. 1) is greater than the radius for the adjacent distal cross-section (i.e. 2), and the radius at the next angle for that cross-section (i.e. 1) is also greater than the radius for the adjacent distal cross-section (i.e. 2), the boundaries are not changed.

2) If the radius at any angle for any cross-section (i.e. 1) is less than the radius for the adjacent distal cross-section (i.e. 2), and the radius at the next angle for that cross-section (i.e. 1) is also less than the radius for the adjacent distal cross-section (i.e. 2), the boundaries are not changed.

3) Provided that neither number 1 nor number 2 above applies, the following is checked. If the absolute value of the difference between the radius for any cross-section (i.e. 1), and the adjacent distal cross-section (i.e. 2) for any angle is greater then 40 percent of the height spacing between the two adjacent cross-sections, the outer boundaries of both cross-sections are revised. The larger radius is decreased by one quarter of the difference between the two radius, and the smaller radius is increased by the same amount.

i.e. if the radius at cross-section 1, angle 1 (R1,1) = 16.0 and the radius at cross-section 2, angle 1 (R2,1) = 10.0 and the height spacing between the cross-section was 10.0. R1,1 would be revised from 16.0 to 14.5 and R2,1 would be revised from 10.0 to 11.5.

The resulting cortical bone outer boundaries are displayed on sheet 2 of the Excel program, next to the previously determined cortical bone outer boundaries. If any of the cortical bone outer boundaries had been revised the program displays them in a **bold** font. Note that, if there are any warped finite elements the ANSYS program will not run. Although the above method does eliminate some warped elements it does not insure that no warped elements will be created.

In addition to trying to prevent warped elements, the program checks that the diameter of the distal portion of the prosthesis is not larger than the prosthesis mid stem diameter, and similarly, that the mid stem prosthesis diameter is not larger than the diameter of the prosthesis at the bone cut surface. This ensures that the prosthesis can be

inserted with a minimum amount of bone removal, and that there is an uniform fit between the prosthesis and bone.

The total length of scanned bone used in this research for each case was 160 mm. This corresponds to seventeen cross-sections, each 10 mm apart. The most distal 20 mm is assumed to be composed of bone without prosthesis. The most distal part of the prosthesis starts at this height. The prosthesis center is assumed to be in a vertical line up to the mid stem. The mid stem is defined as being 40 mm below the most proximal cross-section. Therefore, the height from the distal portion of the prosthesis to the mid stem is 100 mm. The center line of the proximal portion of the prosthesis is allowed to be tilted in both the medial-lateral and the anterior-posterior plane.

The prosthesis parameters that were used to create the prosthesis portions of the finite element input files are show in Table 3.1 and 3.2 for Case 1 and Case 2, respectively. The calculated parameters are: (a) the medial-lateral diameter for the distal stem; (b) the medial-lateral diameter for the mid stem; (c) the height to the medial bone cut surface from the distal stem (H2); (d) the prosthesis medial angle; (e) the prosthesis lateral angle; (f) the length from distal stem center to the center of the neck post in the anterior-posterior plane (L1); (g) the anterior-posterior diameter for the distal stem; (h) the anterior-posterior diameter for the mid stem; and (i) the anterior-posterior diameter for the bone cut surface.

Table 3.1 Case 1: Prosthesis Parameters

Prosthesis Input Parameters	Enter Left or Right in next column	left	
Front (Medial - Lateral) View			
Ratio of Prosthesis to Cortical Bone			
@ distal stem	rPtoBdsml	0.50	
@ mid stem	rPtoBmsml	0.50	
@ bone cut surface	rPtoBbcml	0.50	
Diameter (distal stem)	Dds(ml)	15.55	mm
Diameter (mid stem)	Dms(ml)	19.15	mm
Height to mid stem from distal end	H1	100.00	mm
Height to bone cut from distal end	H2	154.76	mm
Prosthesis Medial Angle	Ang1	88.07	deg
Prosthesis Lateral Angle	Ang2	97.23	deg
Angle of bone cut	Ang3	150.00	deg
Neck to Shaft Angle	Ang4	128.00	deg
Width from Distal Stem Center to Center of Neck Post	W1	62.20	mm
Height from Bone Cut to Center of Neck Post	H3	48.30	mm
Diameter of Neck Post	Dnp(ml)	16.50	mm
Neck Post Angle	Ang5	150.00	deg
Side (Anterior - Posterior) View			
Ratio of Prosthesis to Cortical Bone			
@ distal stem	rPtoBdsap	0.50	
@ mid stem	rPtoBmsap	0.50	
@ bone cut surface	rPtoBbcap	0.50	
Length from Distal Stem Center to Center of Neck Post (if tilt is towards anterior enter a positive number)	L1	0.00	mm
Diameter (distal stem)	Dds(ap)	14.65	mm
Diameter (mid stem)	Dms(ap)	14.65	mm
Diameter (bone cut surface)	Dbcs(ap)	22.36	mm
Diameter of Neck Post	Dnp(ap)	16.50	mm

Table 3.2 Case 2: Prosthesis Parameters

Prosthesis Parameters	Enter Left or Right in next column	left	
Front (Medial - Lateral) View			
Ratio of Prosthesis to Cortical Bone			
@ distal stem	rPtoBdsml	0.50	
@ mid stem	rPtoBmsml	0.50	
@ bone cut surface	rPtoBbcml	0.50	
Diameter (distal stem)	Dds(ml)	14.14	mm
Diameter (mid stem)	Dms(ml)	18.89	mm
Height to mid stem from distal end	H1	100.00	mm
Height to bone cut from distal end	H2	149.96	mm
Prosthesis Medial Angle	Ang1	78.47	deg
Prosthesis Lateral Angle	Ang2	97.23	deg
Angle of bone cut	Ang3	150.00	deg
Neck to Shaft Angle	Ang4	128.00	deg
Width from Distal Stem Center to Center of Neck Post	W1	62.20	mm
Height from Bone Cut to Center of Neck Post	H3	48.30	mm
Diameter of Neck Post	Dnp(ml)	16.50	mm
Neck Post Angle	Ang5	150.00	deg
Side (Anterior - Posterior) View			
Ratio of Prosthesis to Cortical Bone			
@ distal stem	rPtoBdsap	0.50	
@ mid stem	rPtoBmsap	0.50	
@ bone cut surface	rPtoBbcap	0.50	
Length from Distal Stem Center to Center of Neck Post (if tilt is towards anterior enter a positive number)	L1	-10.73	mm
Diameter (distal stem)	Dds(ap)	14.52	mm
Diameter (mid stem)	Dms(ap)	14.52	mm
Diameter (bone cut surface)	Dbcs(ap)	23.00	mm
Diameter of Neck Post	Dnp(ap)	16.50	mm

3.12 Nodes

The next step in the creation of the finite element input file is the determination of the nodes for all of the elements in the finite element model, which includes the cortical bone, cancellous bone, interface (porous coating or cement), prosthesis stem and neck elements. The user is requested to enter the following finite element model information: (a) the number of elements from the inner radius to the outer radius of the prosthesis; (b) the number of elements from the inner radius to the outer radius of the porous coating (or cement) interface; (c) the number of elements from the inner radius to the outer radius of the cancellous bone; (d) the number of elements from the inner radius to the outer radius of the cortical bone; (e) the porous coating (or cement) thickness; (f) the minimum allowable cancellous bone thickness; (g) the maximum allowable change in the cortical bone inner boundary from one cross-section to the next (this is requested to avoid warped elements); and (h) the minimum allowable cortical bone thickness.

The total number of elements from the inner radius to outer radius for each cross-section (NeT) is equal to:

$$NeT = PEfRiRo + IEfRiRo + CanBEfRiRo + CBEfRiRo$$

where PEfRiRo = the number of elements from the inner radius to the outer radius of the prosthesis

IEfRiRo = the number of elements from the inner radius to the outer radius of the porous coating (or cement) interface

CanBEfRiRo = the number of elements from the inner radius to the outer radius of the cancellous bone

CBEfRiRo = the number of elements from the inner radius to the outer radius of the cortical bone

The number of Elements per cross-section (ElempCS) is equal to:

$$ElempCS = (NeT)(360/SA)$$

where SA = the angular spacing between nodes

The number of Nodes per cross-section (NodespCS) is equal to:

$$NodespCS = ElempCS + 1$$

The 1 comes from the node in the center of the prosthesis that the inner set of prosthesis elements are attached to.

The maximum node number in the model (NumNode) is equal to:

$$NumNode = (Slices + 9)(NodespCS) + (360/SA)(PEfRiRo) + 1$$

where Slices = the number of cross-sections

The nine (9) comes about in the following way. The upper bone/prosthesis cross-section is rotated twice (2) to model the geometry between the most proximal cross-section and the bone cut surface. The prosthesis neck contains eight layers of elements. Since the final layer does not need to contain any nodes beyond the prosthesis nodes, only seven (7) of these layers get multiplied by the number of nodes per cross-section. This

method of node numbering was used so that there is a fixed number of nodes (NodespCS) between the nodes of adjacent layers.

The actual number of nodes (ActNumNodes) defined in the model is a somewhat smaller number given by the following equation:

$$\text{ActNumNodes} = (\text{Slices} + 2)(\text{NodespCS}) + (8)\{(360/\text{SA})(\text{PEfRiRo}) + 1\}$$

The maximum element number in the model (NumElem) is equal to:

$$\text{NumElem} = (\text{Slices} + 8)(\text{ElempCS}) + (360/\text{SA})(\text{PEfRiRo})$$

The eight (8) comes about in the following way. There are (Slices-1)(ElempCS) elements in "Slices" cross-sections, i.e. in 17 cross-sections there are only 16 times the number of elements per cross-section elements. To the (Slices-1) number we need to add the elements for the 2 rotated sections and 7 of the 8 sets of elements for the prosthesis neck section, so we have (Slices-1 + 2 + 7) which equals (Slices + 8). Since the final layer does not need to contain any elements beyond the prosthesis elements, this layer does not get multiplied by the number of elements per cross-section. Similarly, this method of element numbering was used so that there is a fixed number of elements (ElempCS) between the elements of adjacent layers.

The actual number of elements (ActNumElem) defined in the model is a somewhat smaller number given by the following equation:

$$\text{ActNumElem} = (\text{Slices} + 1)(\text{ElempCS}) + (8)\{(360/\text{SA})(\text{PEfRiRo})\}$$

A check is performed to insure that the maximum allowable change in the cortical bone inner boundary from one cross-section to the next is within the user defined limit. The check is performed from the distal end up. The inner boundaries of the cortical bone nodes of the most distal cross-section (i.e. 17) is compared to the inner boundaries of the next adjacent proximal cross-section (i.e. 16). If the boundaries of the proximal cross-section (i.e. 16) is greater than or less than the boundaries of the distal cross-section (i.e. 17), plus or minus the user defined limit for any angle, the values of the boundaries of the proximal cross-section (i.e. 16) for that angle are revised to be at the user defined limit. Then the boundaries of that cross-section (i.e. 16) would be compared to the boundaries of the next adjacent cross-section (i.e. 15). This method is repeated until the boundaries of all of the cross-sections are adjusted as required to meet the user defined limit. The reason the check is performed from the distal end up is because the inner boundaries of the distal cortical bone tend to be much more uniform in shape, and less sensitivity to the choice of the CT number that was used to define the boundaries.

A check is then performed to make sure that the cortical bone thickness is equal to or greater then the minimum cortical bone thickness defined by the user. If the thickness of the cortical bone is thinner then the user defined limit for any angle, the inner boundaries of the cortical bone for that angle is moved in to meet the minimum thickness requirement. It should be noted that since this check is performed after the first check, it is possible that the second check may "undo" the changes performed in the first check. The resulting cortical bone boundaries are displayed on sheet 2 of the Excel program, next to the previously determined cortical bone boundaries. If any of the cortical bone

boundaries had been revised the program displays them in a **bold** font. Since bone is being "removed" to insert the prosthesis from the medullar canal, the inner boundaries of the cortical bone will be revised, if needed, to allow room for the prosthesis, interface layer and a minimum user defined thickness for the cancellous bone layer. A cancellous bone section is required in each cross-section for element connectivity.

The location of the most medial cortical bone node is determined. The location of this node is needed to determine the starting location for the rotation section that creates nodes from the most proximal cross-section to the bone cut surface. For a right femur this would be the most positive x node. For a left femur this would be the most negative x node. The most proximal prosthesis node is equal to the height from the mid stem to the bone cut surface, divided by the tangent of the prosthesis medial angle, plus one-half the prosthesis mid stem diameter.

The distal to mid stem slopes of the prosthesis in the medial-lateral and anterior-posterior planes is equal to the change in diameter from mid stem to distal stem, divided by the height from the mid stem to distal stem. This height has been set to a constant value of 100 mm for this study. The tilt of the prosthesis, if any (towards the anterior or the posterior side), is calculated next. This tilt is equal to the arc tangent of the length from the distal stem center, to the center of the neck post, divided by the height from the center of the neck post to the mid stem. In addition to the proximal portion of the prosthesis being tilted in the anterior-posterior plane, it may also have a taper in this plane, i.e. the proximal portion could be wider then the mid stem portion. The anterior-

posterior proximal taper is defined as being equal to the arc tangent of the change in prosthesis radius, from the bone cut surface to the mid stem, divided by 40.

The center of the most distal cross-section has a x, y, z coordinate of (0,0,160), for a right femur +X is Medial, +Y is Anterior, and +Z is Inferior. Similarly, for a left femur +X is Lateral, +Y is Anterior, and +Z is Inferior. The bone distal to the prosthesis is assumed to be cancellous bone in the region directly below the most distal portion of the prosthesis and interface layer. The same x and y node locations are used for the bone nodes distal to the prosthesis, as used in the most distal cross-section containing the prosthesis, except for the nodes defining the cortical bone. This insures properly shaped elements in the distal portion of the model.

Since there is no CT data available for the geometry of the bone at the surface in which the bone is cut, a rotation method is used to approximate the geometry in this region. The nodes of the most proximal cross-section are rotated about a point, located at the most median node, plus 6 divided by the tangent of the bone cut angle. The desired bone cut angle is inputted by the user. A second set of nodes is defined as being centered between the set of nodes of the most proximal cross-section and the rotated set just created. By including the 6 divided by the tangent of the bone cut angle term in the rotated equation, better shaped elements are created, since the three cross-sections (the most proximal cross-section, and the two "rotated" cross-sections) do not share a common node. If the rotation occurred strictly about the most medial cortical bone node, all three layers would have that node as a common node, and the elements sharing that node would be poorly shaped. This node would have a Z value of 0, in the method used

the most medial cortical bone node has a Z value of 0, -3, and -6 for the most proximal cross-section and the two "rotated" layers, respectively.

The shape of the portion of the prosthesis extending beyond the bone is assumed to vary linearly, from its shape at the bone cut surface, to its shape at the top of the neck post. Eight element layers are used to model this section of the prosthesis.

The programs creates ASCII text node files containing the x, y and z locations of all of the nodes which are used to create the finite element input file. ASCII text files of the 3-D outer boundaries of the cortical bone and prosthesis are created. The user is given the option to plot the 2-D nodal boundaries for the 17 cross-sections, as well as, the option to plot the 3-D cortical bone and or the 3-D prosthesis outer boundaries using Mathcad programs. The Mathcad program used to plot the node boundaries is **NODEPLOT.MCD**. The limits of the plots were manually selected for each case to contain the largest cross-section (section 1). The same boundaries were used for all sections of the same case. Appendix A contains the 2-D node boundaries plots for Case 1. **CB3DPLOT.MCD** is used to plot the 3-D cortical bone plots and **3DPPLOT.MCD** is used to plot the 3-D outer boundaries of the prosthesis. The 3-D cortical bone outer boundary plots are shown in Figure 3.10 and 3.11 for Case 1, and Case 2, respectively. Similarly, Figure 3.12 and 3.13 contain the 3-D prosthesis plots for Case 1 and Case 2. The bone tilt, mentioned previously, shown in Figures 3.6 and 3.7 has been removed from the data as can be seen from Figures 3.10 and 3.11. Figures 3.10 and 3.11 also contain the nodes associated with the outer boundaries of the cortical bone of the two rotated layers.

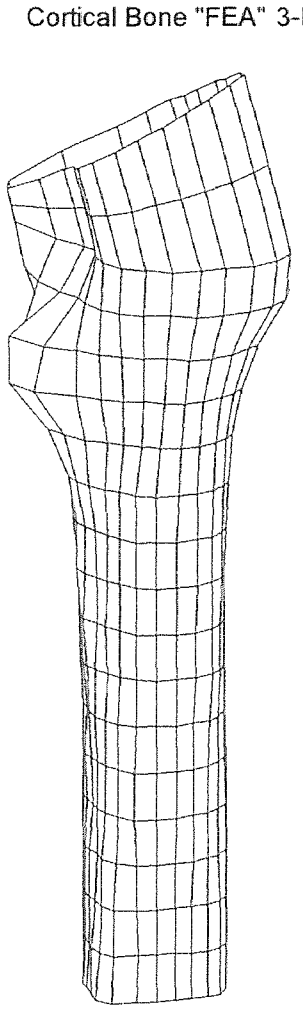

Figure 3.10 Case 1: 3-D Cortical Bone Outer Boundary Plot

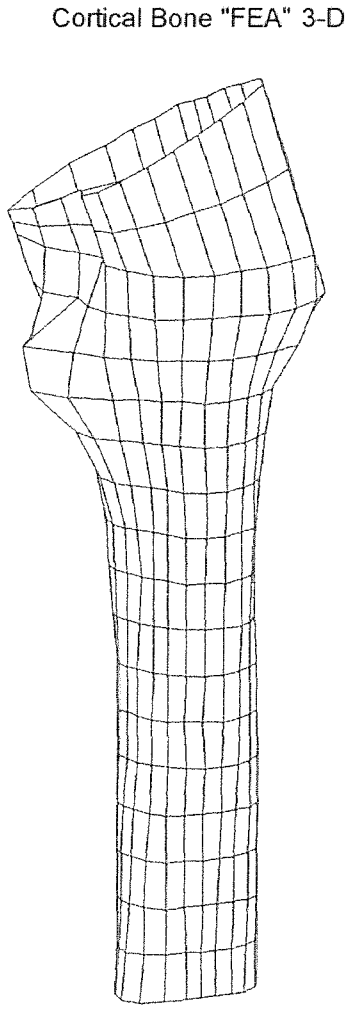

Figure 3.11 Case 2: 3-D Cortical Bone Outer Boundary Plot

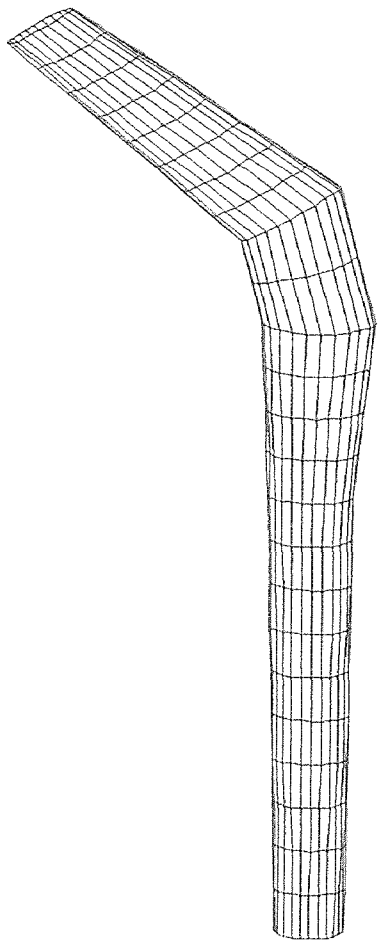

Figure 3.12 Case 1: 3-D Prosthesis Outer Boundary Plot

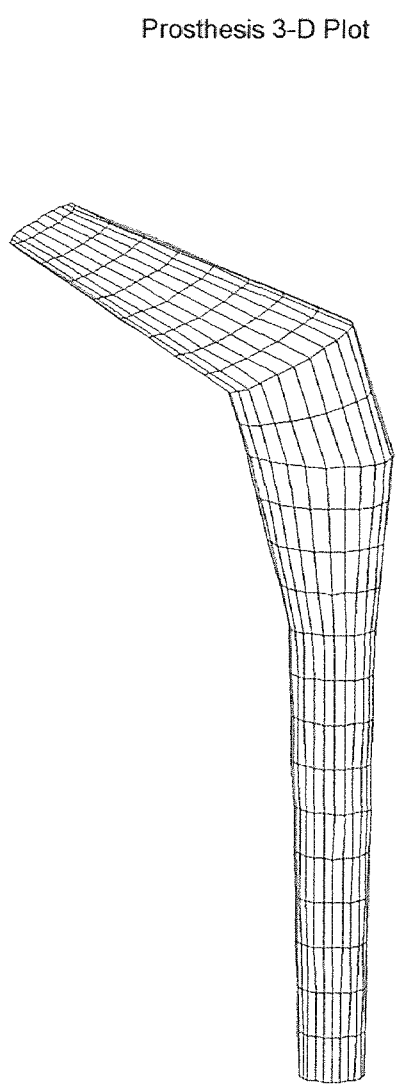

Figure 3.13 Case 2: 3-D Prosthesis Outer Boundary Plot

3.13 Average Computed Tomography Number

The average CT number is determined for each 2-D cortical bone area by taking the average of the CT number of all of the pixels contained in the 2-D area of interest. Each 2-D area represents either the top or bottom surface of an element. The user is requested to input the values of the constants ("A" and "B") that relate the CT number to density in the linear equation listed below:

$$\text{Density} = (A)(CT\#) + B \quad (g/cm^3)$$

The program reads the revised cortical bone boundaries previously printed to sheet 2 of the Excel program. For each truncated pie shape cortical bone 2-D area the boundaries of the smallest box containing this area is determined. Figure 3.14 shows two truncated pie shape areas representing two cortical bone 2-D areas (the shaded portions of Figure 3.14) and the corresponding smallest boxes in which each 2-D area is contained.

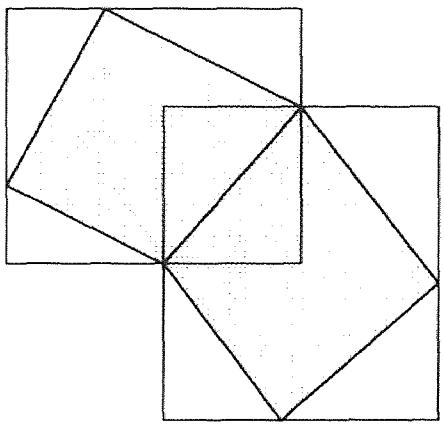

Figure 3.14 Cortical Bone Box Boundaries

The corresponding upper and lower limits for each box containing a 2-D cortical bone area is determined. The boundaries of two of the four lines defining a 2-D cortical bone area is given by the angles in which the area is contained, i.e. if the angular spacing between elements is 15 degrees there would be a cortical bone element area whose two lines are defined by 0 degrees and 15 degrees, etc. The slope and y intercept for the remaining two line bounding the 2-D cortical bone area is determined for each cortical bone section. The location of each pixel in each box (from Xmin,Ymin to Xmax,Ymax; see Figure 3.15) containing a cortical bone 2-D area is check to see if it is inside the four lines defining the cortical bone. If it is, a value of 1 is added to a running count of the number of pixels contained in that area and its CT number is added to a running sum. The total number of pixels contained in a 2-D cortical bone is determined as well as the average CT number.

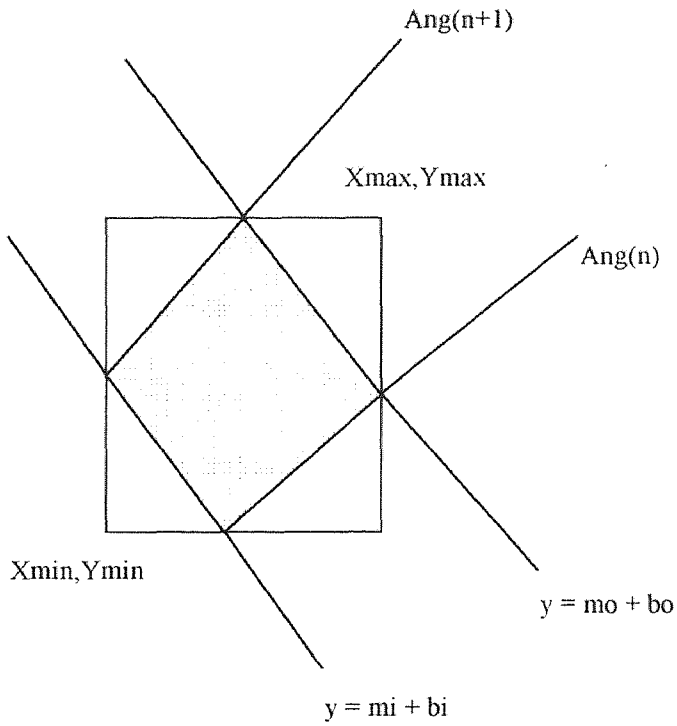

Figure 3.15 Lines defining a 2-D Cortical Bone Area

Based on the average CT# the bone density of each 2-D cortical area is calculated using the linear equation stated above. The density, average CT#, sum of the CT#s, and number of pixels contained in each 2-D cortical bone area is printed to sheet 2 of the Excel program. As a check of "element size" the program will print in **bold** font any pixel count value that is less than 100. An example of the cortical bone data printed to sheet 2 of the Excel program for cross-section 1, Case 1 is shown in Table 3.3.

3.14 Finite Element Model Input File

This module creates the finite element input file, which includes the cortical bone, cancellous bone, interface (porous coating or cement), prosthesis stem and neck elements. The user is requested to enter the following finite element model information: (a) the name of the ANSYS input file to be created; (b) the prosthesis material (i.e. Titanium); (c) the prosthesis Young's modulus in MPa; (d) the prosthesis Poisson's ratio; (e) the interface (between bone and prosthesis) material (i.e. PMMA); (f) the interface material Young's modulus in MPa; (g) the interface material Poisson's ratio; (h) the cancellous bone Young's modulus in MPa; (i) the cancellous bone Poisson's ratio; (j) the values of the constants ("A" and "B") that relate the CT number to the cortical bone density in the following linear equation: Density = (A)(CT#) + B (g/cm^3); (k) the strain rate (in 1/sec) that relates the cortical bone density to Young's modulus in following equation: $E = 3790(\text{strain rate})^{0.06}(\text{Density})^3$ (MPa); (l) the cortical bone Poisson's ratio; (m) the medial-lateral, posterior-anterior and superior-inferior joint force in Newtons; (n) the medial-lateral, posterior-anterior and superior-inferior greater trochanter muscle force in Newtons.

Table 3.3 Case 1; Cross-section 1; Cortical Bone Data

File Name = c:\thesis\Case1s1.dat

X center =	177	Xcbcen =	3.598
Y center =	124	Ycbcen =	0
Z Height =	0		
X range =	277	min CT# =	1280
Y range =	208		

Ang Num	Angle	X min	Y min	Revised X min	Revised Y min	X max	Y max	Revised X max	Revised Y max	Density	Avg	Sum CT	Count
1	15	22.359	5.140	**16.145**	**3.411**	26.214	6.168	26.214	6.168	1.14	1264	1099328	870
2	30	20.046	9.509	**14.666**	**6.590**	21.331	10.280	21.331	10.280	1.18	1320	813248	616
3	45	14.649	11.051	**12.315**	**9.319**	17.733	14.135	17.733	14.135	1.19	1331	625424	470
4	60	10.794	12.336	**9.250**	**11.414**	12.593	15.677	12.593	15.677	1.22	1364	552336	405
5	75	6.168	10.023	**5.681**	**12.730**	8.481	18.504	8.481	18.504	1.26	1417	497440	351
6	90	3.598	13.621	**2.827**	**13.179**	3.598	23.130	3.598	23.130	1.25	1400	707152	505
7	105	1.028	9.509	**-1.972**	**12.730**	-2.827	24.158	-2.827	24.158	1.16	1295	828640	640
8	120	-5.397	15.677	**-5.536**	**11.414**	-10.023	23.644	-10.023	23.644	1.24	1385	1119088	808
9	135	-2.056	5.654	**-8.595**	**9.319**	-25.443	29.041	-25.443	29.041	1.20	1345	2381856	1771
10	150	-7.196	6.168	**-10.943**	**6.590**	-36.494	23.130	-36.494	23.130	1.19	1324	4234384	3197
11	165	-10.280	3.598	**-12.419**	**3.411**	-34.438	10.280	**-33.045**	**9.818**	1.32	1483	4364256	2943
12	180	-3.084	0.000	**-12.923**	**0.000**	-21.845	0.000	-21.845	0.000	1.48	1679	2321056	1382
13	195	-5.140	-2.313	**-12.419**	**-3.411**	-14.135	-4.626	-14.135	-4.626	1.48	1678	672752	401
14	210	-3.084	-3.855	**-10.943**	**-6.590**	-10.794	-8.224	-10.794	-8.224	1.29	1453	95920	**66**
15	225	-7.196	-10.794	**-8.595**	**-10.729**	-9.252	-12.850	-9.252	-12.850	1.31	1470	108768	**74**
16	240	-1.542	-8.995	**-6.112**	**-11.414**	-6.682	-17.733	-6.682	-17.733	1.17	1303	237168	182
17	255	1.542	-7.453	**-3.091**	**-13.630**	-2.056	-20.817	-2.056	-20.817	1.08	1189	247344	208
18	270	3.598	-20.046	**1.851**	**-17.509**	3.598	-21.588	3.598	-21.588	1.07	1187	257472	217
19	285	8.738	-19.275	**6.179**	**-16.333**	9.252	-21.074	9.252	-21.074	1.12	1242	445776	359
20	300	13.621	-17.219	**9.250**	**-11.431**	14.649	-19.018	14.649	-19.018	1.11	1230	720816	586
21	315	17.219	-13.621	**12.315**	**-9.897**	19.275	-15.677	19.275	-15.677	1.15	1285	769456	599
22	330	20.817	-10.023	**14.828**	**-8.598**	24.158	-11.822	24.158	-11.822	1.21	1354	811088	599
23	345	23.644	-5.397	**16.145**	**-3.411**	27.756	-6.425	27.756	-6.425	1.18	1310	1064768	813
24	360	25.700	0.000	**16.649**	**0.257**	29.298	0.000	29.298	0.000	1.13	1253	1111408	887

Linearly elastic, ANSYS element type 45 (3-dimensional, 8 node, homogeneous and isotropic, 3 degree of freedom elements allowing only translation about the X, Y and Z axis), are used for all of the elements in the model. There were 2,544 elements and 2,691 nodes in each model. The prosthesis was modeled using two elements in the radial direction per cross-section. The interface, cancellous bone and cortical bone were modeled with one element in the radial direction per cross-section.

The material properties used in the finite element models are listed in Table 3.4. The Young's modulus of the cortical bone elements varied as a function of density. The maximum cortical bone Young's modulus was 24,724 MPa and 27,194 MPa for Case 1 and Case 2, respectively. The minimum cortical bone Young's modulus was 3,556 MPa and 2,927 MPa for Case 1 and Case 2, respectively.

Table 3.4 Finite Element Model Material Properties

Material	Young's Modulus (MPa)	Poisson's Ratio
Cortical bone	$E = 3790(\varepsilon)^{0.06}\rho^3$	0.30
Cancellous	1,000	0.30
Cement (PMMA)	2,000	0.33
Prosthesis (Titanium)	100,000	0.29

In the finite element models the following boundary conditions and loads are assumed. The most distal set of nodes are fixed in X, Y and Z. This imposes a zero displacement condition on these nodes, meaning that these nodes cannot translate any amount in any direction. The joint force is evenly distributed among the most proximal

set of prosthesis neck nodes. The greater trochanter muscle force is evenly distributed among all of the cortical bone nodes contained in the bone cut layer, within plus or minus 30 degrees (posterior-anterior) of the lateral cortical bone nodes. The joint force and greater trochanter muscle force used in the finite element models are shown in Table 3.5.

Table 3.5 Joint and Greater Trochanter Muscle Force

Joint Force	Newtons
X Medial(-) Lateral(+)	642
Y Posterior(-) Anterior(+)	196
Z Superior(-) Inferior(+)	1750
Greater Trochanter Muscle Force	
X Medial(-) Lateral(+)	-490
Y Posterior(-) Anterior(+)	-150
Z Superior(-) Inferior(+)	-1006

This module reads in the ASCII node files created in the Nodes module. The number of materials defined in the model equals three (1 for the prosthesis, 1 for the interface material and 1 for the cancellous bone) plus the number of cortical bone elements. Since each cortical bone element can have a different average CT number, and therefore, a different Young's modulus, there needs to be a different material number for each cortical bone element to be able to assign each cortical bone element its own Young's modulus.

Node connectivity for each element is also defined in this module. As stated in the Nodes section (3.12) there is a fixed number of nodes (NodespCS) between the nodes

of adjacent cross-sections. Four of the eight nodes of an element comes from one cross-section and the other four come from an adjacent cross-section. For example if nodes n1, n2, n3 and n4 are the four nodes in cross-section N of an element, the remaining four nodes located in cross-section N+1 are (n1 + NodespCS), (n2 + NodespCS), (n3 + NodespCS) and (n4 + NodespCS).

Each set of the four node defining a "distal" or "proximal" section of an element is a 2-D Cortical Bone Area (see Figure 3.15) for which an average CT number has been determined (see section 3.13 Average CT Number). The average of the average CT number for each of the two 2-D Cortical Bone Areas defining an element is used as the CT number for that element. For the elements created by rotating of the most proximal bone cross-section, the average CT numbers of the 2-D Cortical Bone Areas for the rotated cross-section are used. As stated previously the Young's modulus for each element is determined by converting the average CT number into a density, and then converting the density into a strain rate depended Young's modulus, using the following equations:

$$\text{Density} = (A)(CT\#) + B \quad (g/cm^3)$$

$$E = 3790(\text{strain rate})^{0.06}(\text{Density})^3 \quad (MPa)$$

Each element in the model is associated with a material number, and each material number is associated with a Young's modulus and Poisson's ratio.

Additional code is added to the end of the input file that causes the file to be automatically executed when it is read in ANSYS. The ANSYS input file is written to worksheet 3 of the Excel program **CTPROG.XLS**. The user needs to do the following

to create the ASCII text FEA input file that can be read by ANSYS; with worksheet #3 active, select File; Save As; (Formatted Text (Space Delimited)); then enter the file name. Note, only the data on worksheet 3 (the ANSYS FEA input file) will be saved to that file, so one may wish to save the file using "Save" prior to issuing the "Save As" command. The file extension for the ASCII text FEA input file will change from a ".xls" to a ".prn".

3.15 Simulated Right Femur Computed Tomography Data

The Computed Tomography Data Analysis Program was designed to process data from either a left or right femur. The CT data analysis program accesses different sub-programs depending of whether the data is for a left or right femur. Since both Case 1 and Case 2 are for left femurs, a simple Visual Basic module (**CREATERI.XLS**) was created using Microsoft Excel 5.0a to convert the seventeen different data files (one for each cross-section) of Case 2 into data files corresponding to a right femur. This newly created data file was processed though all the programs to insure that the program would access the correct sub-programs for a right femur.

3.16 ANSYS Finite Element Analysis Runs

At this point, all of the steps required to create an ANSYS three-dimensional finite element input file have been discussed. Each finite element input file created in this research contained over 8,000 lines of code. It must be pointed out that the Computed Tomography Data Analysis Program creates these files without requiring the user to enter a single line of code.

The finite element input files contain the following information: (a) a list of all of the nodes and their 3-dimensional coordinates; (b) a list of all of the elements and their node connectivity and associated material number; (c) a material property list containing Young's modulus and Poisson's ratio for each material; (d) a list of nodes which are fixed (zero displacement in X, Y, and Z); (e) a list of nodes and associated values of forces representing the joint force and greater trochanter muscle force; and (f) code that automatically causes ANSYS to enter the solution phase.

The file extension for the ASCII text, FEA input file created in the FEA Input File module (see 3.14) was changed from a ".prn" to a ".dat" because the ANSYS finite element programs data file default extension is ".dat". If no warped elements or other errors exist in the model only the following command needs to be issued in the ANSYS program "/input,*filename*,dat" to completely solve the FE model. The "/input,*filename*,dat" command results in ANSYS reading the ASCII text, FEA input file, which contains all of the node, element, boundary conditions and loads data. Commands are contained in the FEA input file that will cause ANSYS to continue into the solve mode if no modeling errors occurred. Unfortunately the initial steps taken to eliminate warped elements, from occurring in the model, was not 100% successful. In each of the models one warped element face still existed resulting in ANSYS given an error message and not entering the solution stage. As a result of this the last three lines of code starting with "/SOLU" was deleted from the ASCII text FEA input file. Now, when the "/input,*filename*,dat" command was entered ANSYS remained in the PREP7 (modeling mode). The nodes associated with the warped face was revised. In the Case 1, one

cortical bone thick model file, an error element occurred because face 3 of element 1788 was warp. The x value of two of the nodes associated with face 3 of this elements (nodes 1804 and 1925) was revised as shown below:

	Node	from	to
from	1804	-29.812	-28.46275
	1925	-24.415	-25.76425

The screen used to eliminate warped elements was revised and is discussed in section 3.11.

The models were run interactively after the required nodal position adjustments were made. The six components of stress (σx, σy, σz, τxy, τxz, and τyz) for each node along the medial/lateral and anterior/posterior planes were recorded. An excel/visual basic program (**FEADATA.XLS**) that accessed a Mathcad program (**STRESSRT.MCD**) was created to computed the von Mises and maximum shear stress for each of these nodes using the components of stress obtained from the ANSYS runs.

CHAPTER 4

RESULTS AND DISCUSSIONS

4.1 Results

This study consisted of the analysis of the stress in a femur with a prosthesis involving (1) a titanium stem prosthetic with cement, (2) the comparison of the stress patterns for a male femur (Case 1) and a female femur (Case 2), and (3) a comparison to the previous results (Chang 1994). The stresses in the proximal femur and the cement interface are of particular interest, because of the problem of proximal stress shielding and clinical loosening of the femoral component due to fatigue failure of the cement. A material, such as the cement interface, subjected to fluctuating stresses which are below the ultimate tensile strength of the material may fail after repeated cycling. This phenomenon is termed fatigue. Fatigue failure begins with the generation of a fatigue crack which occurs at a point of high stress concentration. Tensile stress, and to a lesser degree shearing stress leads to fatigue crack propagation. The fluctuating stresses, required for fatigue failure, occur due to the changing stress patterns that occur during normal activities; i.e. walking, running, chair raising and seating, stair climbing etc. Two other theories of failure, the maximum shear stress theory and the maximum distortion energy theory are discussed in section 1.8.

The normal, maximum shear and von Mises stress distribution along the lateral and medial sides of the prosthesis, interface, cancellous bone and cortical bone are displayed in Appendix B for Case 1 and Case 2. The stresses along the anterior and posterior sides were much lower and are not presented. A summary of the maximum and

minimum normal, von Mises, and maximum shear stresses for Case 1 and Case 2, are contained in Table 4.1.

Table 4.1 Case 1 and Case 2 Finite Element Analysis Results

	Case 1			Case 2		
	Prosthesis			**Prosthesis**		
	Normal	vonMises	max Shear	Normal	vonMises	max Shear
max	63.6520	64.2478	40.6512	71.1290	71.3776	39.5971
min	-69.5590	3.8556	2.2575	-78.1680	1.1041	0.6059
	Interface Inner			**Interface Inner**		
	Normal	vonMises	max Shear	Normal	vonMises	max Shear
max	1.4274	6.7765	4.4603	1.6175	6.1320	3.6618
min	-5.3098	0.2979	0.0978	-3.6987	0.2626	0.1052
	Interface Outer			**Interface Outer**		
	Normal	vonMises	max Shear	Normal	vonMises	max Shear
max	1.6430	7.0869	4.6876	1.8057	7.0999	4.3604
min	-4.5466	0.3560	0.1441	-2.9095	0.2798	0.1110
	Cancellous Bone Inner			**Cancellous Bone Inner**		
	Normal	vonMises	max Shear	Normal	vonMises	max Shear
max	0.9115	6.0483	3.9667	0.9907	4.3631	2.8026
min	-3.5104	0.1386	0.0633	-2.2033	0.1191	0.0504
	Cancellous Bone Outer			**Cancellous Bone Outer**		
	Normal	vonMises	max Shear	Normal	vonMises	max Shear
max	1.0883	6.1454	4.0382	1.2387	4.2743	2.7468
min	-3.3235	0.1892	0.0867	-2.4536	0.1606	0.0670
	Cortical Bone Inner			**Cortical Bone Inner**		
	Normal	vonMises	max Shear	Normal	vonMises	max Shear
max	23.2710	24.4171	14.9057	27.6990	29.3432	17.0328
min	-26.6530	0.3778	0.1574	-30.8770	0.4627	0.1803
	Cortical Bone Outer			**Cortical Bone Outer**		
	Normal	vonMises	max Shear	Normal	vonMises	max Shear
max	36.9320	35.9019	20.2318	48.4440	46.9498	23.8220
min	-42.0560	0.6660	0.3280	-42.6630	0.2524	0.1077

As stated previously, for the loads applied, the stresses in the medial-lateral plane were greater then the stresses in the anterior-posterior plane. The titanium prosthesis stem is in tension on the lateral side and compression on the medial side. The maximum

tensile stress, on the surface of the prosthesis along the interface, occurs at the mid-distal lateral side. The maximum tensile stress was 64 MPa for Case 1 and 71 MPa for Case 2. The maximum shear stress was 41 MPa for Case 1 and 40 MPa for Case 2.

The maximum tensile stress in the interface (cement) occurred at the proximal medial side of the cement-bone interface. It was 1.6 MPa for Case 1 and 1.8 MPa for Case 2. The maximum shear stress in the cement was greater then the maximum tensile stress. The maximum shear stress also occurred at the cement-bone interface as opposed to the prosthesis-cement interface. For Case 1 the maximum shear stress in the cement occurred at the most proximal medial section and was 4.7 MPa. It occurred at the most distal medial section for Case 2 and was 4.4 MPa. The maximum shear stress versus longitudinal location was U shaped for both Case 1 and Case 2 (see Appendix B6). The maximum von Mises stress occurred at the cement-bone interface and was 7 MPa for both Case 1 and Case 2.

The tensile stress in the cancellous bone was less than 2 MPa for both Case 1 and Case 2. The maximum shear stress in the cancellous bone was 4.0 MPa for Case 1 and 2.8 MPa for Case 2.

The greatest cortical bone tensile stress occurred at the outer distal-lateral side. It was 37 MPa for Case 1 and 48 MPa for Case 2. The tensile stress on the lateral side generally decreased proximally. In fact, the tensile stress at the lateral proximal end was close to zero. The medial portion of the cortical bone was in compression. The maximum shear stress also occurred in the outer portion of the cortical bone. For Case 1

it occurred on the distal medial side and was 20 MPa. For Case 2 it occurred on the distal lateral side and was 24 MPa.

The maximum tensile stresses for Case 2 (female) for the prosthesis, cement and cancellous bone were about 9% to 14% higher then for Case 1 (male). The maximum tensile stresses in the cortical bone were about 19% to 31% higher. The maximum shear stress was higher for Case 1 (male) in the prosthesis, cement and cancellous bone, but lower in the cortical bone, then for Case 2 (female). The stress patterns were quite similar for the male femur (Case 1) and the female femur (Case 2) in the medial-lateral plane. The stresses in the anterior-posterior plane tended to be small and the stress patterns between Case 1 (male) and Case 2 (female) were not as consistent as in the medial-lateral plane.

The maximum tensile stress along the lateral prosthesis boundary for Case 1 was 64 MPa and it occurred mid stem in this study. Chang (1994) reported a maximum tensile stress along the lateral prosthesis boundary of only 23 MPa, occurring proximally. The maximum tensile stress between the cement and the bone at the lateral interface was 1.6 MPa (distal) versus 13.4 MPa (proximal). The maximum shear stress between the cement and the bone at the medial interface 4.7 MPa (proximal) versus 2.5 MPa (proximal). The maximum shear stress between the cement and the bone at the lateral interface 3.3 MPa (distal) versus 8.0 MPa (proximal). The maximum von Mises stress along the medial femoral surface was 29 MPa (distal) versus 17 MPa (distal). The maximum von Mises stress along the lateral femoral surface was 36 MPa (distal) versus 31 MPa (proximal). As seen from the above, there tended to be differences between the

results obtained in this study and the results obtained by Chang (1994) for the same CT data file (Case 1).

4.2 Discussions

A 3-D finite element analysis of a femur with prosthesis was performed for two cases. Computed tomography was used to obtain the geometry and material properties of the cortical bone. One of the most important aspects of the prosthesis design is the load transfer to the proximal portion of the femur. In this study the most proximal portion of the femur was not scanned and a rotation method had to be used to model this critical region. The primary goal of this study was to develop a Computed Tomography Data Analysis Program that could take a CT data files as an input and output a 3-D finite element file of femur with a prosthesis. Since the most proximal portion of the femur was not scanned there was no choice but to used a method to simulate this section of the femur. Future scans should include the proximal portion of the femur so that the actual bone geometry and bone density in this area can be modeled.

The cancellous bone was modeled as having an uniform Young's modulus. This method of assigning properties to the cancellous bone was chosen so that the results could be compared directly with the results from Chang (1994), who used the same CT data files and cancellous bone properties. Since this portion of the femur bone makes contact with the interface layer (cement/porous coating) its properties greatly effect the load transferred to the cortical bone. In future models the properties of cancellous bone should be inputted based on the CT values either using the relationship between density

and Young's modulus developed by Carter and Hayes (1977), or the relationship developed by Rho et al., (1995).

All elements in the model were linear elastic, homogeneous and isotropic. Ideally bonded surfaces were assumed for all interfaces. The use of linear elastic, homogeneous and isotropic elements for the prosthesis and bone is the standard modeling assumption found in the literature (Harrigan and Harris 1991, Keaveny and Bartel 1993 a,b and 1994, Skinner et al., 1994, Huiskes and Van Rietbergen 1995, Mann et al., 1995). However, the interface layer has been modeled in the literature using non-linear gap elements, elements with Coulomb friction and or shear-strain properties. The use of linear elastic, homogeneous and isotropic element properties with ideal contact was used for the interface elements for two reasons (1) this modeling technique requires the minimum amount of computer memory and run time, on the present NJIT computer system used to run ANSYS a model with non-linear properties would take an excessive amount of time to run and may exceed the user's allotted space and (2) this was the modeling assumption used in the study in which these results were compared (Chang 1994).

Only one load case was run of the finite element model. This load case was meant to simulate normal gait for a 154 pound patient. Loads were 2.6 times body weight. The load was represented by a single joint force and a single muscle force so the results represent a static stress condition and not the actual dynamic stress condition that occurs in the bone. The effects of stress shielding and the resulting bone remodeling were not considered.

In order for the ANSYS finite element program to run the node locations of some outer cortical bone elements have to be repositioned. For Case 1 and Case 2, 4 nodes of the 456 outer cortical bone nodes needed to be modified, on each model. In the finite element models created in this study, the elements were 15 degrees apart. In the previous models (Chang 1994) the elements were 22.5 degrees apart. The spacing of the outer cortical bone elements along a radial arc was 8.4 mm apart in this model and 12.6 mm apart in Chang (1994) model, at the locations in which the nodes were adjusted. Although, repositioning of the nodes was undesirable, the largest required movement was less than 1.4 mm. This number is small compared with the spacing between cross-sections (10 mm) and is less then the increase in the overall resolution of the model (8.4 mm from 12.6 mm). Therefore, this required repositioning will have a minimum effect of the results and is within the overall accuracy of the model's mesh.

Convergence runs performed on a linear elastic, homogeneous and isotropic model of the femur with prosthesis using elliptical cross sections showed that at even at a much larger model size than the single layer cortical bone model used in this study, convergence is not reached. Two methods were used for checks of convergence of the simple elliptical model. The first method compared the maximum equivalent stress obtained from an individual model to the estimated maximum equivalent stress, considering the effect of discretization error, as predicted by the FEA solver (ANSYS). The second method compared the maximum equivalent stress predicted for each of the models. The maximum equivalent stress along the medial and lateral outer surfaces of the prosthesis, and the maximum equivalent stress along the medial outer surfaces of the

femur bone were the locations chosen to estimate convergence. The calculated stresses were very sensitive to the number of radial elements in a cross-section. Since a single layer was used to model the interface, cancellous bone and cortical bone in this study, the validity of the stress results may be suspect. The "single layer" model mesh was based on the model size used by Chang (1994), and therefore, comparison of results to that model is valid.

The maximum tension stress in the cement determined in this study 1.6 MPa and 1.8 MPa, for Case 1 and 2, respectively, are within the fatigue strength of the cement (8 - 10 MPa). The von Mises stress in the cement was 7 MPa which is very close to the fatigue limit. One must also keep in mind that the most strenuous load case possible was not used (Bergmann et al., 1995). Therefore the actual stresses in the cement may be higher then those reported here. The stress observed in the cancellous bone were all very low. This is a direct result of the low Young's modulus associated with the cancellous bone (1,000 MPa). The lowest Young's Modulus used for the cortical bone was 3,556 MPa and 2,927 MPa for Case 1 and Case 2, respectively. Therefore, between the cancellous bone and cortical bone there was a step change in modulus as opposed to a smooth transition. In the actual bone there is probably a smoother transition then the one modeled.

A comparison of the stress levels in the cortical bone without prosthesis was not performed, so the degree of stress shielding that may be induced by the prosthesis was not reported.

The stress levels in general were greater for the female case (Case 2) then for the male case (Case 1). However, the actual body weights may not have been the same as assumed in the model. The loads applied to the model was based on body weight and the same body weight was used for both cases. If the female patient weighed less then modeled the resulting stress levels would have been lower then reported. The Young's modules for the cortical bone of the male case ranged from 3,556 to 24,724 MPa. The Young's modules for the cortical bone of the female case ranged from 2,927 to 27,194 MPa. It was surprising that the female case had a range of Young's modulus that was 15% larger then the male case and had the lowest and highest Young's modulus. It is unclear if this large range of Young's modulus is normal, or if it is due to the modeling method employed, or if it is an indication of a more progressive bone disease condition than observed in the male patient.

There was differences between the stress results of this study and the stress levels reported by Chang (1994) for the same CT data (Case 1). The exact size of the prosthesis used by Chang (1994) was not clearly defined. It is possible that the prosthesis used in this study was slightly larger, which would results in the higher prosthesis stresses observed, since stiffness is proportional to the radius to the fourth power. There were also modeling differences in the neck portion of the prosthesis which would effect the proximal stress levels. It is believed that the stresses reported by Chang (1994) were "mixed material" stress results and this would account for the other differences observed. All nodes in the model except for the nodes associated with the outer cortical bone layer and the prosthesis neck, and prosthesis inner layer are nodes that are shared by two

dissimilar materials. For example, the same node would be shared by a prosthesis element and a cement element, or by a cement element and a cancellous bone element, or by a cancellous bone element and a cortical bone element. Since these materials have different Young's modulus, the nodal stress is different for the different materials. In the post processing method employed in this study the stress levels at each node was obtained for each of the materials associated with that node, whereas, in the method employed by Chang (1994) only one stress level was outputted per node(a "mixed material" stress).

The software program developed by Chang (1994) required the user to have access to the following software packages: Hoops, C, FORTRAN, ANSYS and IDEAS. Since these software items do not come as a standard package it limited the portability and likely acceptance of this tool. The Computed Tomography Data Analysis Program created in this study only requires the use of two common software packages (Microsoft Excel and Math Soft Mathcad) and a finite element processor (ANSYS). This use of common software packages increases the acceptability of the program and makes it easier to update and maintain.

Chang's (1994) software program also required the user to type in long lines of code to access the program i.e. f77 ctfem2por2.F -lhoops -lsuntool -lsunwindow -lpixrect -lX11 -lxgl -lm -L/usr/openwin/lib. The user interface has been made simple by the use of a window base program with custom menu items and user input boxes.

In Chang's (1994) software program the user was required to call up each cross-section and choose an area to be processed. It required the user to manually record the location of the pixel defining the upper left corner point, and to calculate the width and

length between this pixel and the pixel defining the lower right corner of the area to be processed. This required a lot of user interfacing, was time consuming and therefore was not a "selling" point of the program. In the Computed Tomography Data Analysis Program an algorithm was written to quickly find the approximate center of the femur and the maximum area of interest without requiring the user to perform this task.

In Chang's (1994) software program the user had to select a minimum CT number to associate with the cortical boundaries of each cross-section by a trial and error method. The Computed Tomography Data Analysis Program automatically plots out the cortical bone boundaries, versus a range of CT numbers so that the user has a visual aid (see Figures 3,1 and 3.2) in selecting the CT number to use for each cross-section.

CHAPTER 5

CONCLUSIONS AND SUGGESTIONS

5.1 Conclusions

There were two objectives in this study. Both of which were met. The first objective was to develop a Windows based Computed Tomography Data Analysis Program to process CT data files of a proximal femur into a "3-D" finite element model with prosthesis. This was accomplished by creating a data analysis program that utilizes Microsoft Excel 5.0a (and it's Visual Basic Modules) and Math Soft Mathcad 5.0.

The program performs the following tasks: (a) the area of interest in the CT Scans are determine and ASCII "Text" files which can be read by Mathcad are created; (b) the cortical bone inner and outer boundaries versus various CT Numbers are automatically plotted for each cross-section, using Dynamic Data Exchange between the Excel program and a Mathcad program; (c) color displays of the area of interest for each cross-section are automatically plotted for each cross-section, using Dynamic Data Exchange between the Excel program and a Mathcad program; (d) the centers of the cortical bone as well as the inner and outer boundaries are calculated for each cross-section; (e) 3-D images of the inner and outer cortical bone boundaries are plotted; (f) a prosthesis is fitted into the cortical bone, based on the bone geometry and user inputs; (g) the nodes that define the geometry of the prosthesis, interface layer, cancellous bone and cortical bone, including the prosthesis neck are determined; (h) 2-D nodal boundaries for each cross-section are plotted as well as 3-D cortical bone and prosthesis outer boundaries; (i) the average CT Numbers of all of the pixels contained in each two dimensional element boundary is calculated; and (j) an ANSYS finite element input file is created.

The Computed Tomography Data Analysis Program has been designed to be very versatile and user friendly. A menu item was created in the Excel program which contains the programs modules in the sequential order in which the user needs to run them. Throughout the CT data analysis program the use of input boxes with default values has been incorporated. These input boxes allow the user to vary many parameters without needing to revise the source code. The following is a list of some of the parameters the user can vary: (a) the size of the CT data matrix; (b) the spacing between the pixels; (c) the spacing between cross-sections; (d) the number of cross-sections; (e) the relationship between CT number and density for the CT scanner being used (all of which allows this program to be used for a wide varied of CT data files from different CT scanners); (f) the prosthesis size relative to the size of the femur receiving the prosthesis in the medial-lateral and anterior-posterior planes at three locations; (g) the bone cut angle; (h) the prosthesis neck to shaft angle; (i) the location of the center of the prosthesis neck relative to the prosthesis stem; (j) the neck post diameter in the medial-lateral and anterior-posterior planes; (k) the neck post angle (items (f) through (k), allows the user to vary the prosthesis size and shape to optimize the resulting stress distribution); (l) the angular spacing between elements in the finite model; (m) the number of prosthesis, interface, cancellous and cortical bone elements in the model; (n) the interface thickness; (o) the prosthesis and interface material properties; (p) the joint force and trochanter muscle force to applied (items (l) through (p), allows the user to define the "mesh" of the finite element model and to easily vary the load cases to be applied to the model).

The second objective was to run the finite element models obtained from this program for the two cases studied, and to compare the results obtained with the previous

reported results for Case 1 (Chang 1994). There were differences in the stress results of this study and the stress levels reported by Chang (1994) for the same CT data (Case 1). These differences are believed do be due to the use of slightly different prosthesis shaped stems and the reporting of "mixed material" stresses by Chang (1994).

The von Mises stress in the cement was 7 MPa, for the load case modeled, which is very close to the fatigue limit. Since this is not the most strenuous load case possible, fatigue failure of the cement joint is a possibility.

The fact that, case 2 (the female patient) had a 15% larger range of Young's modulus then the male case may be an indication of a more progressive bone disease condition in that patient.

In summary, a method to create a three-dimensional finite element model of a femur with a prosthesis from CT data of the femur was developed. This method is useful in determining the resulting stress pattern that would be induced by a particular prosthesis, allowing one to optimize the prosthesis selection for a particular femur geometry and bone state of health. The method allows the determination of the material properties of the femur, i.e. density and Young's modulus, from the CT data. This method also allows the investigation of new prosthesis shapes and materials to be evaluated pre-clinically. One can also used this method to predict the expected failure mode and location. It can also be used as a evaluation tool to determine why a particular implant failed.

The main advantage of this tool is that an estimate of the stress pattern induced in the actual femur in which the implant is to be installed can be assessed prior to surgery, and an alternate implant can be chosen and analyzed if required.

5.2 Suggestions

In CT scans the bone geometry is normally typical of an arthroplasty patient but the material properties (density) are calibrated to represent average bone properties. It is suggested that during a CT scan, that two standards with known different densities be properly prepared and scanned also. These standards should be used to determine the relationship between CT number and density in place of the present method of assuming certain densities at certain locations.

The present program only allows the prosthesis shape to be varied as a function of the size of the bone in which it is being implanted. The program could be further enhanced by allowing the use of other prosthesis options, i.e. prosthesis with collars, prosthesis with different amounts of porous coatings, standard existing prosthesis shapes and sizes. The program could also be revised to allow the use of a distal tip with its own material properties.

A model containing the femur head geometry should be run to determine the stress levels in the femur without a prosthesis so that the degree of stress shielding can be determined.

The finite element modeling section of the program should be updated to allow the use of non-linear interface elements as done by Keaveny & Bartel, (1993 a,b and 1994), Huskies and Van Rietbergen (1995), and Mann et al., (1995). A bone adaptation model could also be incorporated into the solution phase as done by Weinans et al., (1994), Huiskes and Van Rietbergen (1995).

APPENDIX A

2-D NODE BOUNDARIES PLOTS FOR CASE 1

Node Plot
Cross- Section # 1

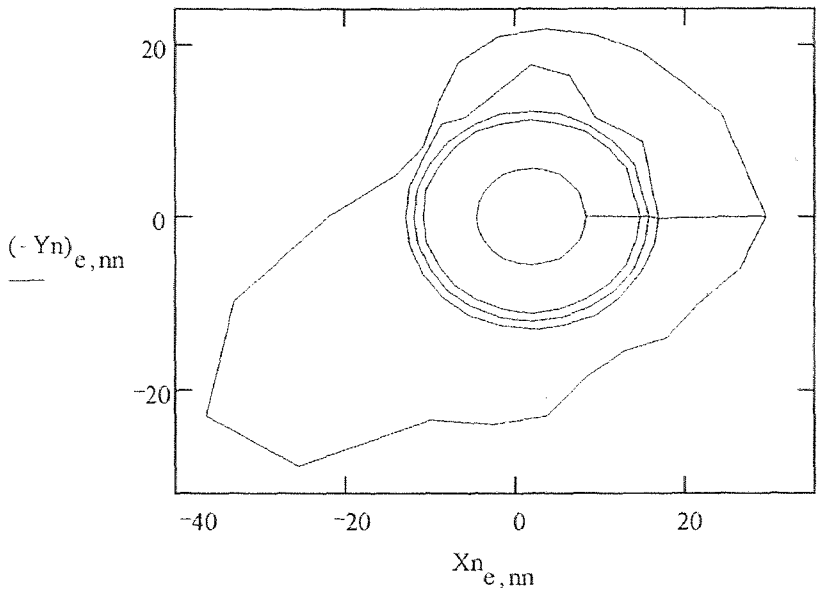

Appendix A1: Case 1; Cross-section 1; Node Boundaries

Node Plot
Cross- Section # 2

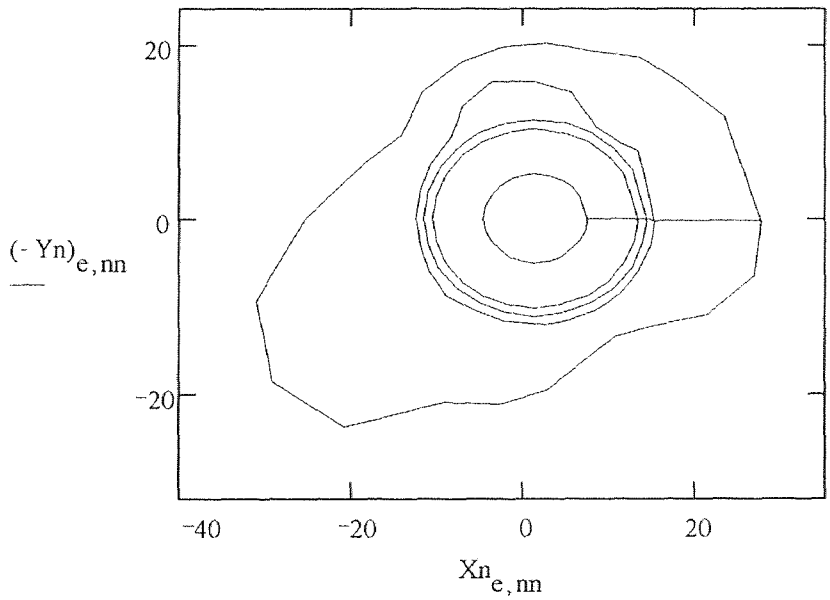

Appendix A2: Case 1; Cross-section 2; Node Boundaries

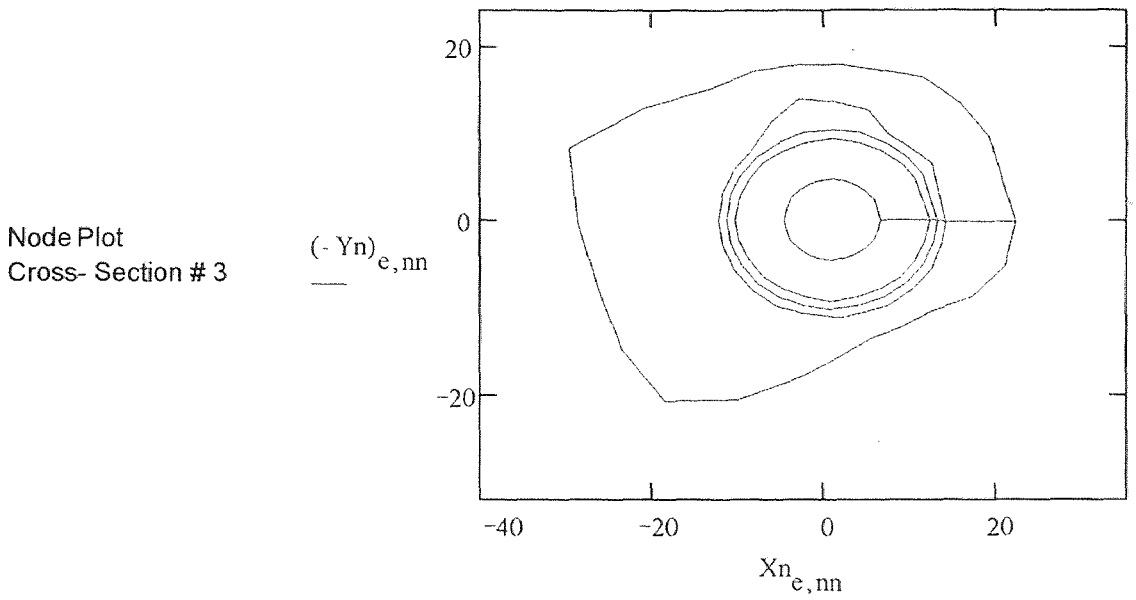

Appendix A3: Case 1; Cross-section 3; Node Boundaries

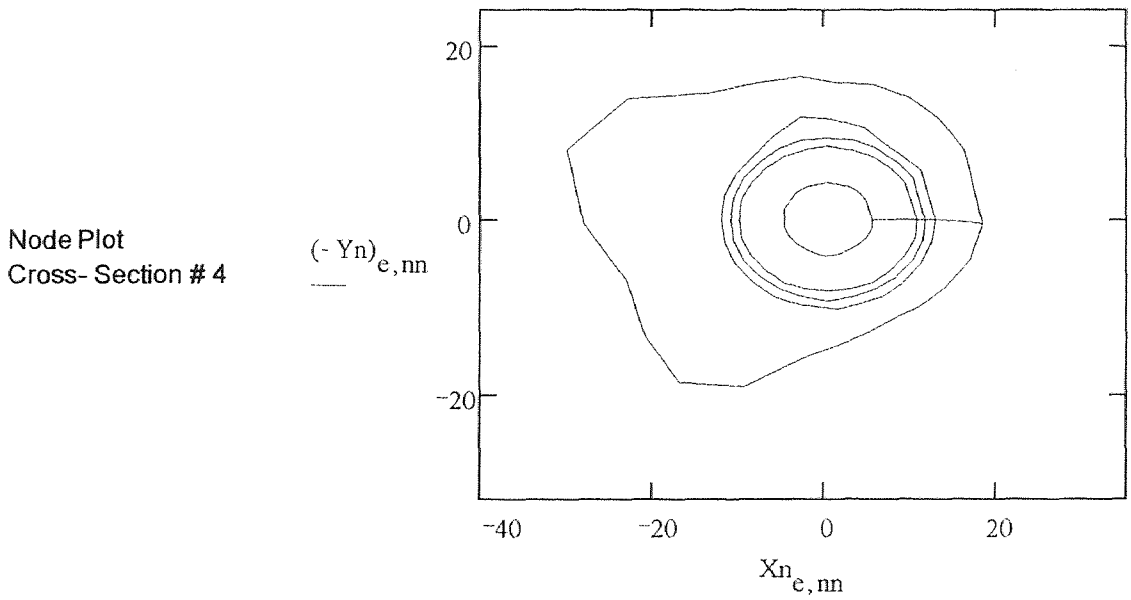

Appendix A4: Case 1; Cross-section 4; Node Boundaries

Node Plot
Cross- Section # 5

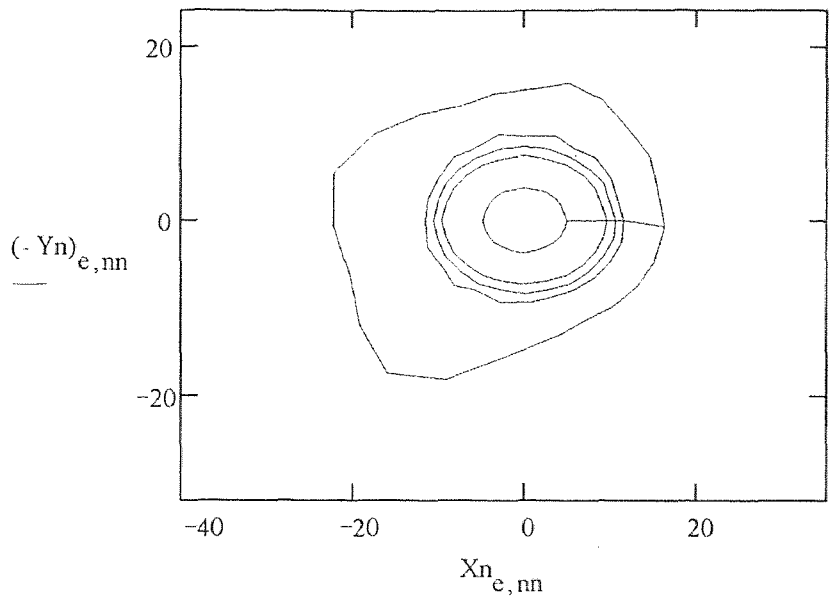

Appendix A5: Case 1; Cross-section 5; Node Boundaries

Node Plot
Cross- Section # 6

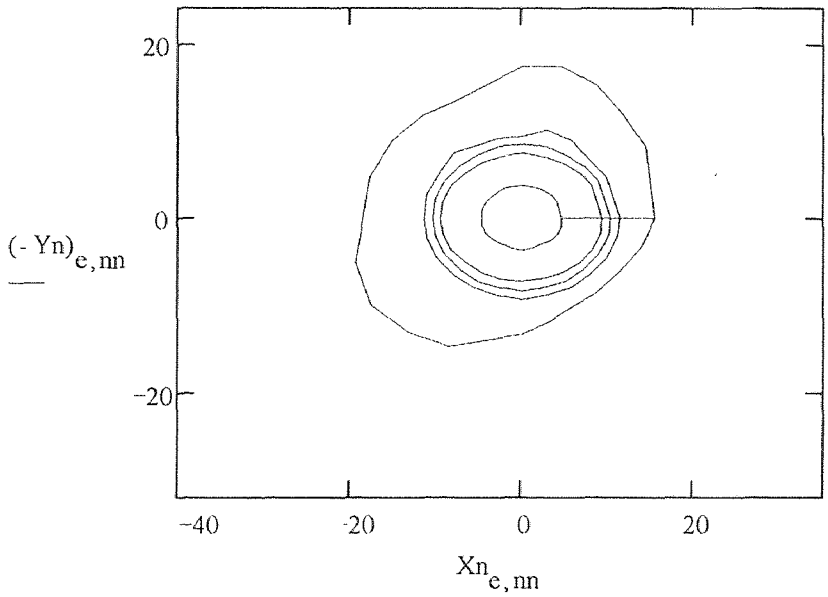

Appendix A6: Case 1; Cross-section 6; Node Boundaries

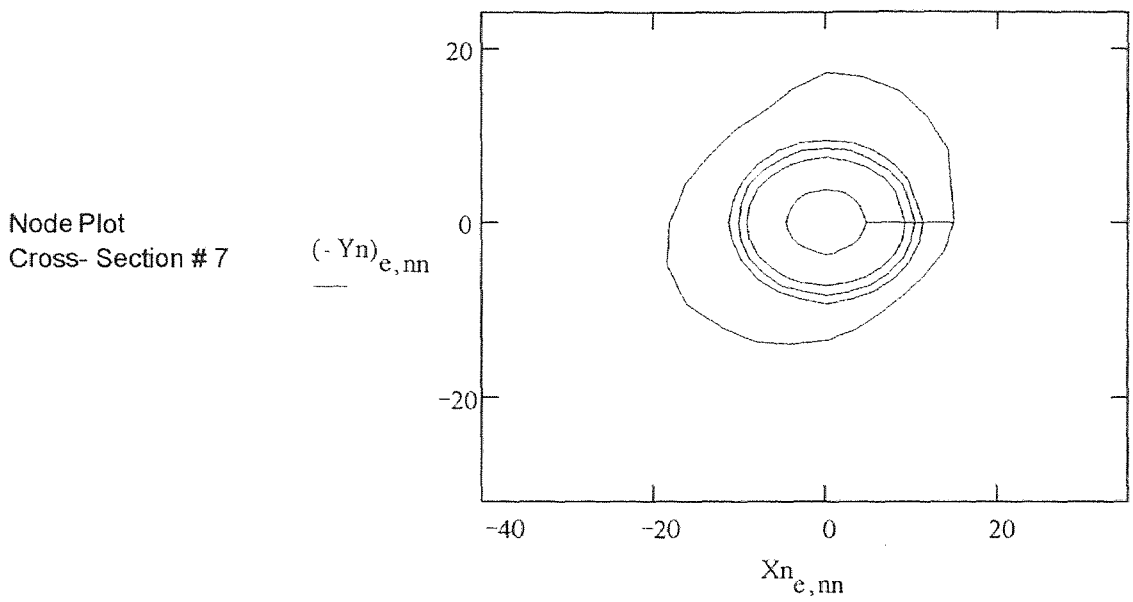

Appendix A7: Case 1; Cross-section 7; Node Boundaries

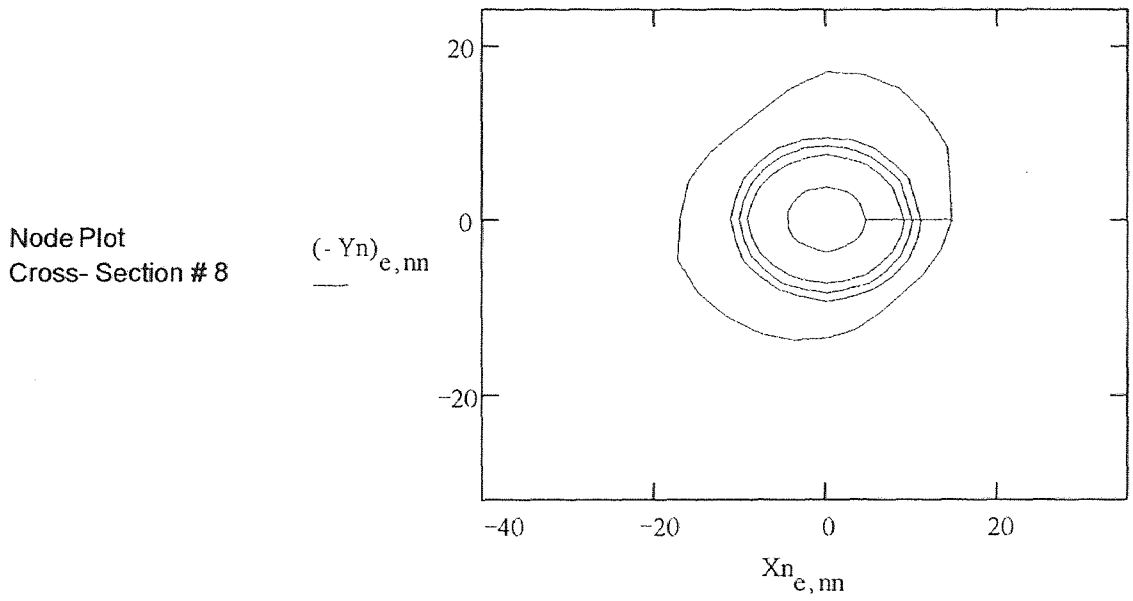

Appendix A8: Case 1; Cross-section 8; Node Boundaries

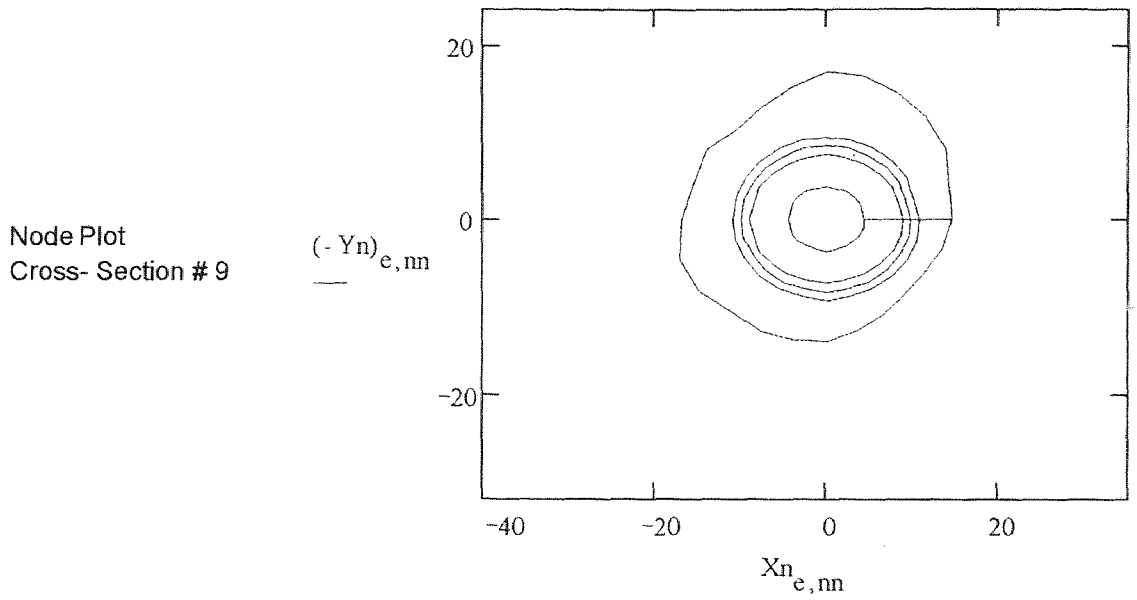

Appendix A9: Case 1; Cross-section 9; Node Boundaries

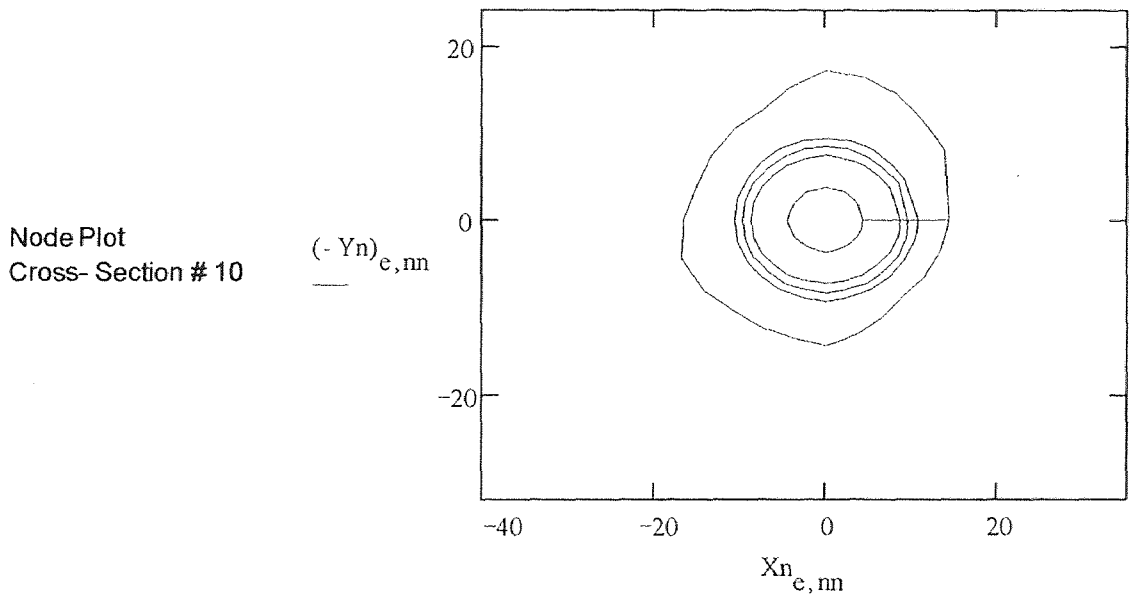

Appendix A10: Case 1; Cross-section 10; Node Boundaries

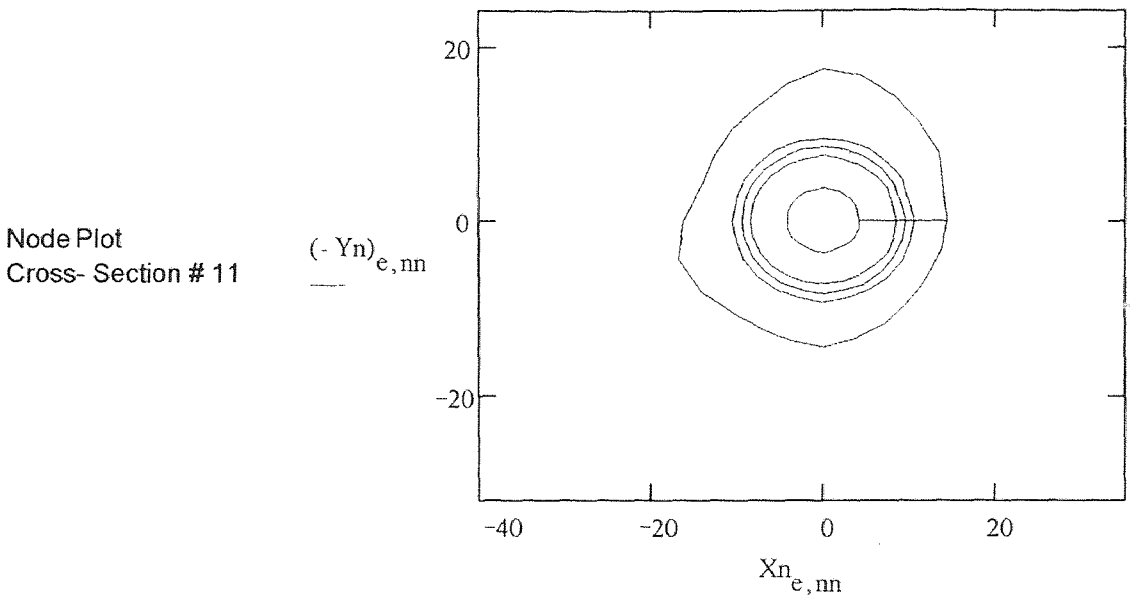

Appendix A11: Case 1; Cross-section 11; Node Boundaries

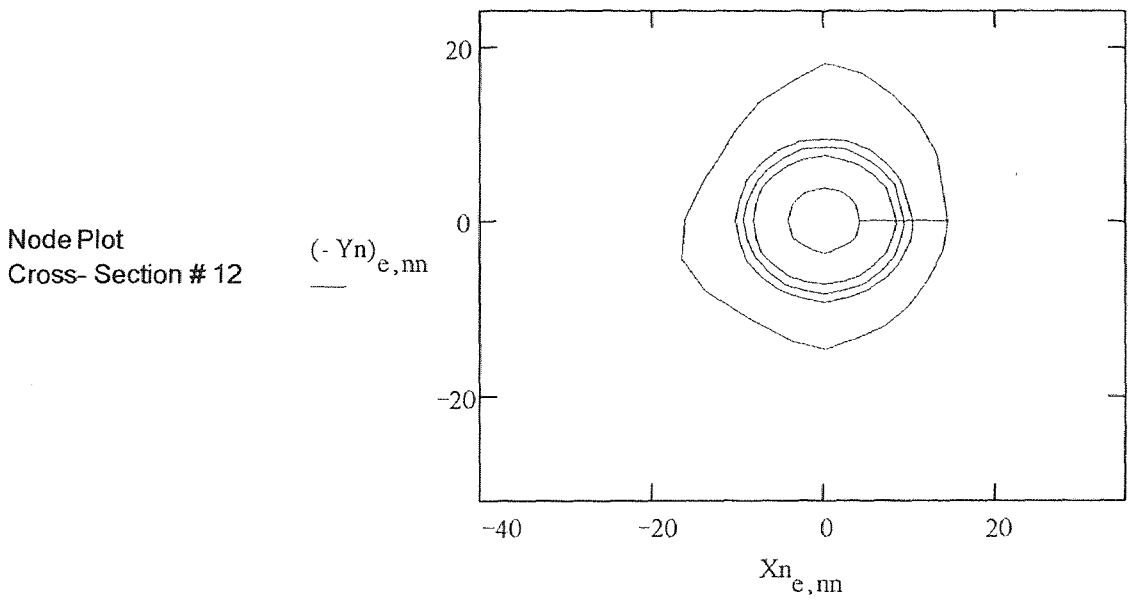

Appendix A12: Case 1; Cross-section 12; Node Boundaries

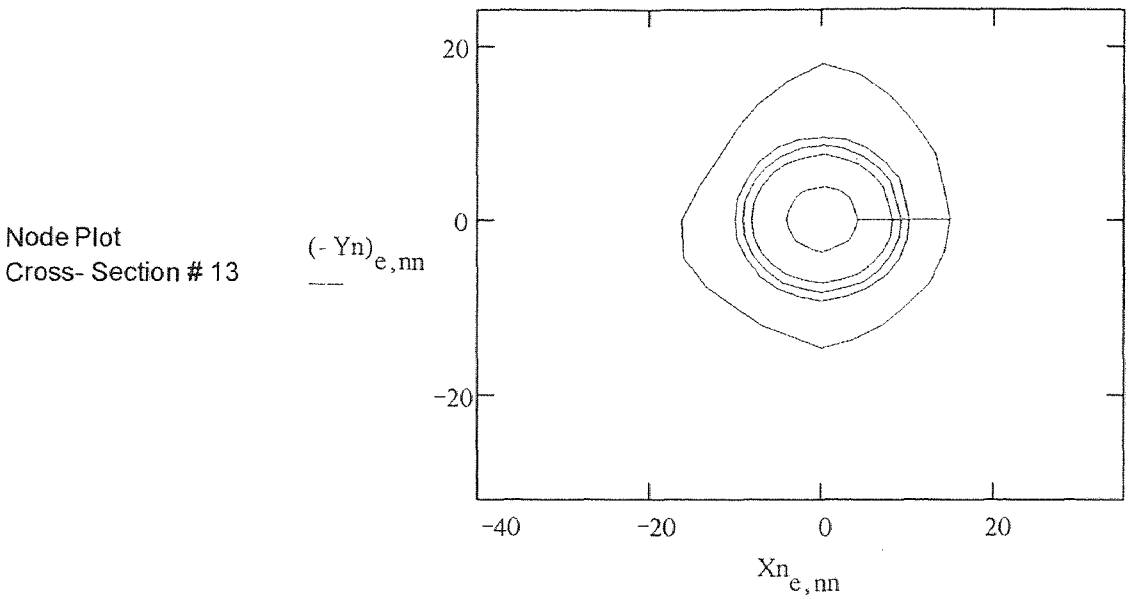

Appendix A13: Case 1; Cross-section 13; Node Boundaries

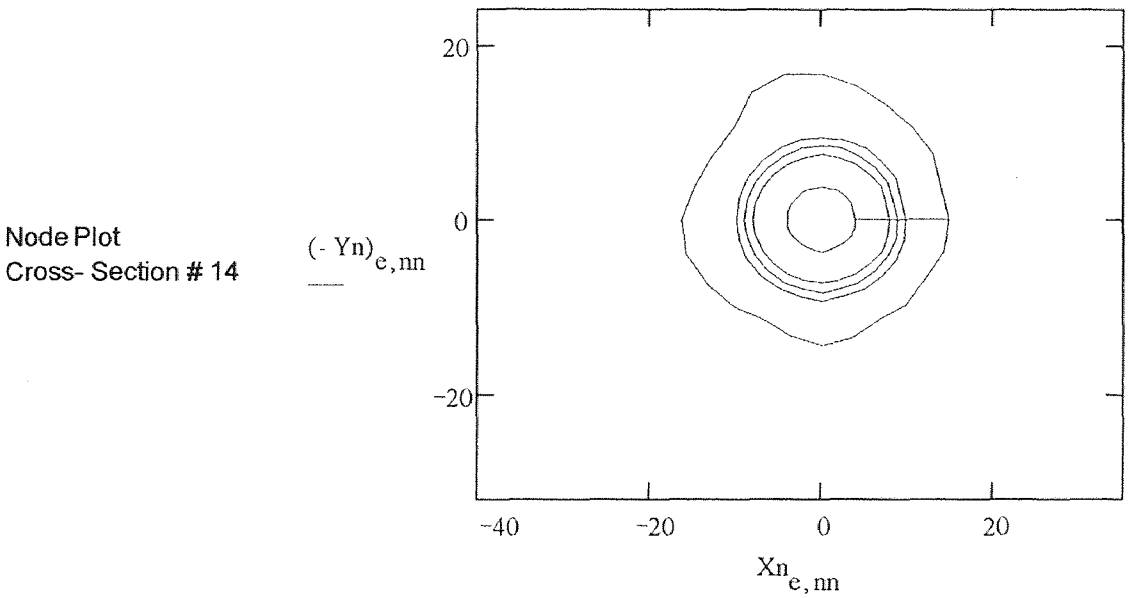

Appendix A14: Case 1; Cross-section 14; Node Boundaries

Node Plot
Cross- Section # 15

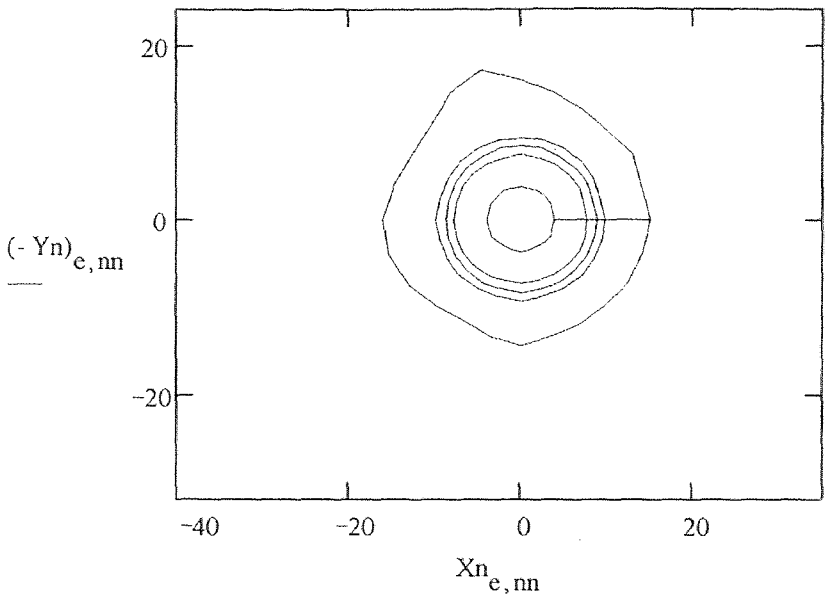

Appendix A15: Case 1; Cross-section 15; Node Boundaries

Node Plot
Cross- Section # 16

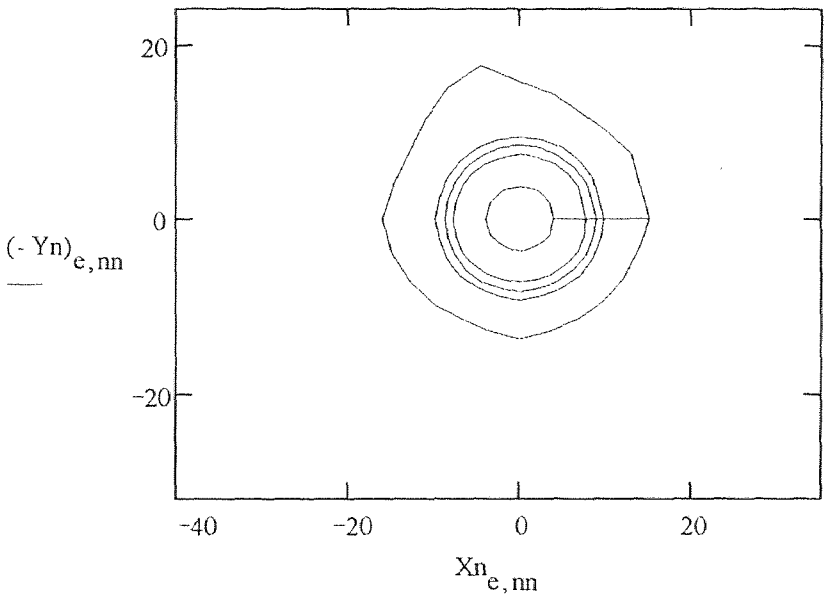

Appendix A16: Case 1; Cross-section 16; Node Boundaries

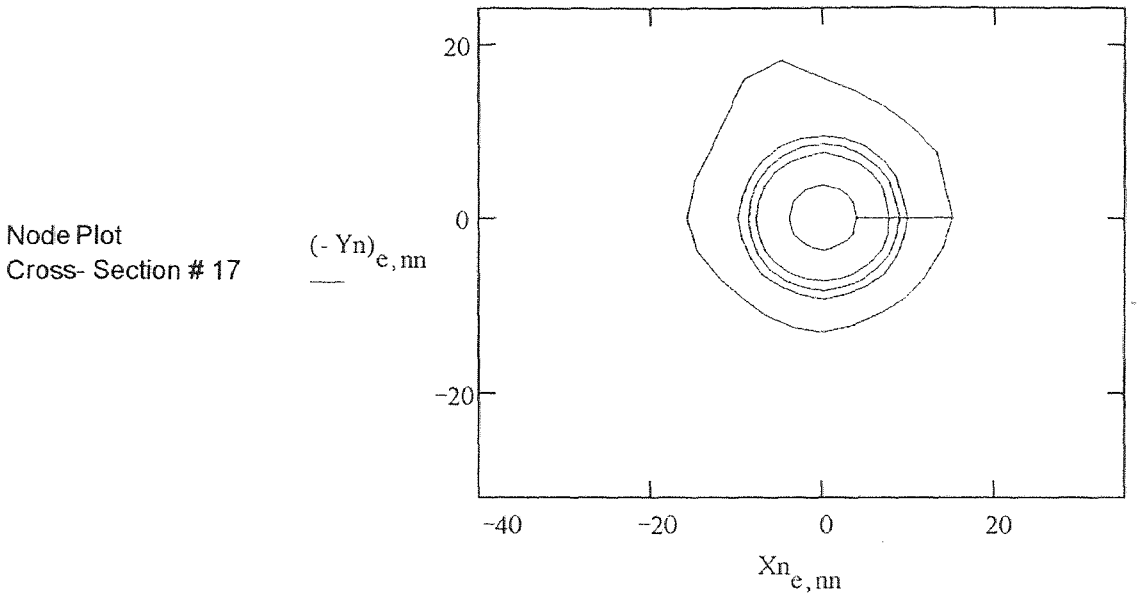

Appendix A17: Case 1; Cross-section 17; Node Boundaries

APPENDIX B
STRESS DISTRIBUTION OF FEMUR WITH PROSTHESIS

Lateral Side Along Prosthesis

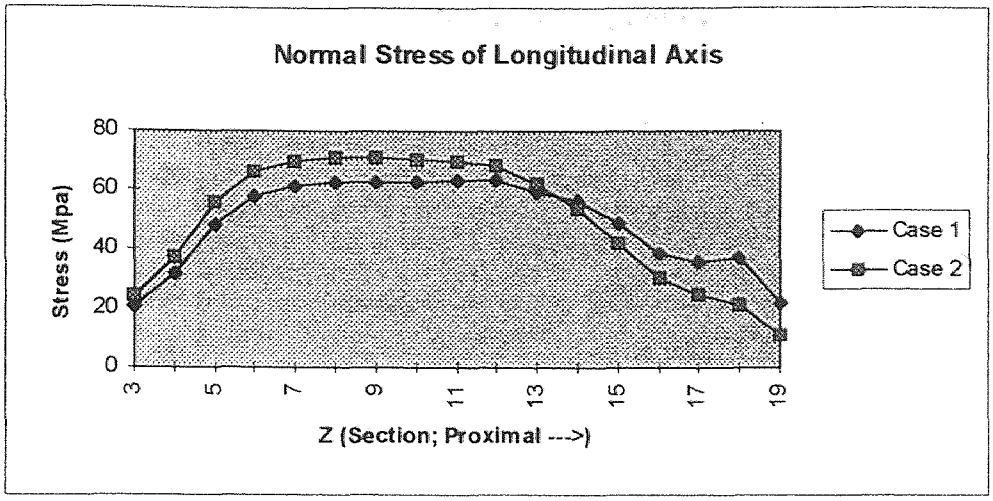

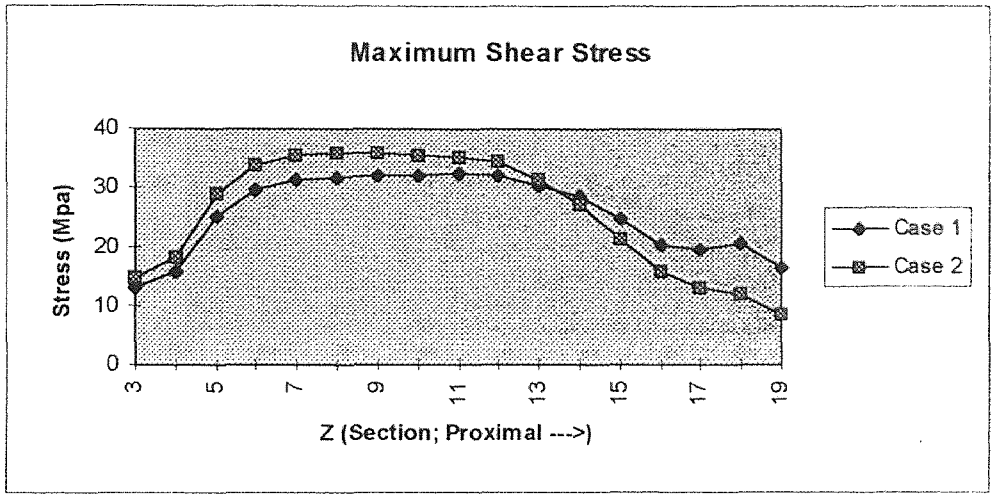

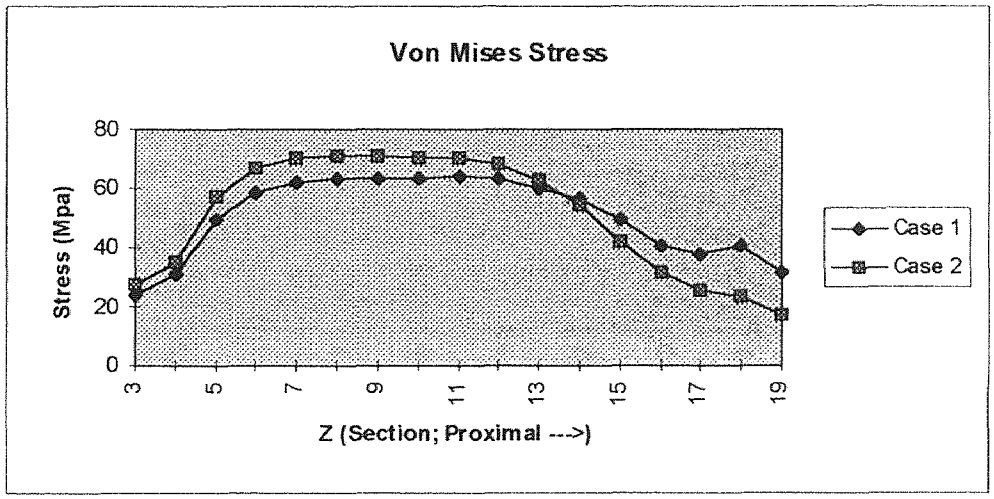

Appendix B1: The stress distributions of lateral side along prosthetic stem surface

Medial Side Along Prosthesis

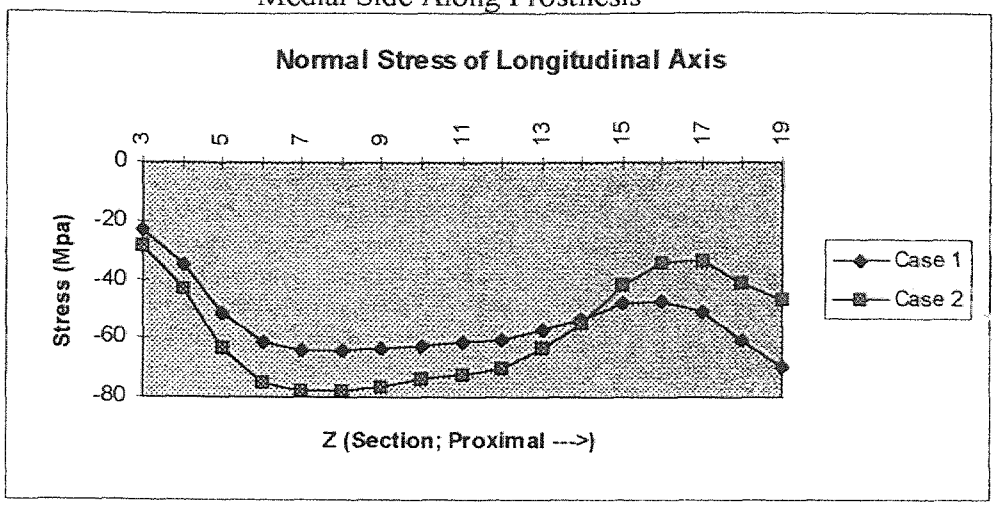

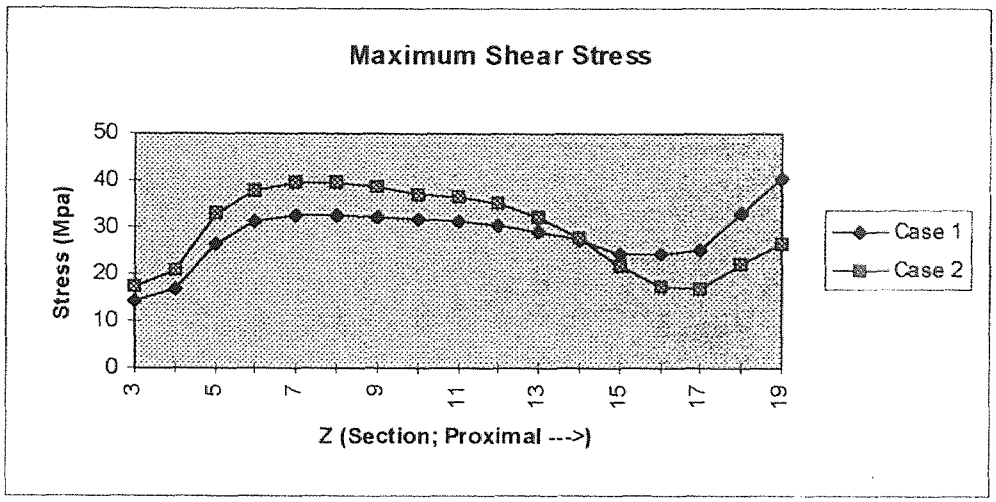

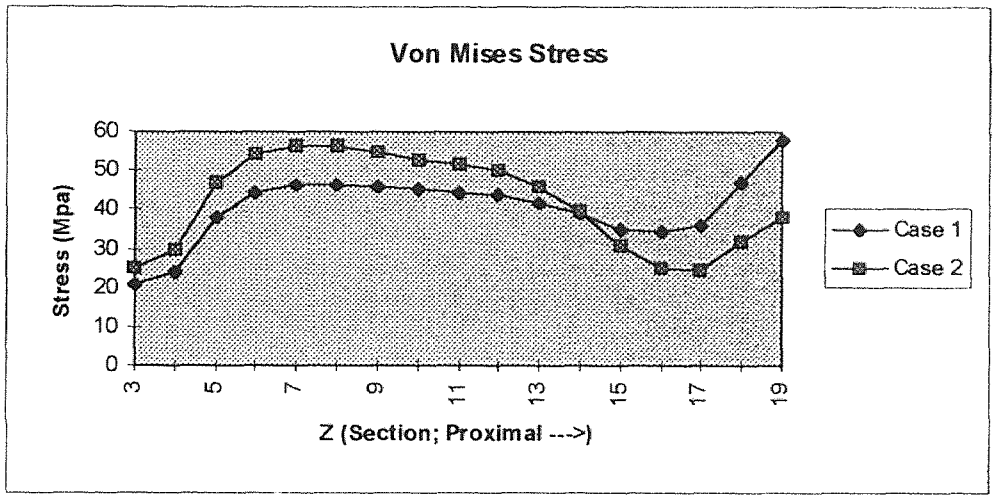

Appendix B2: The stress distributions of medial side along prosthetic stem surface

Lateral Side Along Interface (Inner)

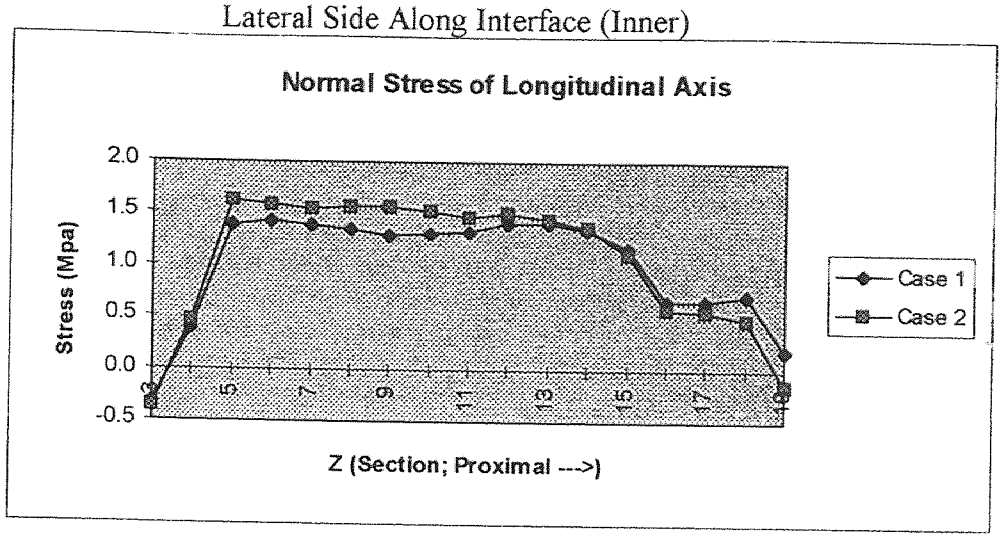

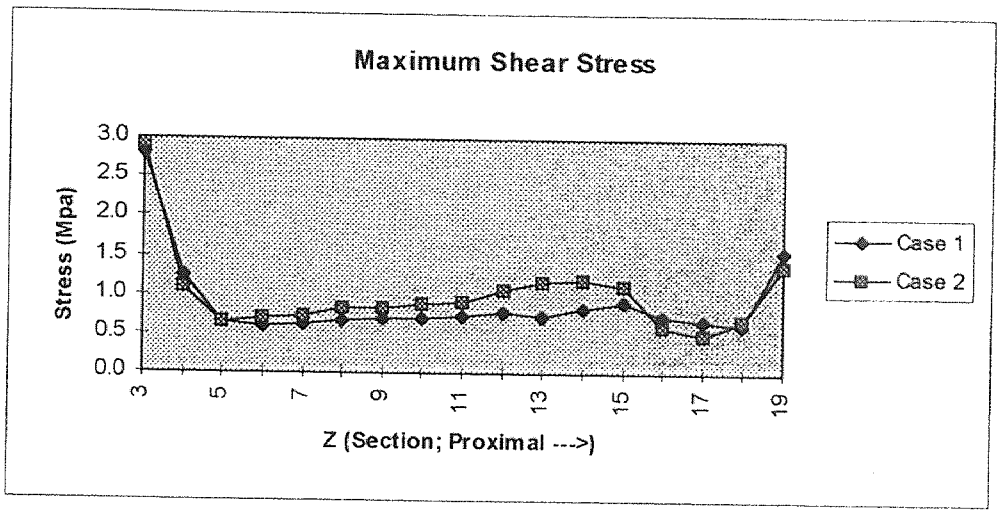

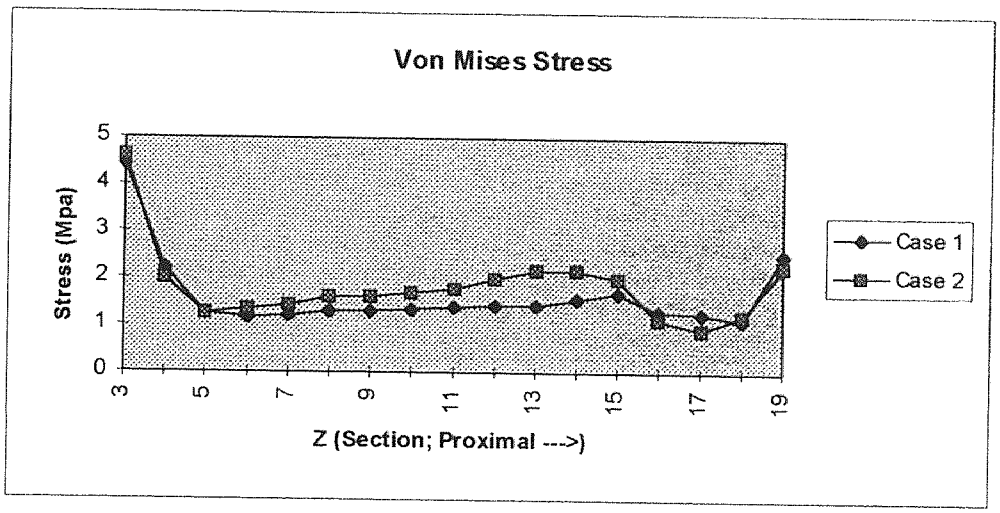

Appendix B3: The stress distributions of lateral side along Interface (Inner)

Medial Side Along Interface (Inner)

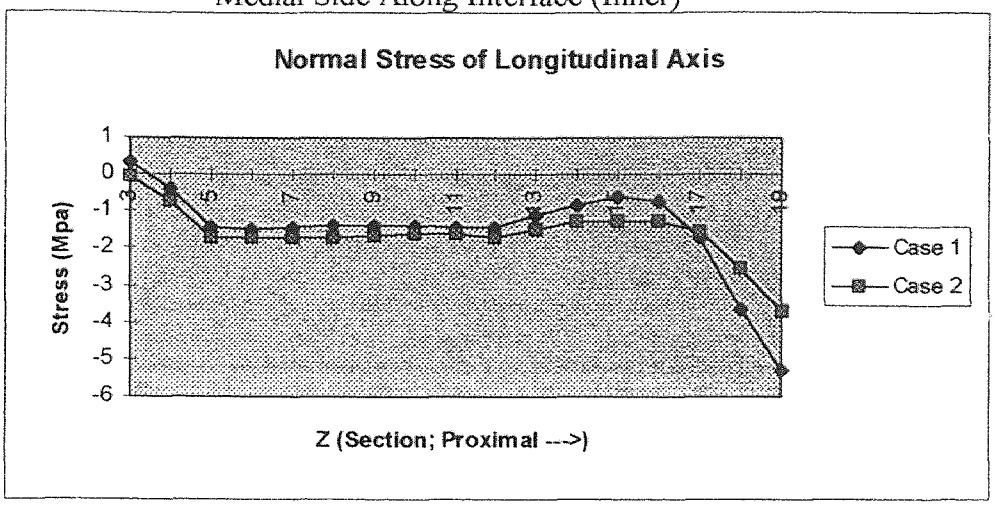

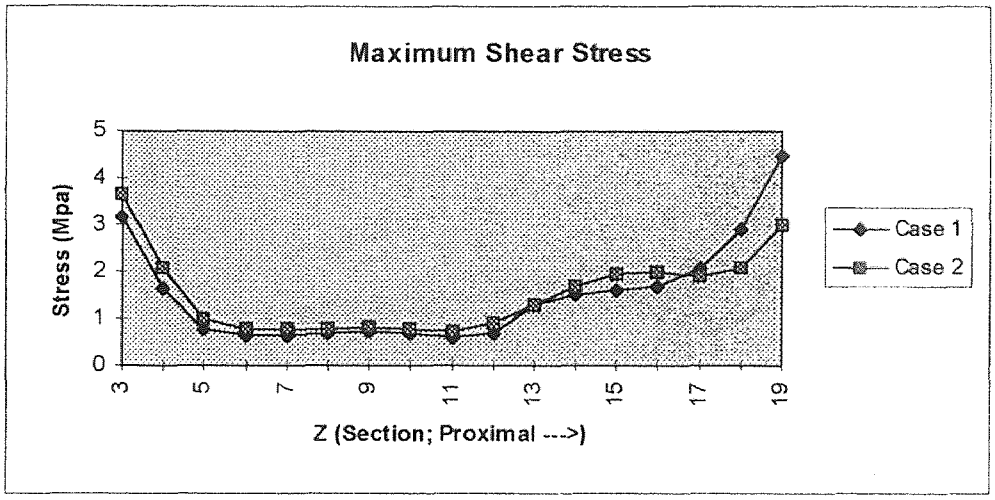

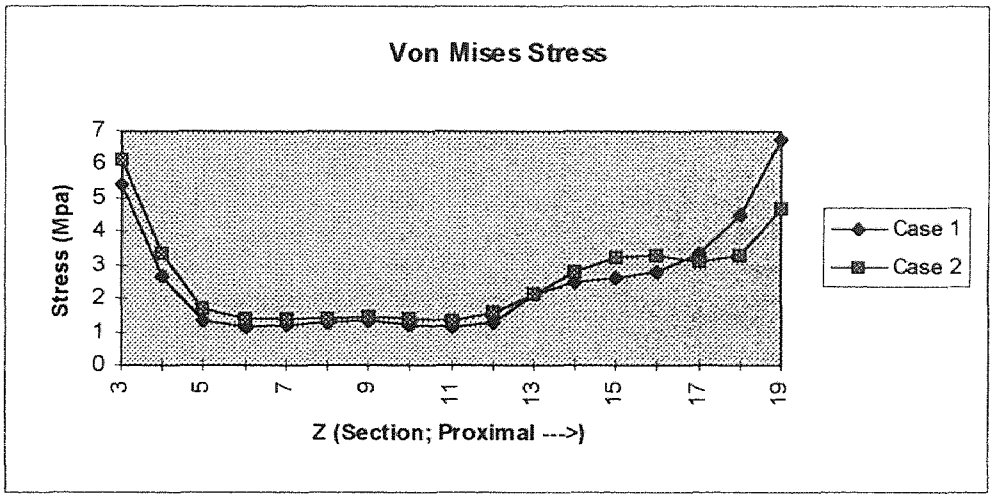

Appendix B4: The stress distributions of medial side along Interface (Inner)

Lateral Side Along Interface (Outer)

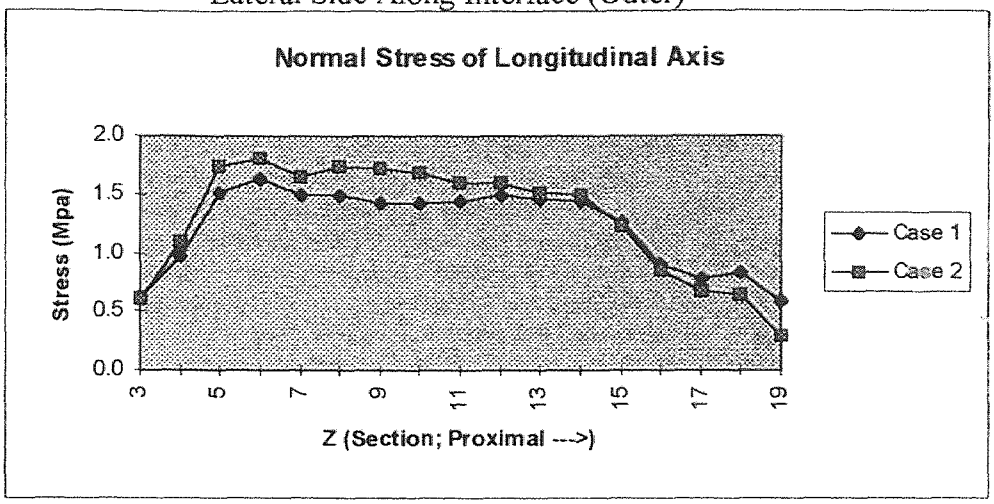

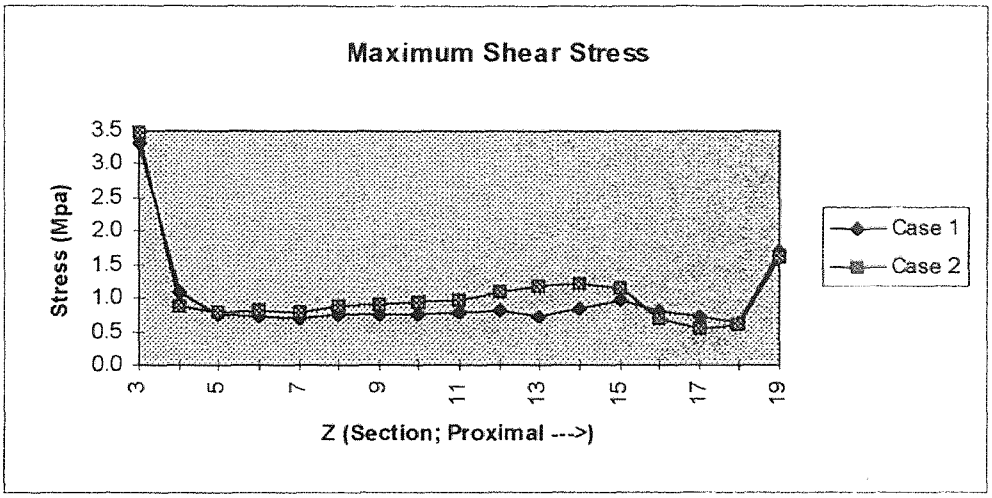

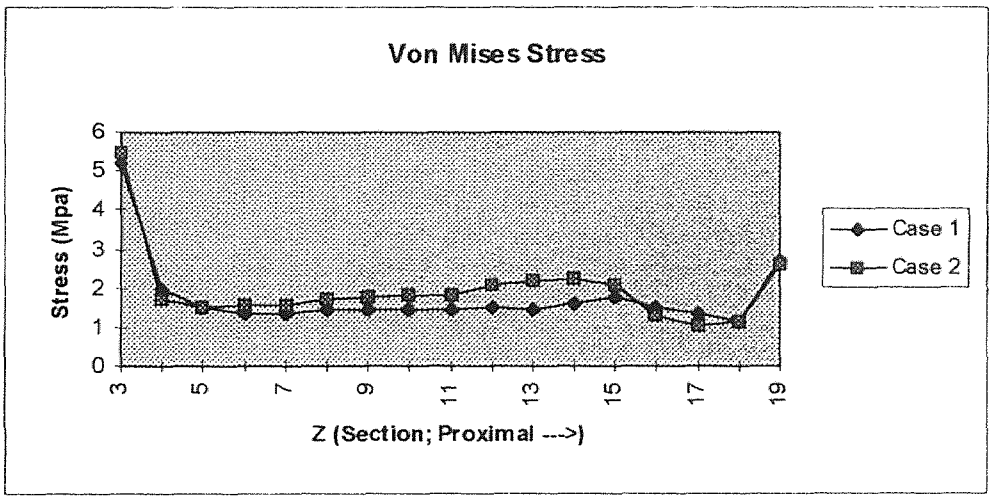

Appendix B5: The stress distributions of lateral side along Interface (Outer)

Medial Side Along Interface (Outer)

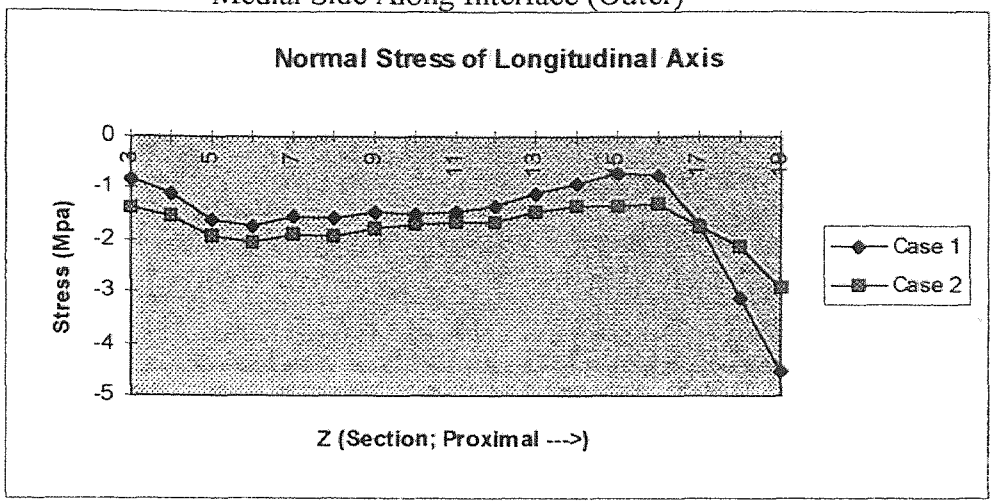

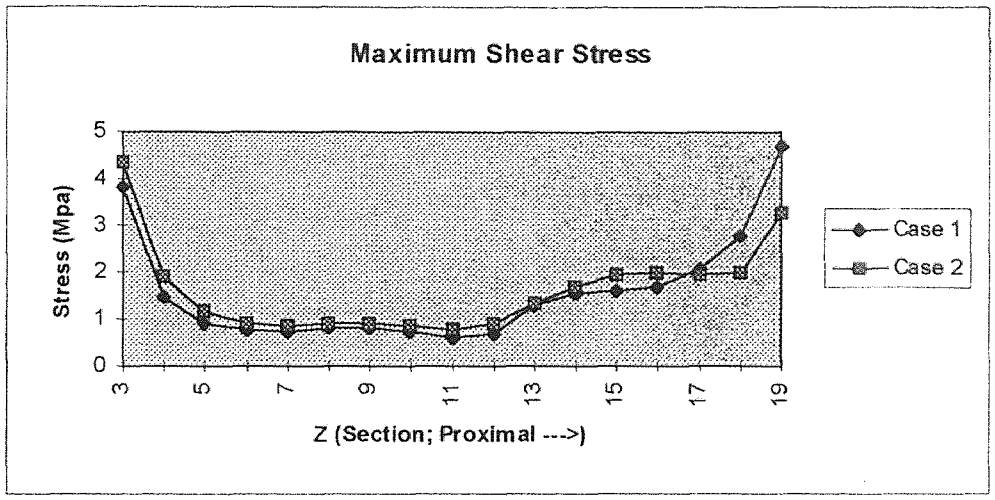

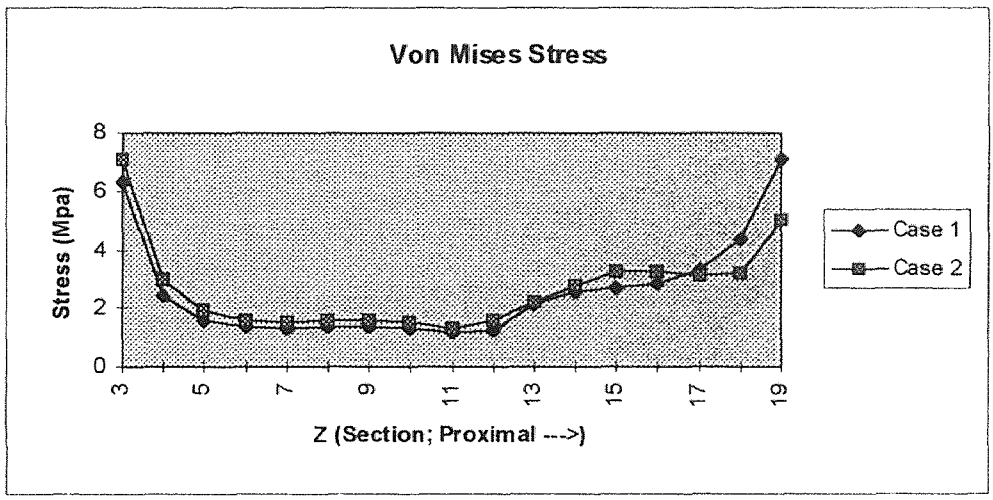

Appendix B6: The stress distributions of medial side along Interface (Outer)

Lateral Side Along Cancellous Bone (Inner)

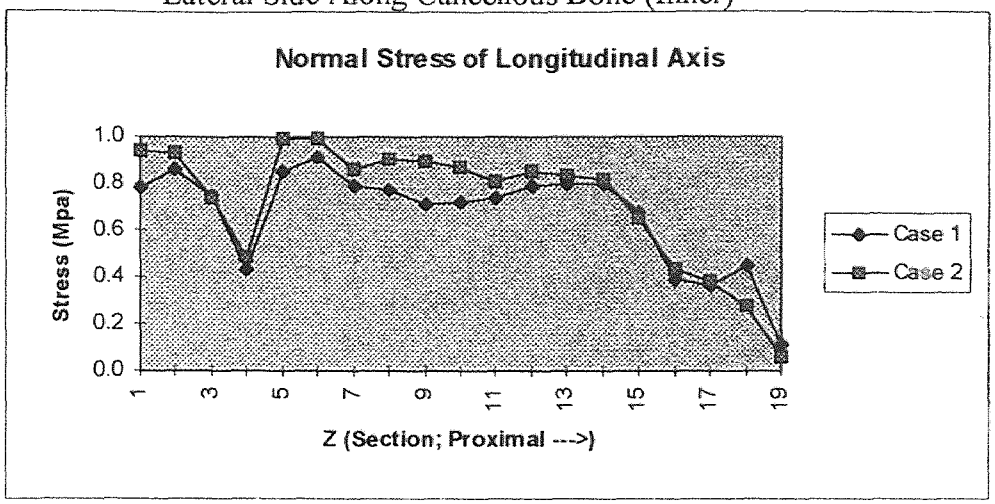

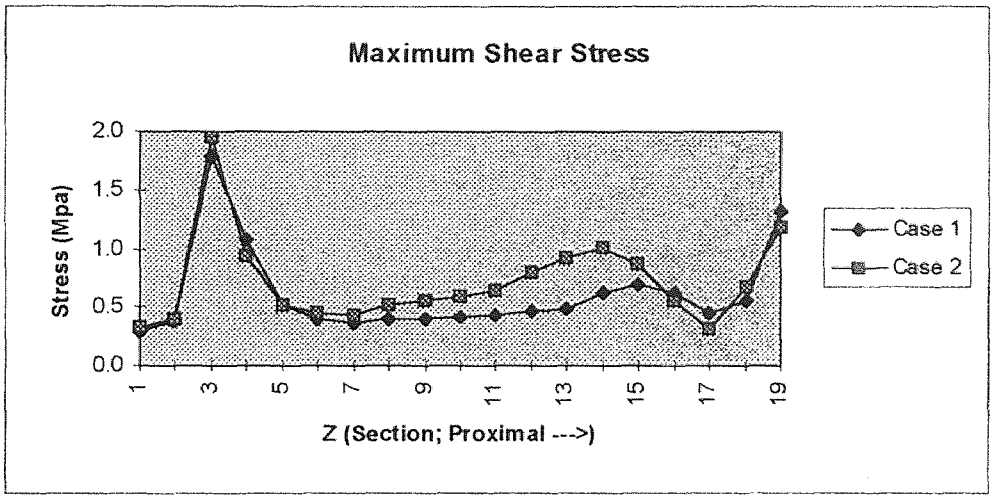

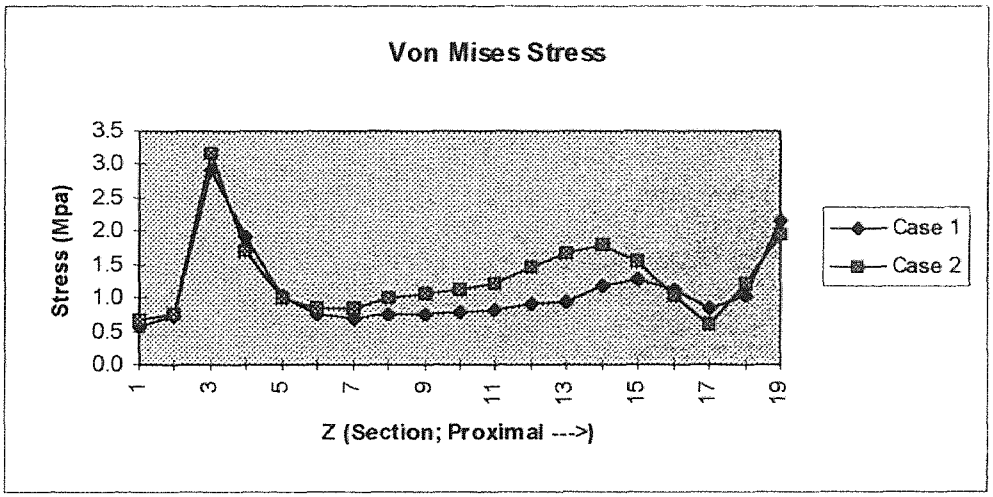

Appendix B7: The stress distributions of lateral side along Cancellous Bone (Inner)

Medial Side Along Cancellous Bone (Inner)

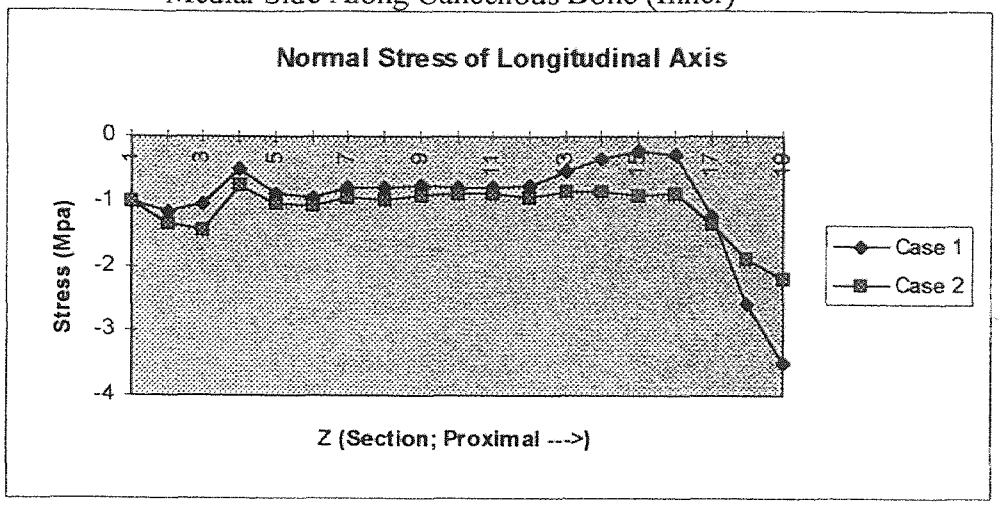

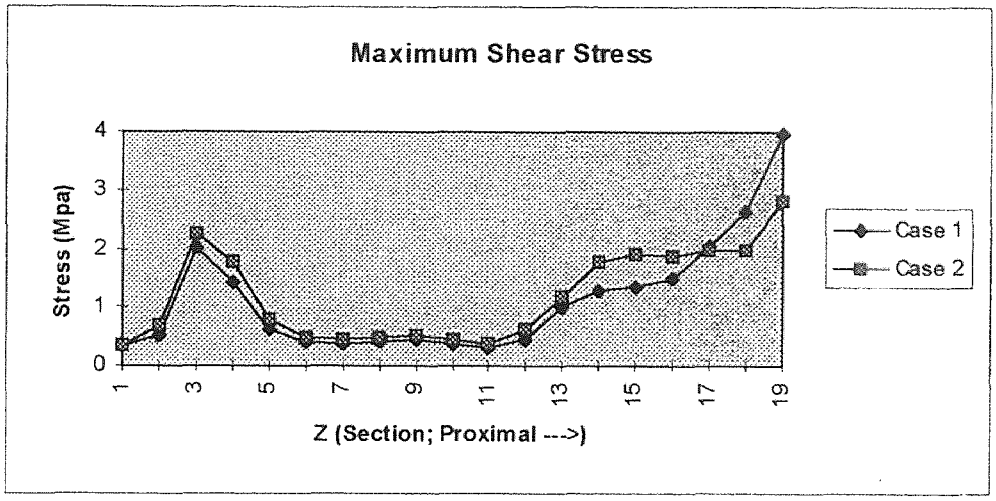

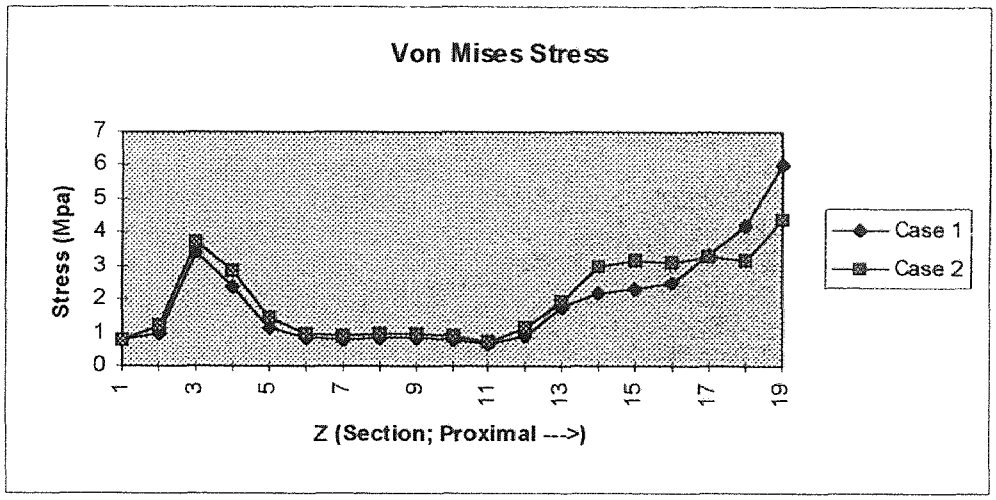

Appendix B8: The stress distributions of medial side along Cancellous Bone (Inner)

Lateral Side Along Cancellous Bone (Outer)

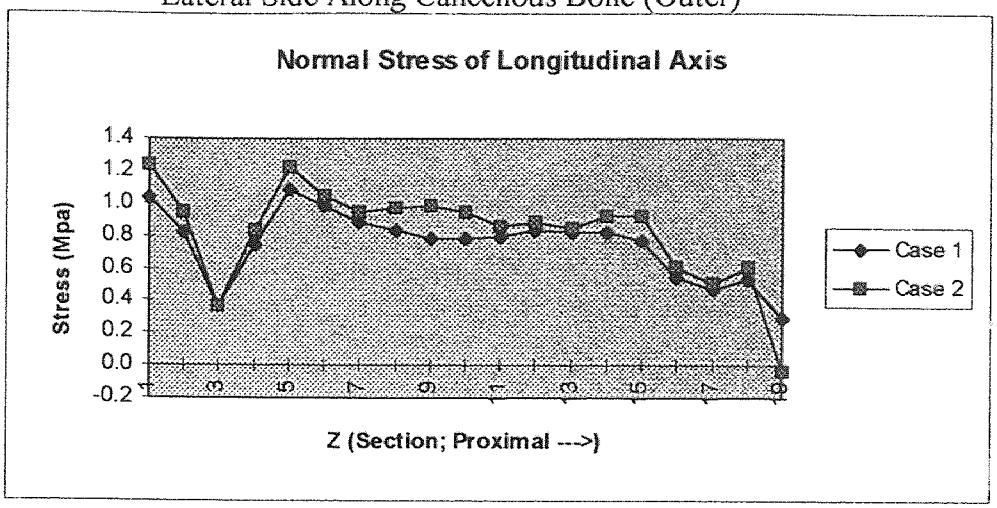

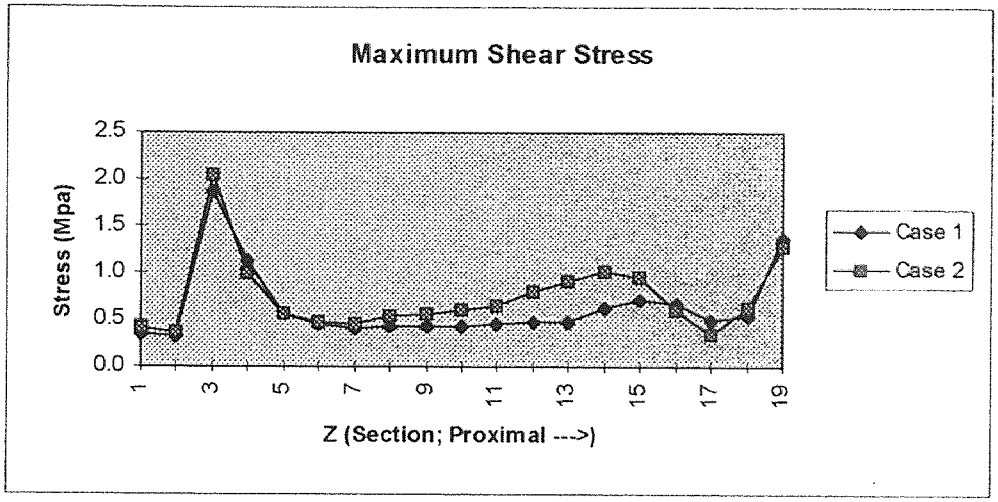

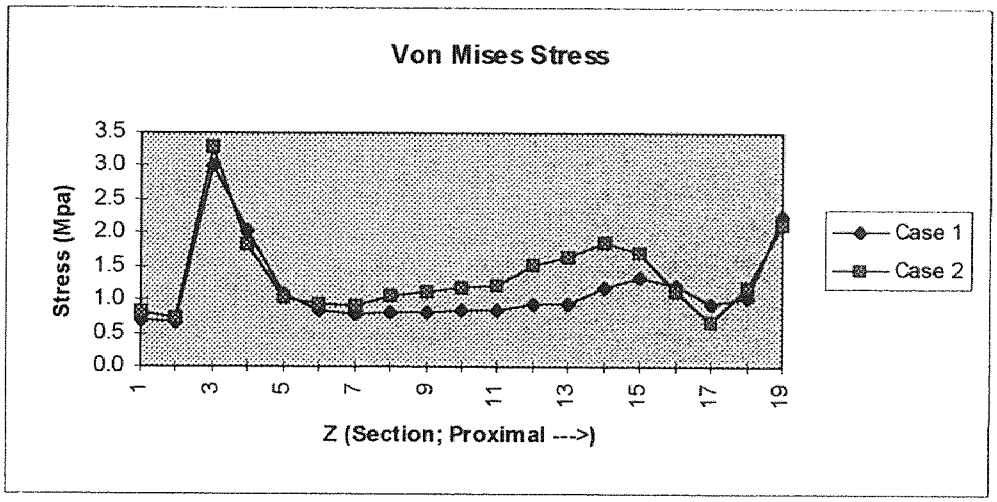

Appendix B9: The stress distributions of lateral side along Cancellous Bone (Outer)

Medial Side Along Cancellous Bone (Outer)

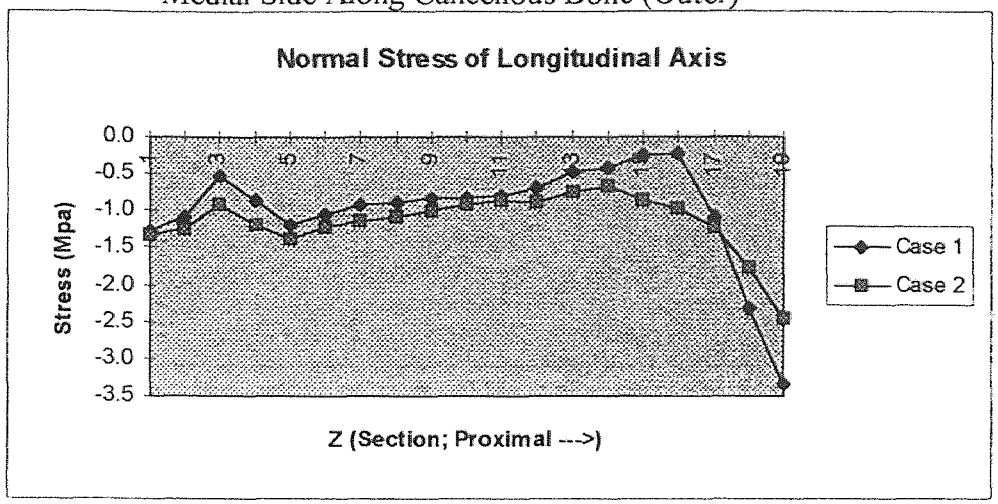

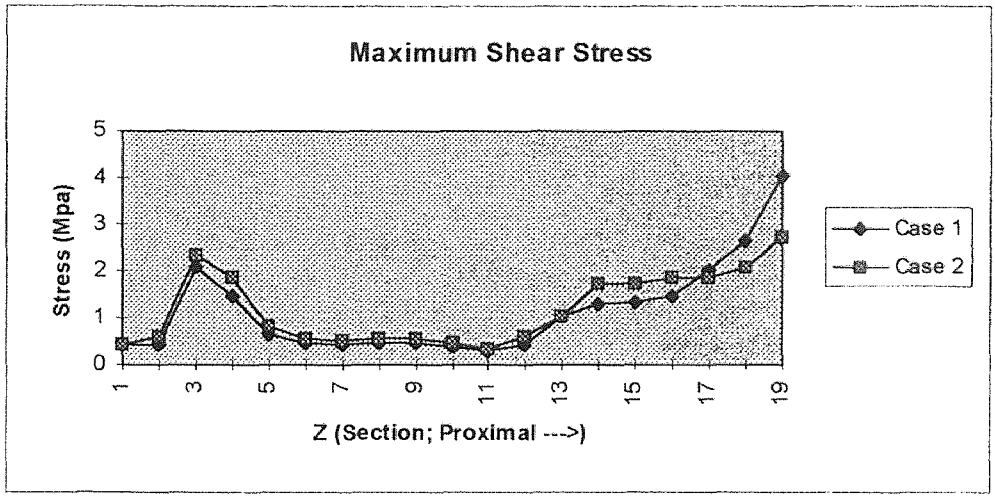

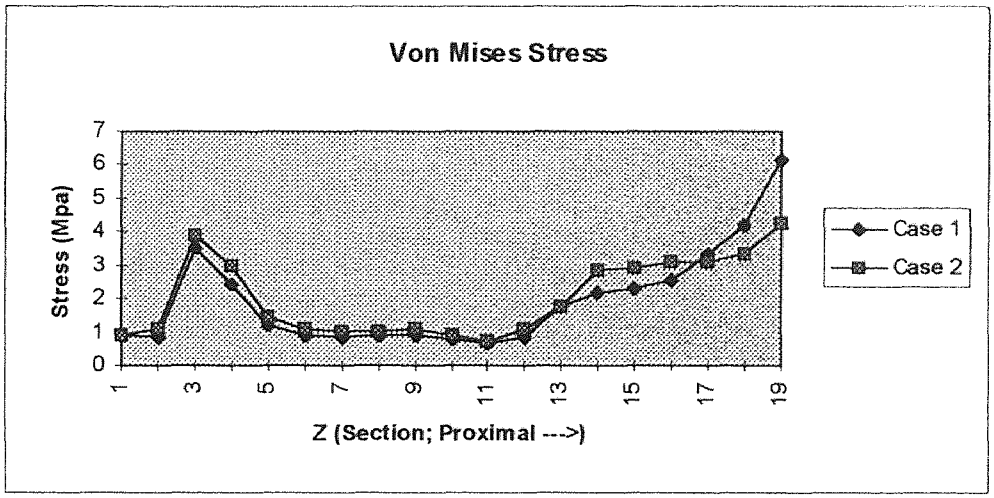

Appendix B10: The stress distributions of medial side along Cancellous Bone (Outer)

Lateral Side Along Cortical Bone (Inner)

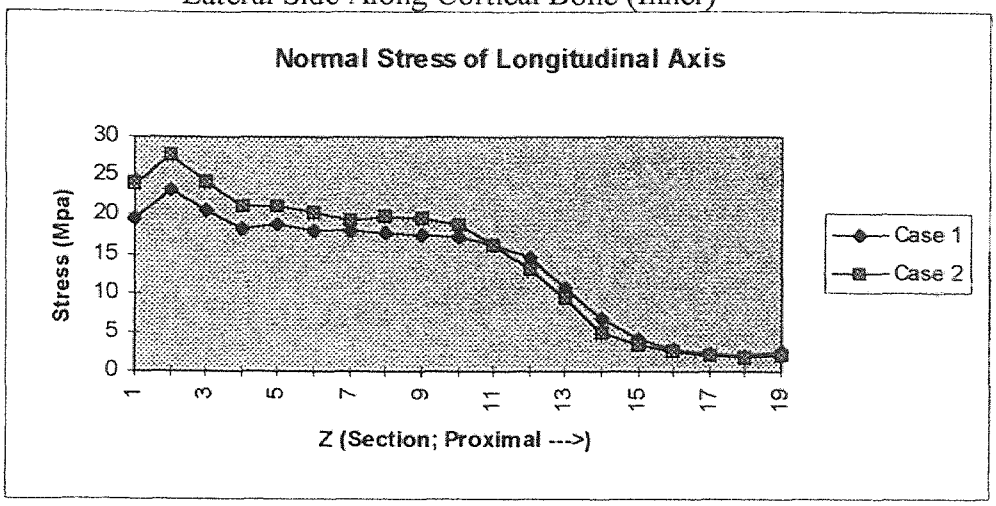

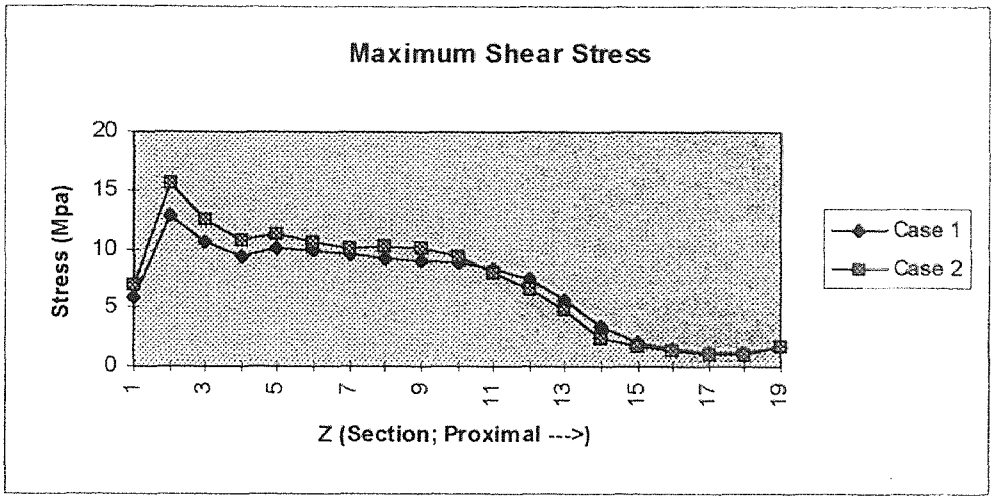

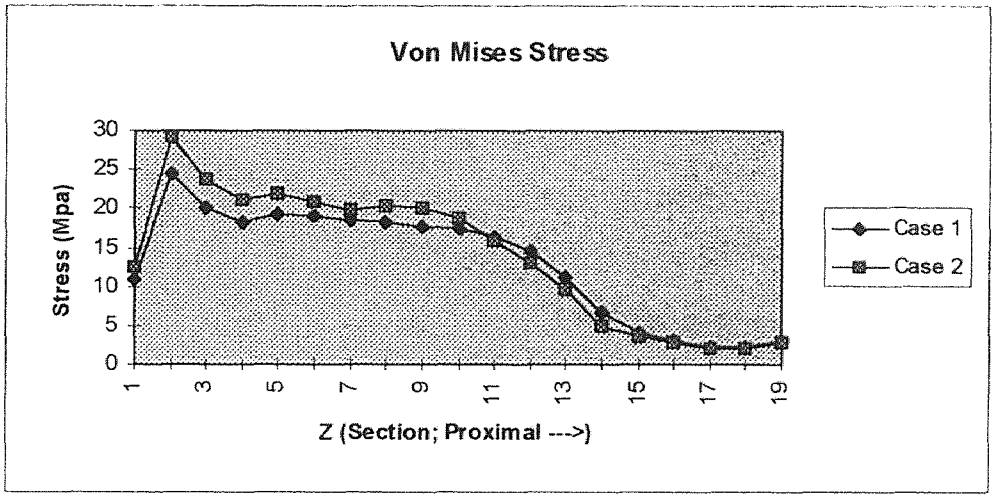

Appendix B11: The stress distributions of lateral side along Cortical Bone (Inner)

Medial Side Along Cortical Bone (Inner)

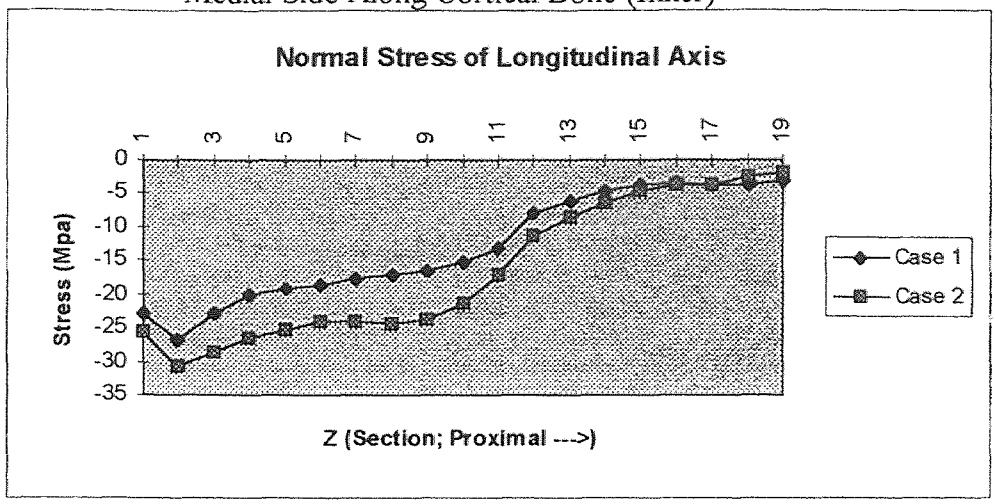

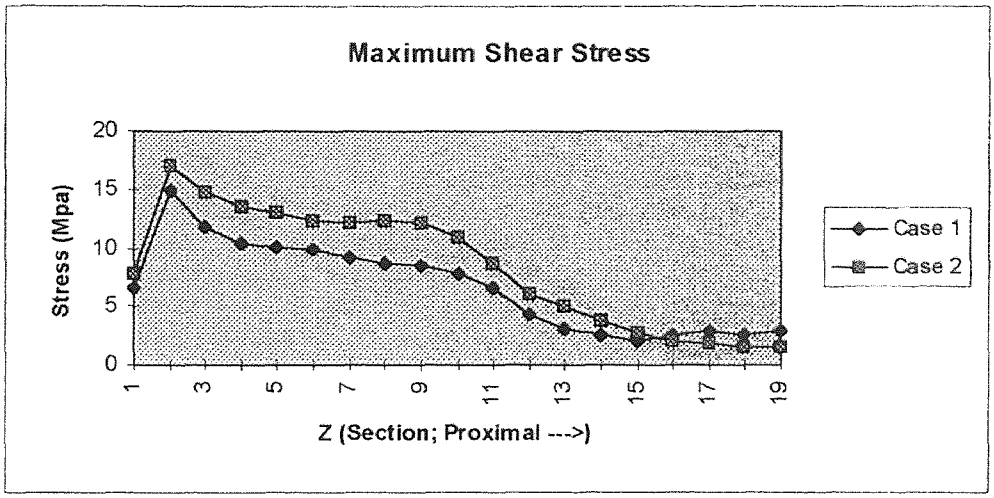

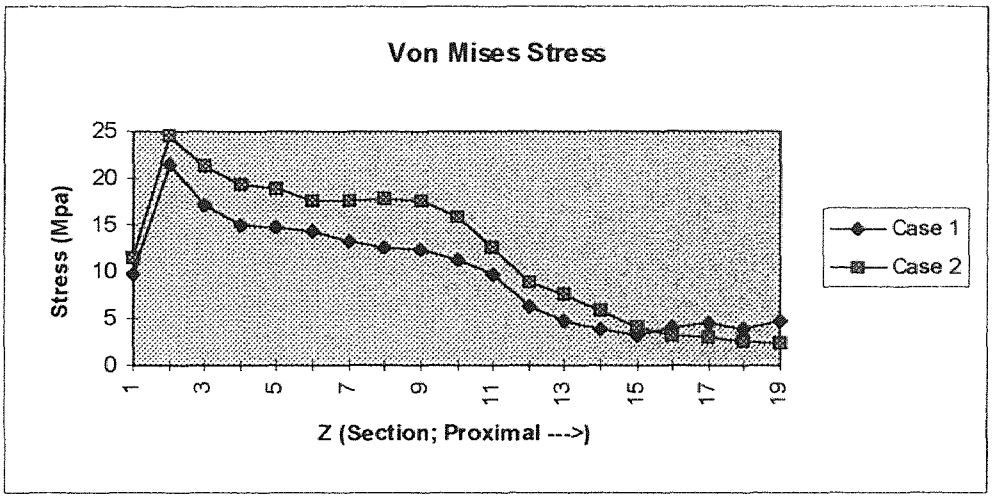

Appendix B12: The stress distributions of medial side along Cortical Bone (Inner)

Lateral Side Along Cortical Bone (Outer)

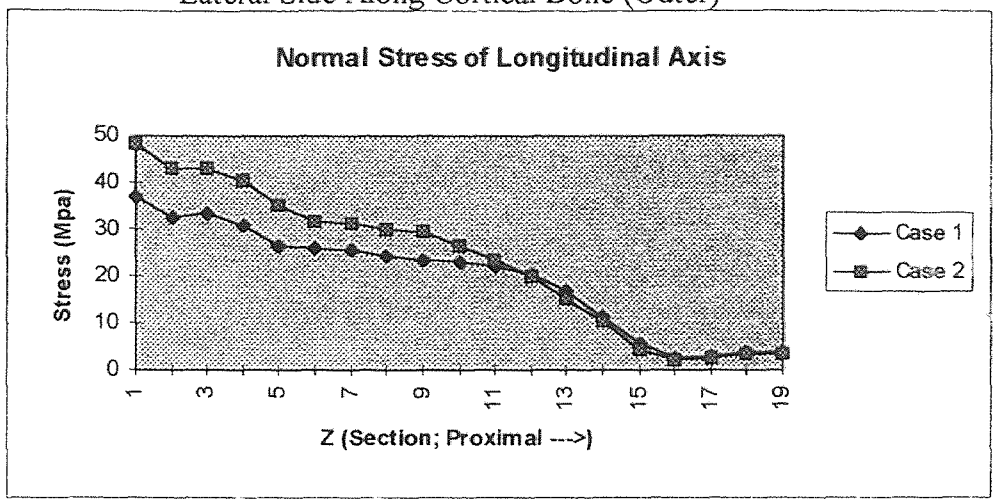

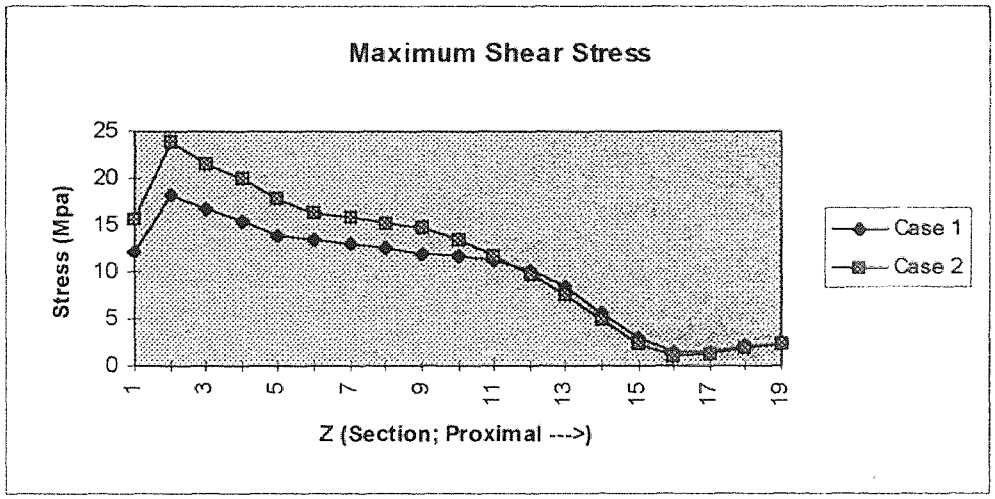

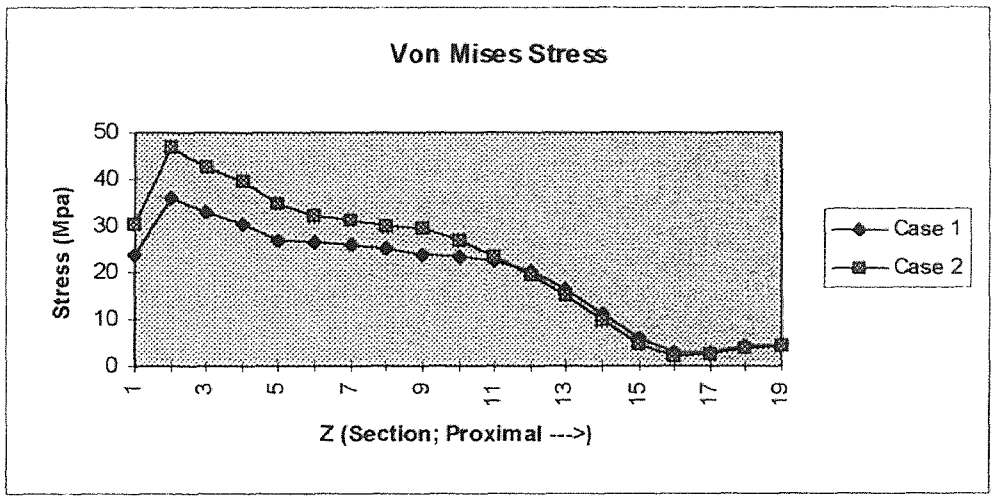

Appendix B13: The stress distributions of lateral side along Cortical Bone (Outer)

Medial Side Along Cortical Bone (Outer)

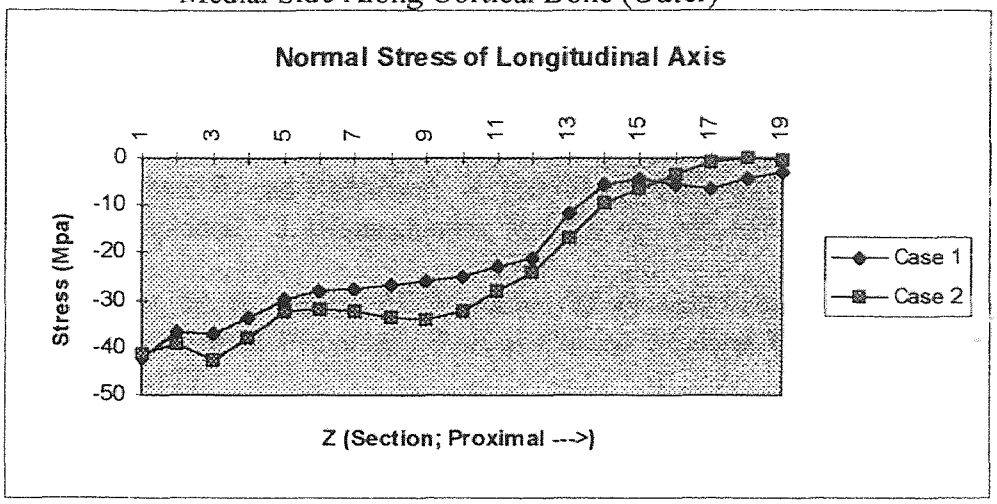

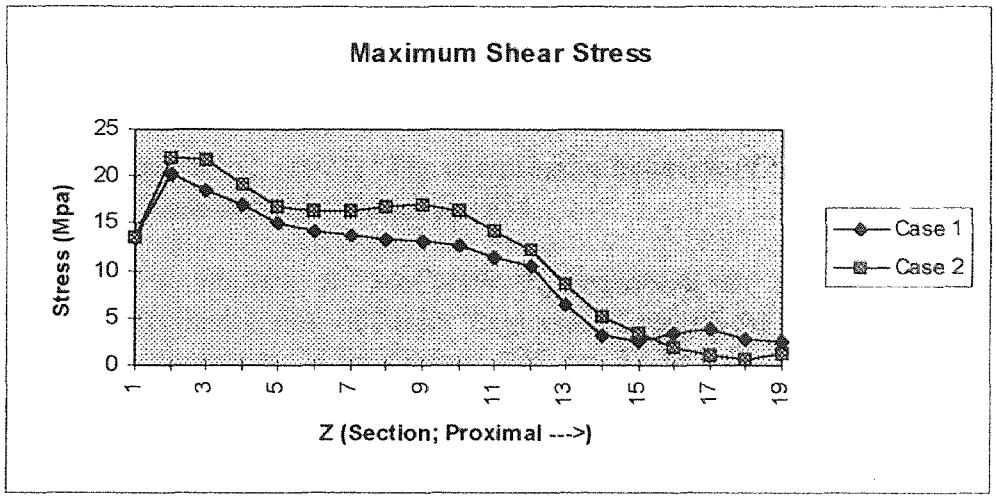

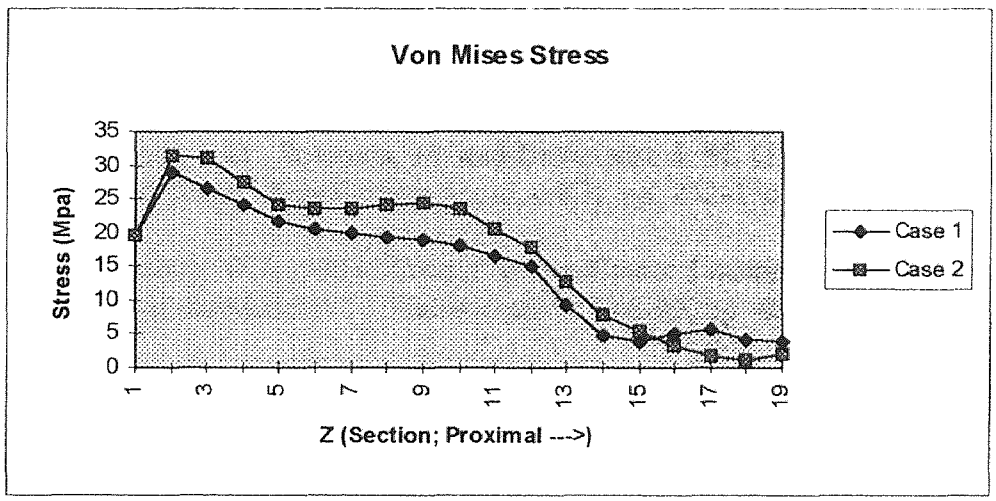

Appendix B14: The stress distributions of medial side along Cortical Bone (Outer)

REFERENCES

Bergmann, G., Graichen, F. and Rohlmann, A. (1993) "Hip Joint Loading during Walking and Running, Measured in Two Patients." J. Biomechanics, Vol. 26, pp. 969-990.

Bergmann, G., Graichen, F. and Rohlmann, A. (1995) "Is Staircase Walking a Risk for the Fixation of Hip Implants?." J. Biomechanics, Vol. 28, pp. 535-553.

Berry, D. J., Harmsen, W. S., Ilstrup, D., Lewallen, D. G. and Cabanela, M. E. (1995) "Survivorship of Uncemented Proximally Porous-Coated Femoral Components." Clin. Orthop. 319, pp. 168-177.

Bourne, R., Rorabeck, C., Burkart, B. and Kirk, P. (1994) "Ingrowth Surfaces." Clin. Orthop. 298, pp. 37-46.

Callaghan, J. J. (1993) "Current Concepts Review The Clinical Results and Basic Science of Total Hip Arthroplasty with Porous-Coated Prostheses." J. Bone and Joint Surg., pp. 299-305.

Carter D. R., and Hayes W. C. (1977) "The compressive behavior of bone as a two-phase porous structure." J. Bone and Joint Surg., pp. 954.

Chandler, H., Clark, J., Murphy, S., McCarthy, J., Penenberg, B., Danylchuk, K., and Roehr, B. (1994) "Reconstruction of Major Segmental Loss of the Proximal Femur in Revision Total Hip Arthroplasty." Clin. Orthop. 298, pp. 67-74.

Chang, W. (1994) "Computer Aided Stress Analysis of the Femur with Prosthetic Hip Stem Utilizing Computed Tomography." Doctoral Dissertation, Department of Mechanical and Industrial Engineering, New Jersey Institute of Technology, Newark, NJ

Cowin, S.C. (1995) "Technical Note: On the Minimization and Maximization of the Strain Energy Density in Cortical Bone Tissue." J. Biomechanics, Vol. 28, pp. 445-447.

Dall, D. M., Learmonth, I. D., Solomon, M. and Davenport, J. M. (1993) "811 Charnley hips followed for 3-17 years." Acta Orthop Scand, 64(3), pp. 252-256.

Delp, S. L. and Maloney, W. (1993) "Effects of Hip Center Location on the Moment-Generating Capacity of the Muscles." J. Biomechanics, Vol. 26, pp. 485-499.

Engh, C., Hooten, J, Jr., Zettl-Schaffer, K., Ghaffarpour, M., McGovern, T., Macalino, G. and Zicat, B. (1994) "Porous-Coated Total Hip Replacement." Clin. Orthop. 298, pp. 89-96.

Estok II, D. M. and Harris, W. H. (1994) "Long-Term Results of Cemented Femoral Revision Surgery Using Second-Generation Techniques An Average 11.7-Year Follow-Up Evaluation." Clin. Orthop. 299, pp. 190-202.

Fyhrie, D. P. and Schaffler, M. B. (1995) "The Adaptation of Bone Apparent Density to Applied Load." J. Biomechanics, Vol. 28, pp. 135-146.

Gilbert, J. L., Bloomfeld, R. S., Lautenschlager, E. P. and Wixson, R. L. (1992) "A Computer-Based Biomechanical Analysis of the Three-Dimensional Motion of Cementless Hip Prostheses." J. Biomechanics, Vol. 25, pp. 329-340.

Harrigan, T. P. and Hamilton, J.J. (1994) "Bone Remodeling and Structural Optimization." J. Biomechanics, Vol. 27, pp. 323-328.

Harrigan, T. P. and Harris, W. H. (1991) "A Three-Dimensional Non-Linear Finite Element Study of the Effect of Cement-Prosthesis Debonding in Cemented Femoral Total Hip Components." J. Biomechanics, Vol. 24, pp. 1047-1058.

Havelin, L. I., Espehaug, B., Vollset, S. E., Engesaeter, L. B. and Langeland, N. (1993) "The Norwegian Arthroplasty Register a Survey of 17,444 Hip Replacements 1987-1990." Acta Orthop Scand, 64(3), pp. 245-251.

Head, W. C., Bauk, D. J. and Emerson, Jr., R. H. (1995) "Titanium as the Material of Choice for Cementless Femoral Components in Total Hip Arthroplasty." Clin. Orthop. 311, pp. 85-90.

Hollister, S. F., Kikuch, N. and Goldstein, S. A. (1993) "Do Bone Ingrowth Processes Produce a Globally Optimized Structure?" J. Biomechanics, Vol. 26, pp. 391-407.

Huiskes, R., and Van Rietbergen, B. (1995) "Preclinical Testing of Total Hip Stems." Clin. Orthop. 319, pp. 64-76.

Katz, R. P., Callaghan, J. J., Sullivan, P. M. and Johnston, R. C. (1995) "Results of Cemented Femoral Revision Total Hip Arthroplasty Using Improved Cementing Techniques." Clin. Orthop. 319, pp. 178-183.

Keaveny, T. M. and Bartel, D. L. (1993a) "Effects of Porous Coating and Collar Support on Early Load Transfer for a Cementless Hip Prosthesis." J. Biomechanics, Vol. 26, pp. 1205-1216.

Keaveny, T. M. and Bartel, D. L. (1993b) "Effects of Porous Coating, With and Without Collar Support, on Early Relative Motion for a Cementless Hip Prosthesis." J. Biomechanics, Vol. 26, pp. 1355-1368.

Keaveny, T. M., Borchers, R. E., Gibson, L. J. and Hayes, W. C. (1993) "Theoretical Analysis of the Experimental Artifact in Trabecular Bone Compressive Modulus." J. Biomechanics, Vol. 26, pp. 599-607.

Keaveny, T. M. and Bartel, D. L. (1994) "Fundamental Load Transfer Patterns for Press-Fit, Surface-Treated Intramedullary Fixation Stems." J. Biomechanics, Vol. 27, pp. 1147-1157.

Kohles, S. S., Vanderby Jr, R., Ashman, R. B., Manley, P. A., Markel, M. D. and Heiner, J. P. (1994) "Ultrasonically Determined Elasticity and Cortical Density in Canine Femora after Hip Arthroplasty." J. Biomechanics, Vol. 27, pp. 134-144.

Mann, K. A., Bartel, D. L., Wright, T. M. and Burstein A. H. (1995) "Coulomb Frictional Interfaces in Modeling Cemented Total Hip Replacements: A More Realistic Model." J. Biomechanics, Vol. 28, pp. 1067-1078.

Marom, S. A. and Linden, M. J. (1990) "Computer Aided Stress Analysis of Long Bones Utilizing Computed Tomography." J. Biomechanics, Vol. 23, pp. 399-404.

McPherson, E. J., Dorr, L. D., Gruen, T. A. and Saberi, M. T. (1995) "Hydroxyapatite-Coated Proximal Ingrowth Femoral Stems." Clin. Orthop. 315, pp. 223-230.

Mullender, M. G., Huiskes, R. and Weinans, H. (1994) "A Physiological Approach to the Simulation of Bone Remodeling as a Self-Organizational Control Process." J. Biomechanics, Vol. 27, pp. 1389-1394.

Munting, E. and Verhelpen, M. (1995) "Fixation and Effect on Bone Strain Pattern of a Stemless Hip Prosthesis." J. Biomechanics, Vol. 28, pp. 949-961.

Pritchett, J. W. (1995) "Femoral Bone Loss Following Hip Replacement." Clin. Orthop. 314, pp. 156-161.

Raut, V.V., Siney, P. D. and Wroblewski, B. M. (1994) "Long-Term Results of Cemented Charnley Revision Arthroplasty for Fractured Stem." Clin. Orthop. 303, pp. 165-169.

Reddy, J. N. (1984) *An Introduction to the Finite Element Method* McGraw-Hill Publishing Company, New York, NY pp. 64-81, 235-242.

Rho, J. Y., Ashman, R. B. and Turner, C. H. (1993) "Young's Modulus of Trabecular and Cortical Bone Material: Ultrasonic and Microtensile Measurements." J. Biomechanics, Vol. 26, pp. 111-119.

Rorabeck, C., Bourne, R., Laupacis, A., Feeny, D., Wong, C., Tugwell, P., Leslie, K. and Bullas, R. (1994) "A Double-Blind Study of 250 Cases Comparing Cemented with Cementless Total Hip Arthroplasty" Clin. Orthop. 298, pp. 156-164.

Rossi, P., Sibelli, P., Fumero, S. and Crua, E. (1995) "Short-Term Results of Hydroxyapatite-Coated Primary Total Hip Arthroplasty." Clin. Orthop. 310, pp. 98-102.

Rubin, C., and McLeod, K. (1994) "Promotion of Bony Ingrowth by Frequency-Specific, Low-Amplitude Mechanical Strain." Clin. Orthop. 298, pp. 165-174.

Sadegh, A. M., Luo, G. M. and Cowin, S. C. (1993) Bone Ingrowth: An Application of the Boundary Element Method to Bone Remodeling at the Implant Interface." J. Biomechanics, Vol. 26, pp. 167-182.

Skinner, H. B., Kilgus, D. J., Keyak, J., Shimaoka, E. E., Kim, A. S. and Tipton, J. S. (1994) "Correlation of Computed Finite Element Stresses to Bone Density after Remodeling Around Cementless Femoral Implants." Clin. Orthop. 305, pp. 178-189.

Sotereanos, N. G., Engh, C. A., Glassman, A. H., Macalino, G. E. and Engh, Jr., C. A. (1995) "Cementless Femoral Components Should Be Make From Cobalt Chrome." Clin. Orthop. 313, pp. 146-153.

Tonino, A. J., Romanini, L., Rossi, P., Borroni, M., Greco, F., Garcia-Araujo, C., Garcia-Dihinx, L., Murcia-Mazon, A. Hein, W. and Anderson, J. (1995) "Hydroxyapatite-Coated Hip Protheses." Clin. Orthop. 312, pp. 211-225.

Van Rietbergen, B., Weinans, H., Huiskes R. and Odgaard, A. (1995) "A New Method to determine Trabecular Bone Elastic Properties and Loading using Micromechanical Finite-Element Models." J. Biomechanics, Vol. 28, pp. 69-81.

Weinans, H., Huiskes, R. and Grootenboer, H. J. (1992) "The behavior of adaptive bone-remodeling stimulation models." J. Biomechanics, Vol. 25, pp. 1425-1441.

Weinans, H., Huiskes, R. and Grootenboer, H. J. (1993) "Quantitative Analysis of Bone Reactions to Relative Motions at Implant-Bone Interfaces." J. Biomechanics, Vol. 26, pp. 1271-1281.

Weinans, H., Huiskes, R. and Grootenboer, H. J. (1994) "Effects of Fit and Bonding Characteristics of Femoral Stems on Adaptive Bone Remodeling." J. Biomechanical Eng, Vol. 116, pp. 393-400.

Xenos, J. S., Hopkinson, W. J., Callaghan, J. J., Heekin, R. D., and Savory, C. G. (1995) "Osteolysis Around an Uncemented Cobalt Chrome Total Hip Arthroplasty." Clin. Orthop. 317, pp. 29-36.